Title	Development of High-Sensitivity Optical Fiber Sensor Based on Optical Pulse Correlation
Author(s)	Song, Hongbin
Citation	高知工科大学, 博士論文.
Date of issue	2008-03
URL	http://hdl.handle.net/10173/368
Rights	
Text version	author

Development of High-Sensitivity Optical Fiber Sensor Based on Optical Pulse Correlation

Hongbin Song

A dissertation submitted to
Kochi University of Technology
in partial fulfillment of the requirements
for the degree of

Doctor of Philosophy

Graduate School of Engineering

Kochi University of Technology

Kochi, Japan

March 2008

Abstract

To develop a real-time high-sensitive optical fiber sensing system, this dissertation comprehensively concerns a time-based sensing concept proposal, real-time sensing system construction, polarization fluctuations compensation, field experiment, and performance estimation in long-range monitoring.

Optical pulse correlation sensing system employs the time modulation of the optical signal propagating in the optical fiber transmission lines, which is completely different from the conventional methods based on the modulation of other parameters of the optical signal such as the intensity, wavelength, phase and frequency. The propagation time drift generated in the optical signal caused by the environment conditions such as temperature, stress or pressure around the optical fiber transmission lines was monitored by using the SHG optical pulse correlation measurement.

Chapter 2 presents the optical pulse correlation sensing concept. The time-drift based optical pulse correlation sensing concept is proposed and the corresponding correlation measurement method is presented. The theoretical analysis and the fundamental sensing characteristics of the optical pulse correlation sensor are discussed in theory.

Chapter 3 illustrates the mechanism of the optical pulse correlation sensing system. By using the differential detection of two correlation signals generated in orthogonal polarization directions, high-sensitivity sensing is realized. The temperature and strain

monitoring characteristics are investigated. As the correlation signals simultaneously sensitive to the temperature change and stress impacted on the monitoring fiber, the discrimination of temperature and strain monitoring is discussed in theory.

Chapter 4 improves the sensing structure and compensates the polarization fluctuation in correlation signals resulted from the birefringence fluctuations in a single-mode fiber via retracing beam. Since the birefringence fluctuations in a single-mode fiber originate from the time-dependant difference variation of two orthogonal components of an optical beam, if the orthogonal components experience the same variations at any time along the single-mode fiber, it is available to neutralize the birefringence fluctuations. This method is introduced into the optical pulse correlation sensing system and the fluctuations in the correlation signals are compensated. At the same time, the sensitivity is nearly doubled due to the double-pass monitoring by virtue of the reflection from FRM. Finally, a field experiment on the temperature monitoring outside of the lab is carried out.

Chapter 5 investigates the performance of the optical pulse correlation sensing system in long-range monitoring in theory and experiment. The effects of loss impact, dispersion effect and nonlinear impairments on the correlation sensing system with long monitoring fiber are discussed in theory. Finally, the time drift monitoring characteristics of the optical pulse correlation sensing system with monitoring fiber of length 30 km, 50 km and 60 km are investigated in experiment.

Chapter 6 summarizes the main results in this work.

Table of Contents

Abstract

Chapter 1: Introduction

Chapter 2: Optical Pulse Correlation Sensing Concept

Chapter 3: Optical Pulse Correlation Sensing System

Chapter 1

Introduction

1.1 Research background

The rapid development of semiconductor laser and optical fiber technology for the communication purpose has promoted the step of optical fiber sensors. Optical fiber sensing technology has demonstrated its superiority to the traditional mechanical sensors and electric sensors as shown in table 1.1.

Table 1.1 Comparison of traditional sensors and optical fiber sensor

	Traditional sensors	Optical fiber sensors
Immune to Electro-magnetic interference	×	○
No need power supply	×	○
Multiplexing	×	○
Remote sensing	⊗	○
Online monitoring	⊗	○
Compact structure	⊗	○
Resistance to chemical corrosion	×	○

Therefore, optical fiber sensors have been widely used in many fields such as industry, environment, biology, health monitoring of civil engineering, and inertial navigation [1-6]. Recently, the application of optical fiber sensing technology with long-range

monitoring ability to disaster prediction such as slope collapse, earthquake and tsunami is becoming a hot topic, due to the direct alarming sending by taking advantage of the optical fiber cables for communication network [7]. Fig.1. illustrates the schematic diagram of an optical fiber sensing system for slope collapse monitoring [7]. By sending the monitoring signal to the communication network via fiber cables for communication purpose, the alarming signal can be directly sent to the user terminal.

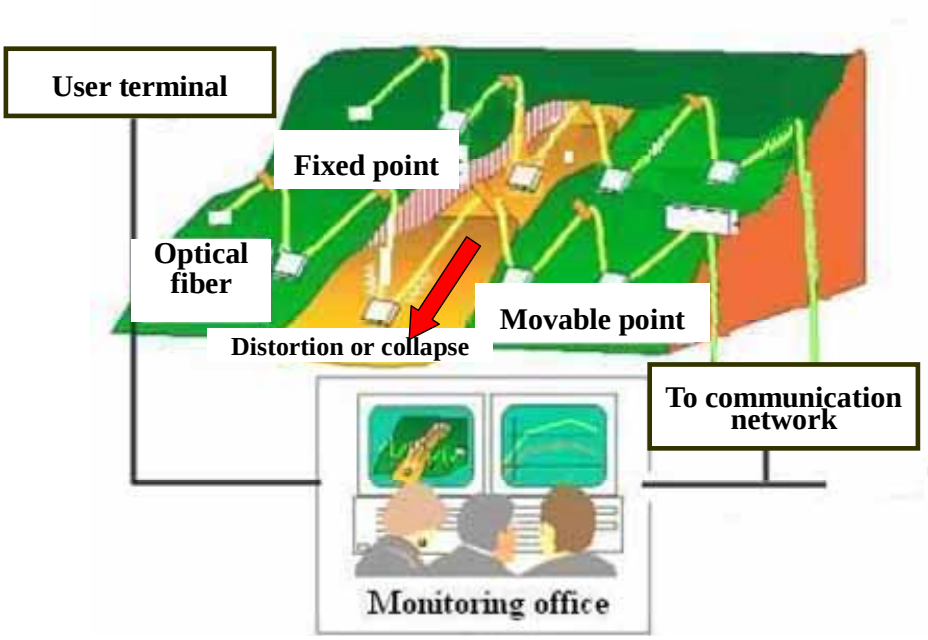

Fig.1.1 Optical fiber sensing system for slope collapse monitoring

http://www.mlit.go.jp/road/road/new5/05/5-1.html

Since early 1970s, researchers have begun to apply the optical fiber to the sensing system and various kinds of sensing techniques have been developed. There are many classifications of the optical fiber sensing techniques. However, all the optical fiber sensing techniques originate from the modulation of intensity, phase, wavelength, frequency, and polarization, by which the optical signal is determined.

1. Intensity-based optical fiber sensor

Intensity-based optical fiber sensor realizes the sensing according to the optical field

distribution or the power loss caused by micro- or macro-bending [8-10]. Since the optical field distribution is related to the longitudinal and axial distance between the transmitter fiber and a receiver fiber. By using a transducer, the distance between the transmitter fiber and monitoring fiber was modulated by the environment such as temperature and pressure, so the optical power detected by the receiving fiber was modulated and the sensing was realized [8]. For the micro-and macro-bending sensor, the optical intensity is modulated by the distortion of fiber resulted in the power loss [9, 10]. Optical time domain reflectometry (OTDR) belongs to the intensity-based sensor, as it is based on the bending loss [11]. Intensity-based fiber sensors have simple structure. However, they have a series of limitations imposed by various losses in the system that are not caused by the environmental change to be measured. Potential error sources include variable losses due to connectors, splices, and mechanical creep and misalignment of light sources and detectors.

2. Optical fiber interferometer

The optical fiber interferometer is developed based on coherent theory of optical beams. The interference fringe visibility is related to the phase difference between coherent beams. There are mainly four structures: Mach-Zehnder interferometer (MZI), fiber optic gyroscope (FOG) based on Sagnac interference, Michelson interferometer, and Fabry-Perot interferometer (FPI). As the optical path length can be measured on the scale of the wavelength of light, intense researches have been carried out. Mach-Zehnder and Michelson interferometers have been insensitively investigated for acoustic pressure detection in the early stage of fiber sensor development [12, 13]. Hydrophones based on these two interferometers are reported to have high resolution of 0.1% [14]. However, due to the low level of photo elastic or stress-optic coefficients of

the silica glass fibers, a very long sensing fiber is necessary to obtain the desirable sensitivity, which unavoidably makes the sensor thermally unstable and sensitive to vibrations. In addition, due to source-induced phase noise in unbalanced interferometers, a highly coherent source with a relatively long coherence length is normally required [15, 16]. A white light interferometer (WLI) with an accuracy of 0.5 μm was presented by T. Li et.al based on the low coherence of Michelson interferometer, which overcame the limit of the coherence requirement to the light source [17]. But the measurement range is inherently limited by the scanning length of the motor. Another drawback associated with these two types of interferometric sensors is the polarization-fading problem that refers to the interference fringe visibility as a function of the polarization status of the light transmitted inside the fibers [12].

Fiber optic gyroscope obtained the contemporary development with optical fiber hydrophone, which was used to measure the rotation as a replacement of ring laser gyroscope firstly developed by V.Vali and R. E. Shorthill in 1976 [18]. Extrinsic Fabry-Perot interferometer (EFPI) has high resolution and small size, which has been widely used in health monitoring of large scale civil engineering structures, acoustic detection and aircraft [19, 20]. In 1996, Bhatia et al. demonstrated an absolute EFPI system for measuring values of cavity length d ranging from 40 to 300 μm with a demonstrated spectral resolution of 0.1 nm [21]. In 2001 M. Schmidt. et.al. proposed a fiber-optic extrinsic Fabry-Perot interferometer strain sensor with 50 pm displacement [22]. However, EFPI sensors are limited by the weak interferometric signal and difficulty in multiplexing. At present, many researchers are concentrated to solve these problems [23-25].

3. Fiber Bragg Grating sensor

Fiber Bragg grating (FBG) is an important wavelength selection component based on the photosensitivity. After a controllable and effective method for FBG fabrication was devised by G. Meltz et.al. in 1989[26], the intensive studies on the application to add/drop filters, amplifier gain flattening, dispersion compensator and fiber lasers for the communications have begun [27]. As the reflected wavelength is sensitive to the change of grating period or the effective refractive index caused by strain or temperature, it has been used to develop high-sensitivity optical fiber sensor. The typical strain and temperature sensitivity of FGB sensors near 1550 nm are ~1.2 pm/με and ~13 pm/°C, respectively [27, 28].

Except the high sensitivity characteristic, FBG sensor has the multiplexing ability. Various kinds of multiplexing systems based on FBG sensors were developed. In 1990 W.W. Morey et.al. demonstrated a multiplexing FBG sensing system based on a broadband light source interrogation to a chain of FBGs[29]. In 1996 Volanthen et al. demonstrated a broadband interrogation system for distributed grating sensors by using a low-coherence interferometry a tunable filter to measure the local wavelength [30]. In 2004 Peng-Chun Peng et.al. proposed a multiplexing sensor by using a multi-port fiber laser [31].

Although FBG sensors have been developed nearly 30 years, many researchers are embarking on the extensive research on FBG sensor currently due to its high sensitivity and the multiplexing ability [32-33]. However, as FBGs indicates the quantities by the wavelength shift, it is required to monitor the output signal by utilizing an optical spectrum analyzer with high resolution. It must be admitted that optical spectrum analyzer is not suitable for real sensing systems due to the high expense and low

wavelength scanning speed. Therefore, interrogators for FBG sensor are required. Some interrogators are quite simple but are more limited in measurement resolution, dynamic range or multiplexing, and some are more complicated and provide better resolution but are more expensive or need stabilization [34, 35].

4. Brillouin Optical Time-domain Reflectometer (BOTDR)

BODTR is a sensor based on the Brillouin gain in an optical fiber. When two lasers, one is defined as the probe laser and the other is pump laser, are launched into an optical fiber, Brillouin effect will occur if the pump laser frequency is greater than that of the probe laser by the Brillouin frequency shift; the probe laser will be amplified, experiencing Brillouin gain. Since the Brillouin frequency shift depends on the environment around the fiber such as temperature or the strain, the sensing is realized. If the probe intensity emerging from the fiber is monitored following the launch of a pump pulse, an increase in the intensity will be observed whenever Brillouin gain occurs. The time delays between the launch of the pump pulse and these increases in the received probe signal correspond to round-trip times for light traveling to and from the regions of gain. These times provide the position information. Therefore the distribution sensing is available [36-37]. BOTDR is powerful to realize the high-sensitivity distribution monitoring in long-range, however, its response time is required to be several minutes. So it is a little difficult to realize the real-time monitoring.

According to the above introduction, the characteristics of different optical fiber sensors are summarized in table 1.2. It can be seen that for the conventional fiber sensors based on the modulation of intensity, phase, wavelength and frequency of optical signal have various difficulties to realize the real-time high-sensitivity sensing system with long-range monitoring ability fro remote sensing. To overcomes these disadvantages,

we proposed an optical fiber sensing technology based on the modulation of optical tiem delay of optical pulse propagating in an optical fiber.

Table 1.2 Characteristics of conventional fiber sensors

Sensing mechanism	Sensor type	Advantages	Disadvantages
Intensity	Micro-bending sensor Macro-bending sensor OTDR	Simple	•Low sensitivity •Insertion loss dependence
Phase	Interferometer	High sensitivity	• Coherence length dependence •Unable to long-distance monitoring
Wavelength	FBG	•Multipoint monitoring •Intensity independence	•Low sensitivity •Insertion Loss dependence
Frequency	BODTR	•Distribution monitoring •Long-range monitoring	• Coherence length dependence •Difficult to real-time monitoring

1.2 Scope and objective of this work

1.2.1 Optical pulse correlation sensor for time drifts measurement

Time drift in fiber optic devices such as pulse compression fiber, nonlinear optical loop mirrors and Erbium-doped fiber amplifiers due to the optical power and environmental

condition change, limits the performance of all-optical fiber modulation multiplexing/demultiplexing in fiber optic communication system [38], which is adverse for the performance of the optical fiber communication system.

However, the time drift contains abundant information such as the temperature, strain, and pressure around fiber optic transmission lines. Therefore, the monitoring of the drift is valuable for understanding the environment condition around the optical fibers. By detecting time drift in an optical pulse, the environmental conditions around fiber optic transmission lines are available to be monitored. This sensing system is based on the correlation monitoring of traveling pulses, which can be detected according to the overlap of optical signals. The optical correlation in orthogonal directions for differential detection is realized due to the time delay bias in the optical signal correlation unit. The time delay bias also makes it possible to obtain high-sensitivity measurement.

The time resolution of the optical pulse correlation system depends on the pulse width of light source, the time jitter, SHG efficiency and S/N of the O/E detector. A mode-locked LD with low time jitter short pulse is used as the light source. The pulse width can be controlled by using dispersion compensation fiber. By using quasi-phase matching technique, high SHG efficiency is available. The time monitor circuit is bit-rate flexible and does not need high-speed. Therefore, it is potential to realize a time resolution around several femo-seconds [39].

1.2. Scope and objective of this work

This work aims to develop a high-sensitivity optical fiber sensor based on optical pulse correlation. It is focused on the following aspects:

(1) To illustrate the theory of optical pulse correlation and construct the fundamental sensing system

(2) To investigate the fundamental sensing characteristic of the optical pulse correlation sensing system and confirm the feasibility to high-sensitivity temperature and strain measurement

(3) To enhance the sensing performance by improving the sensing structure and verify the improvement

(4) To carry out the field experiment

(5) To investigate the performance of the sensor in the case of long monitoring fiber

The optical pulse correlation theory is proposed in chapter 2, in which the basic of the optical fiber sensor is discussed. Chapter 3 illustrates the construction of the optical pulse correlation sensing system and the fundamental sensing characteristic is investigated. According to the experimental results, the polarization fluctuation caused by the birefringence in the single mode fiber was observed. The polarization fluctuation compensation is described in chapter 4. At the same time, the enhancement of sensitivity and linearity improvement are obtained due to the establishment of double-pass monitoring. Then a temperature monitoring experiment outside of the lab is carried out. Chapter 5 is dedicated to the theoretical and experimental investigation of the optical pulse correlation sensor performance in the case of long monitoring fiber. Chapter 6 summarizes the research results and conclusions. The organization of the dissertation is shown in Fig.1.2.

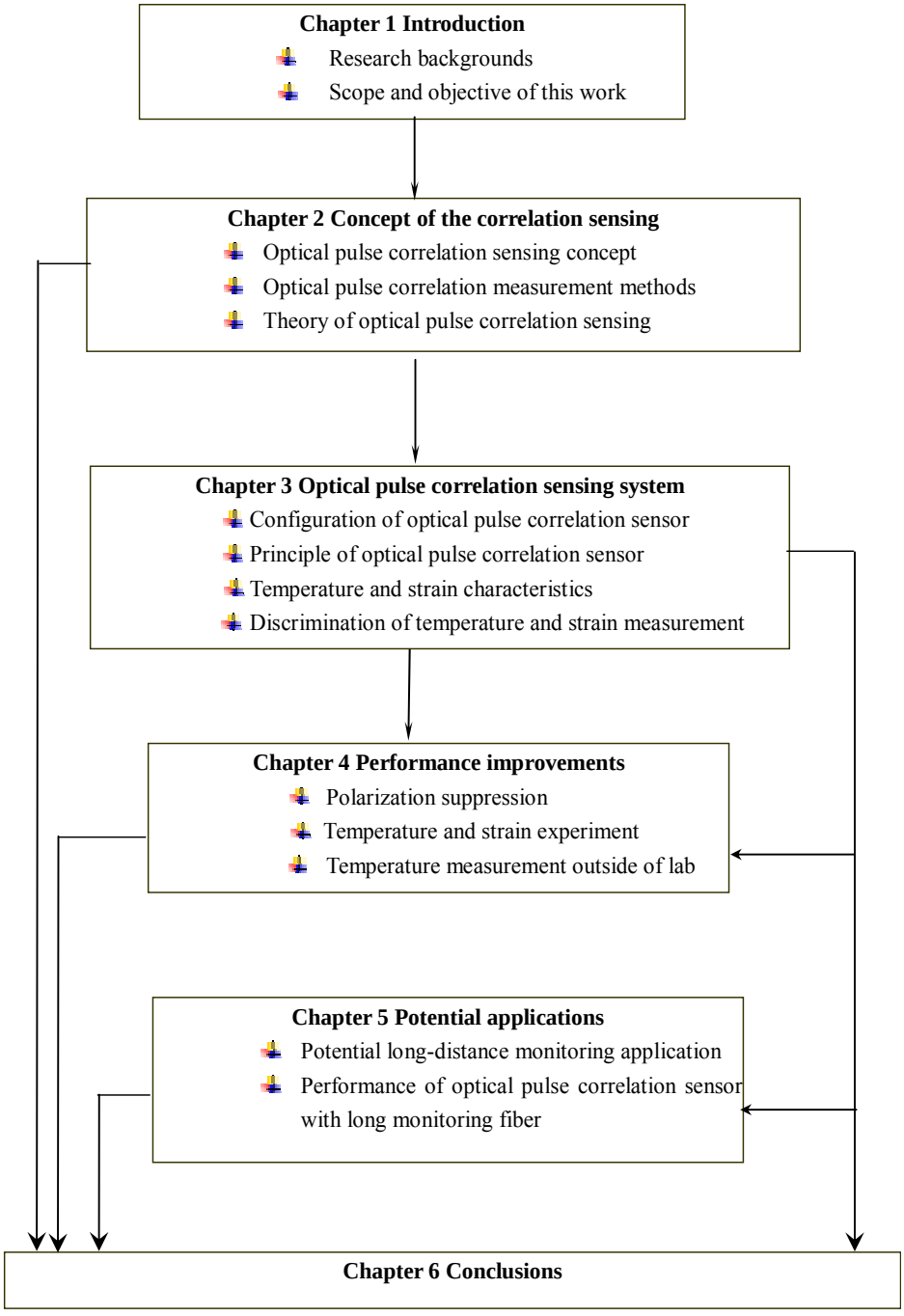

Fig.1.2 Outline of the dissertation

Chapter 2

Optical Pulse Correlation Sensing Concept

2.1 Introduction

Time drift between optical pulses limits the performance of the communication systems utilizing ultra short pulse trains, as the environment condition change is easy to cause the time delay drift of the optical pulses transmitting in the long fiber devices such as pulse compression fiber, nonlinear optical loop mirrors and Erbium-doped fiber amplifiers. Therefore, it is required to monitor and stabilize the time drift within a few pico-seconds in the communication system [38]. However, as the time drift contains abundant environmental information such as the temperature, strain and pressure around optical fiber transmission lines, if the time drifts of optical pulses propagating in the optical fiber transmission lines can be detected, the environmental conditions around optical fiber transmission lines are potential to be monitored. The timing relationship between two optical pulses can be defined as the optical pulse correlation, which can be measured by using the double-frequency nonlinearity of a crystal or the fluorescence of an organic dye solution. Based on the optical pulse correlation concept, a high-sensitivity optical fiber sensor is proposed. In this chapter, the concept of the optical pulse correlation sensor is presented.

2.2 Optical pulse train correlation sensing concept

As an important parameter of optical signal, the time of optical signal reflects condition

of the the optical path. So the sensing can be realized by monitoring the time information of optical signals. The mature of short-pulse generation technique enables the sensor based on the time modulation of optical pulse to have high sensitivity. The time information of the optical pulse is included in the optical pulse correlation, which makes the sensing feasible.

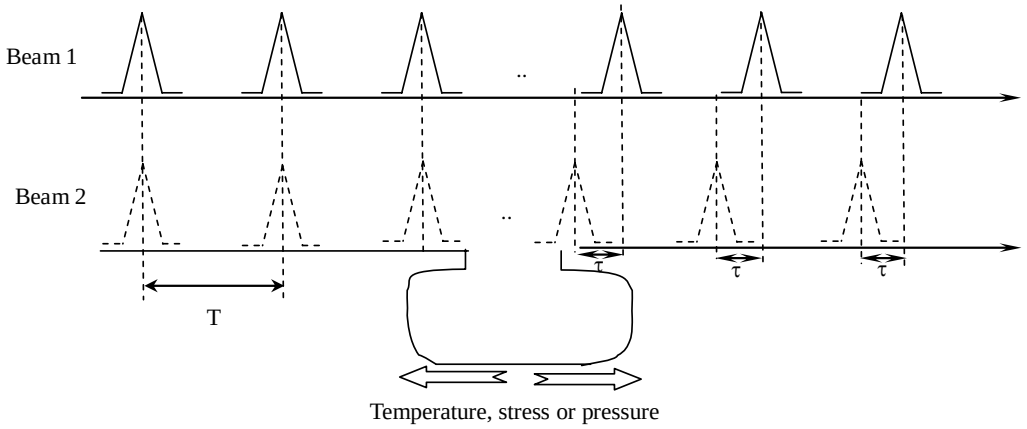

Fig.2.1 Timing drifts in optical fiber

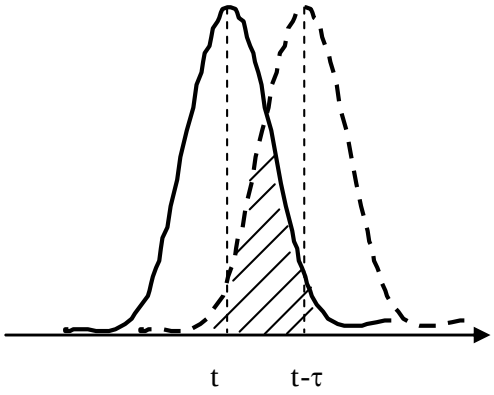

Fig.2.2 Optical pulse correlation measurement

For two optical beams from the same light source transmitting in optical fibres, when they experience the static optical path, the timing relationship between them is constant. However, if there is any change in the environment around one optical fiber such as

temperature, strain or pressure, a time delay of the optical pulse will be generated in this beam as shown Fig.2.1[40]. The timing relationship between two pulses is shown in Fig.2.2, which can be defined as an optical pulse correlation equation and written as

$$I_{correlation}(\tau) \infty \int I(t) I(t-\tau) dt \qquad (2\text{-}1)$$

The correlation between beam1 and beam2 can be measured by using a nonlinear process of second-harmonic generation (SHG) in a crystal or the fluorescence of an organic dye solution. Then the time drift in the monitoring pulse caused by the environment change will be obtained. As a result, the corresponding environment change is available to be measured.

2.3 Optical pulse correlation measurement methods

2.3.1 SHG correlation measurement

SHG is a well-known frequency-doubling nonlinear phenomenon, which is currently being used in ultraviolet generation, microscopy, biological imaging and electric field measurement [41-44]. Combing SHG with the Michelson interferometer with a scanning arm, an autocorrelation scheme was developed and successfully applied to measure the width of low-repetition rate ultra short pulses [45-47].

2.3.1.1 Second-harmonic generation

When two optical waves with frequencies of ω_1 and ω_2 are incident onto a nonlinear crystal, an optical beam with a frequency of ω_3 is generated.

$$\omega_1 + \omega_2 = \omega_3 \qquad (2\text{-}2)$$

If $\omega_1 = \omega_2$,

$$\omega_3 = 2\omega_1 \qquad (2\text{-}3)$$

This phenomenon is defined as the second harmonic generation whose process is demonstrated in Fig.2.3 [44].

The output power of the second harmonic wave can be expressed as

$$P_{2\omega} = \frac{2\pi^2 d_{eff}^2 L^2 P_{\omega}^2 \sin^2(\Delta kL/2)}{\varepsilon_0 c n_{\omega}^2 n_{2\omega} \lambda_{2\omega}^2 A(\Delta kL/2)^2} \qquad (2\text{-}4)$$

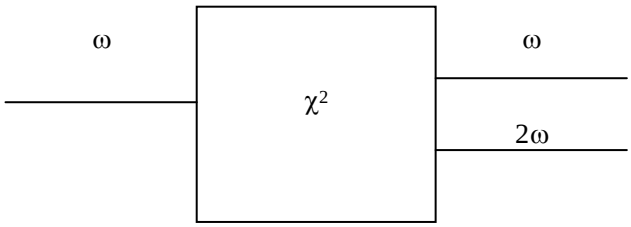

(a)

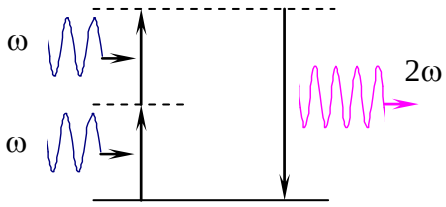

(b)

Fig.2.3 (a) Geometry of second harmonic generation

(b) Energy-level diagram description

Where, d_{eff} is the nonlinear optical constant,

ε_0 is the dielectric constant,

n is the refractive index,

A is the cross area of the input beam,

L is the length of the crystal.

According to Eq. (2-4), a prerequisite for efficient second-harmonic generation is

$\Delta k = 0$. Then $\frac{\sin^2(\Delta kL/2)}{(\Delta kL/2)^2}$ is equal to unit and the second harmonic intensity increases with L^2 [46] $\Delta k = 0$ is called the phase-matching condition. Under the phase-matching condition, we have

$$P_{2\omega} \propto P_{\omega}^2 \tag{2-5}$$

To obtain an efficient SHG, it is required to satisfy the phase-matching condition, that is,

$$\Delta k = k^{(\omega)} - 2k^{(\omega)} = 0 \tag{2-6}$$

i.e.

$$k^{(\omega)} = 2k^{(\omega)} \tag{2-7}$$

In order to satisfy the phase-matching condition described above, there are main two techniques birefringent phase matching and quasi-phase matching.

Birefringent phase matching is a usual technique to satisfy the phase-matching condition in nonlinear crystal, which exploits the natural birefringence of anisotropic crystals.

According to $k^{(\omega)} = \omega n^{(\omega)} / c$, in order to satisfy formula (2-7)

$$n^{(2\omega)} = n^{(\omega)} \tag{2-8}$$

Therefore, the indices of refraction at the fundamental and second-harmonic frequencies must be equal [47]. In normally dispersive materials the index of the ordinary wave or the extraordinary wave along a given direction increases with ω, which makes it impossible to satisfy (2-8) when both ω and 2ω beams are of the same type, that is, when both are ordinary or extraordinary. We can, however, under certain circumstances, satisfy (2-8) by making the two waves have different types.

As the birefringence phase matching is difficult to satisfy the requirement in (2-8), especially in the case of ω and 2ω beams with the same types. Therefore, a special

technique of significant importance called quasi-phase matching is proposed. Quasi-phase matching utilizes a material with spatially modulated nonlinear properties instead of a homogeneous nonlinear crystal material to realize the phase matching [48]. The spatial modulation nonlinear properties are realized by the periodically poling [42]. The growth of second harmonic power is shown in Fig.2.4 Comparing the conversion efficiency in the case of phase matching, quasi-phase matching and non-phase matching, it can be seen that, the efficiency of quasi-phase matching is lower than that the phase matching condition but much higher than the non-phase matching condition. However, by utilizing the material with high effective nonlinearity, the conversion efficiency can be enhanced as high as that in the case of phase matching [48].

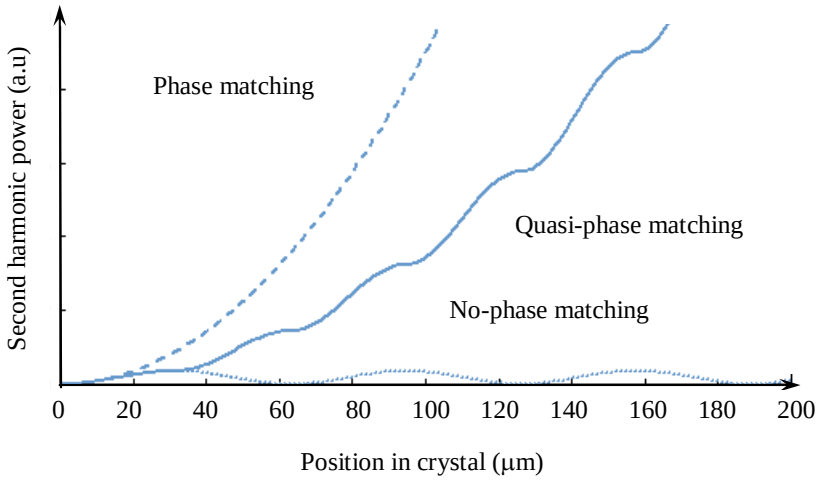

Fig.2.4 Growth of second-harmonic power in a nonlinear crystal [48]

2.3.1.2 SHG intensity correlation measurement

Determination of the duration of a light pulse from measurements of the intensity autocorrelation function can be regarded as a “self-sampling” technique in which one measures a signal proportional to the temporal overlap of the pulse with its time-delayed replica. A typical experimental arrangement for the intensity correlation measurement is

shown in Fig.2.5 [45, 49]. The pulse to be measured is divided into two equal intensity portions, and a time delay τ is introduced between the two components. The pulse *I(t)* and *I(t+τ)* are then focused into a suitable nonlinear crystal for the second harmonic generation. As the pulse duration $\Delta t_{1/2}$ is proportional to the width of the intensity, this approach is widely used to the pulse width measurement [44-47].

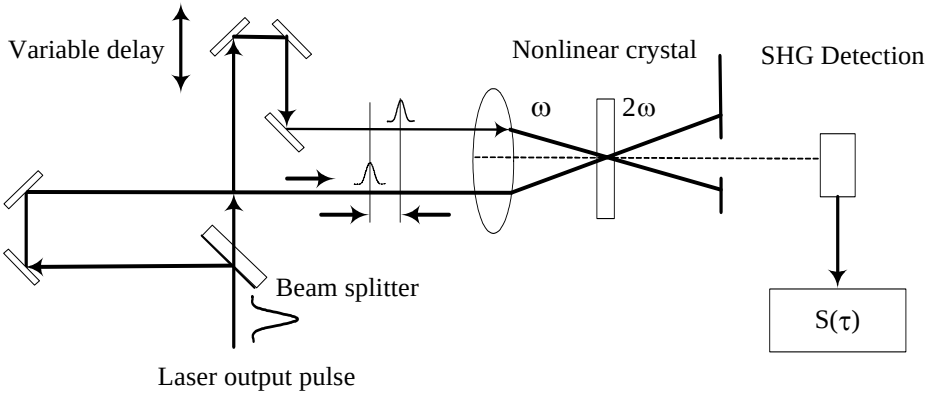

Fig.2.5 Experimental setup for intensity correlation measurement using SHG [45]

By using the experiment setup shown in Fig.2.5, the intensity correlation was obtained as

$$S(\tau) = 1 + 2G^2(\tau) + r(\tau) \qquad (2\text{-}9)$$

Where *r(τ)* is a rapidly varying fringelike component that averages to zero over several optical periods and is generally not observed experimentally [18,19]. When τ=0, a peak value can be obtained, which is defined as the perfect overlap. If *c/n* is the pulse velocity in the medium and *z* is the distance from the perfect overlap, i.e. $\tau = 2nz/c$, S(τ)=1. Thus, one measures the second-order correlation function in the presence of constant background [45]. Therefore, a ratio of 3:1 between the peak and the background can be observed. If the polarizations of two pulses in Fig.2.5 are orthogonal,

the intensity correlation with free-background can be obtained [18]. However, intensity correlation measurement with background provides assurance that the central peak in $G^2(\tau)$ has been obtained.

2.3.2 Two-photon fluorescence methods [45]

Two-photon fluorescence (TPF) method has been widely used to measure the pulse width of mode-locked lasers and spectroscopy in biologics due to its inherent simplicity and its ability to provide a complete measurement of $G^2(\tau)$ with a single pulse[50,51]. A schematic diagram of TPF correlation measurement with a triangle configuration is shown in Fig.2.6 [51]. The investigated pulse is divided into two equal components by a beam splitter, and each component travels equal distances and overlap in a solution of Rhodamine 6 G in ethanol exhibiting two-photon absorption and fluorescence. Neutral density filters were used for attenuation of the μs pulses. A time resolved photograph of the fluorescence trace was taken using a Charge-coupled device(CCD) camera and output from it was given to various measuring devices such as Cathode Ray Oscilloscope and PC monitor. The time-integrated photograph recorded from the side shows enhanced fluorescence where fluctuations or isolated pulses overlap with each other. Correlation occurs in a liquid dye solution that has no absorption at the pulse wavelength but fluoresces in the presence of high intensity by virtue of two-photon absorption. The integrated intensity of fluoresces at any point is proportional to the time averaged fourth power of the optical electric field. For two identical pulses moving in opposite direction, the fluoresces intensity distribution has the same form to Eq.(2-9).

The main advantage of the TPF method is that the spatial distribution of the fluorescence intensity is directly related to second order correlation function $G^{(2)}(\tau)$, also called fourth-order coherence function [51]. However, the measurement precision

of TOF critically depends on the alignment of the two optical beams and to a lesser extent on the intensity difference between two optical pulses.

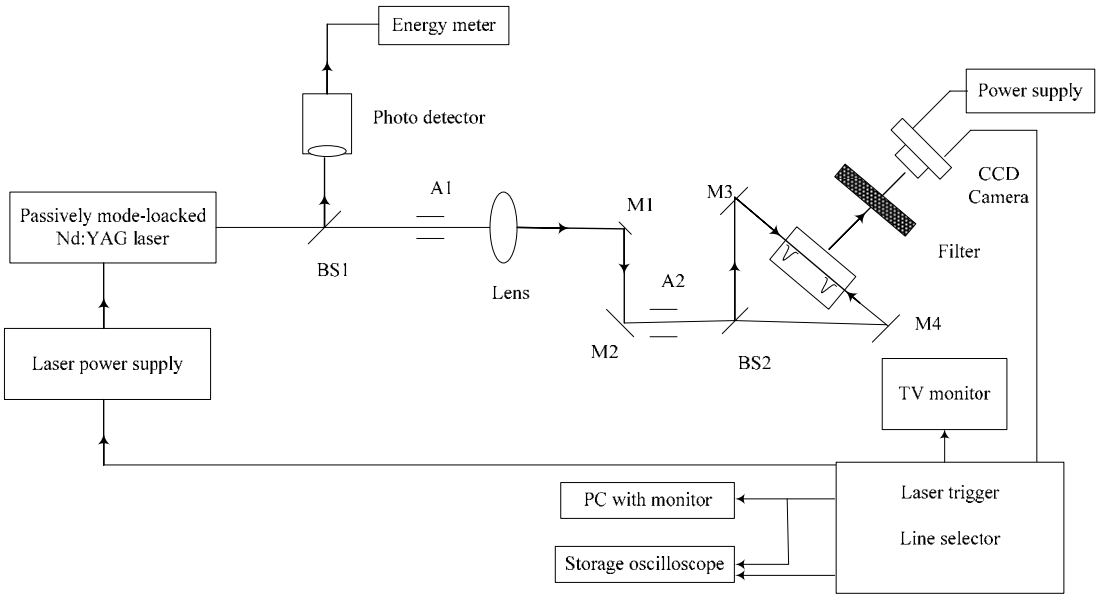

Fig.2.6 Schematic diagram of TPF correlation measurement [51]

2.4 Theory of optical pulse correlation sensing

According to the above description of correlation measurement method, compared with TPF method, SHG correlation has the high precision due to the relatively high nonlinear conversion efficiency under phase-matched condition. Therefore, we use SHG to realize the optical pulse correlation sensing.

As shown in Fig.2.1, the electric fields of beam1 and beam2 can be expressed as [52]

$$e_1^{\omega}(t) = \mathrm{Re}[E_1(t)e^{jw_1 t}] \tag{2-10}$$

$$e_2^{\omega}(t) = \mathrm{Re}[E_2(t-\tau)e^{jw_2(t-\tau)}] \tag{2-11}$$

As beam1 and beam2 come form the same light source, we have

$$e_1^{\omega}(t) = \mathrm{Re}[E(t)e^{jwt}] \tag{2-12}$$

$$e_2^{\omega}(t) = \mathrm{Re}[E(t-\tau)e^{jw(t-\tau)}] \tag{2-13}$$

The electric field from SHG crystal is shown as

$$e^{2\omega}(t) = \mathrm{Re}[E^2(t)e^{j2wt}] \tag{2-14}$$

The total input electric field to the SHG crystal is

$$e_{in}(t) = \mathrm{Re}\{[E(t) + E(t-\tau)e^{-i\omega\tau}]e^{i\omega t}\} \tag{2-15}$$

According to (2-14), the amplitude of the electric field after SHG crystal is the square of the electric field of the input beam. Therefore, the electric field of the output beam is

$$\begin{aligned} E_{out}(t) &= \{[E(t) + E(t-\tau)e^{-i\omega\tau}]\cdot[E(t) + E(t-\tau)e^{-i\omega\tau}]^* \\ &= E^2(t) + E^2(t-\tau) + E(t)E(t-\tau)e^{-i\omega\tau} + E(t)E(t-\tau)e^{i\omega\tau} \end{aligned} \tag{2-16}$$

This SH signal can be detected by using a photo detector. The output current i_d of the photodiode is proportional to the intensity of SH signals. By using a circuit, we obtain a voltage output. Hence, we have

$$\begin{aligned} \mathrm{v(t)} &\propto i_d(t) \propto E_{out}(t)E^*{}_{out}(t) \\ &= [E^2(t) + E^2(t-\tau) + E(t)E(t-\tau)e^{-i\omega\tau} + E(t)E(t-\tau)e^{i\omega\tau}]\cdot[E^2(t) + \\ &\quad E^2(t-\tau) + E(t)E(t-\tau)e^{i\omega\tau} + E(t)E(t-\tau)e^{-i\omega\tau}] \\ &= E^4(t) + E^4(t-\tau) + 4E^2(t)E^2(t-\tau) + s(\tau) \end{aligned} \tag{2-17}$$

Where $s(\tau)$ is an item related to $\cos\omega\tau$ and $\cos 2\omega\tau$.

According to (2-17), it can be seen that *v(t)* is a function of *t*. However, the light beam has a frequency as high as GHz, by using a low speed photo-diode; we can obtain the integration output of (2-17). As $s(\tau)$ is an item contains $\cos\omega\tau$ and $\cos 2\omega\tau$, the integration of $s(\tau)$ becomes to 0. Hence,

$$\mathrm{v}(t) \propto < I^2(t) > + < I^2(t-\tau) > + 4 < I(t) >< I(t-\tau) > \tag{2-18}$$

Where, < > represents the temporal average.

The optical pulse correlation is defined as

$$G^{(2)}(\tau) \equiv \frac{< I(t)I(t-\tau) >}{< I^2(t) >} \tag{2-19}$$

Substitute (2-19) to (2-18) and normalize the output current of detector, we have

$$i_d(t) = 1 + 2G^{(2)}(\tau) \tag{2-20}$$

When there is no any delay between beam 1 and beam 2, that is τ=0, $G^{(2)}(\tau)$=1 [45,52]. If τ_0 <<τ<t+T (τ_0 is the pulse width of beam 1 and beam 2), $G^{(2)}(\tau)$=0. Therefore,

$$i_d(t)\begin{cases} 3 & \tau = 0 \\ 1 & \tau_0 << \tau < t + T \end{cases} \tag{2-21}$$

The relationship between the SHG signal and the time delay of beam1 and beam2 is shown in Fig.2.7. It can be seen that when beam2 locates at the left of beam1 with a large time delay, the SHG signal is too weak due to the correlation signal is 0. But there is still some output due to the existence of the fundamental wave. With beam 2 approaches to beam 1, the overlap part between two pulses is increased, which indicates that the correlation signal is increased. Therefore, the SHG signal is increased. When beam2 completely overlaps with beam1, a maximum of SHG signal is obtained, which is caused by the complete correlation of two pulses.

According to the above description, the optical pulse correlation can be monitored successfully by SHG. Hence according to the intensity correlation signal detected by SHG, the timing relationship between two optical pulses can be measured. Therefore, the environment changes around the monitoring fiber can be monitored successfully.

According to Fig.2.7, there is a corresponding relationship between the time drift and SH signal, from which the sensing is available. However, the sensitivity of this single channel correlation sensing system is not high enough. Moreover, a background exists. In order to obtain a linear sensing region with high sensitivity, a differential detection of two correlation signals in two channels is available by using a nonlinear crystal. The

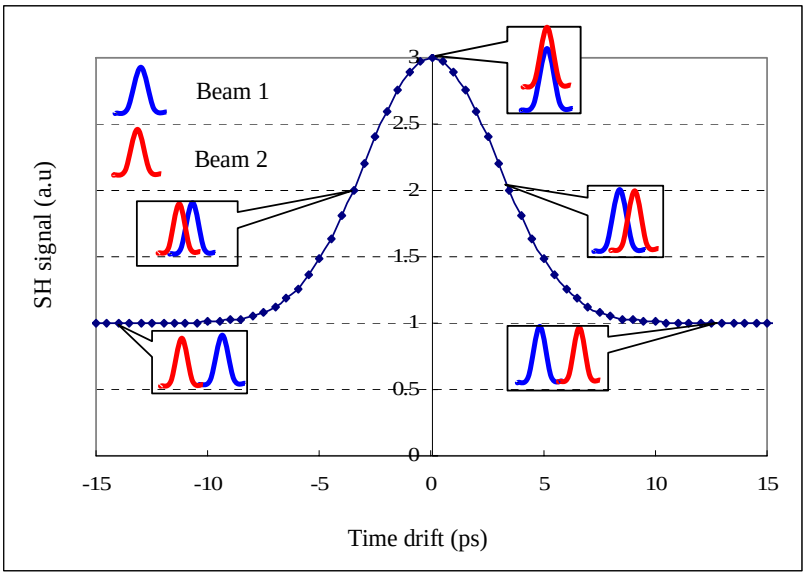

Fig.2.7 SH signal vs. time delay

nonlinearity of a crystal enables it to split one optical beam into two beams orthogonally polarizing with a time delay of T_0. Therefore, two correlation signals can be obtained as shown in Fig.2.8. It can be seen that the correlation signals periodically vary with time delay with a period of T, where T is determined by the repetition rate of the pulse train. In one period, there is a linear region between the peaks of OUT1 and OUT2, which is related to T_0. If the difference between two SH signals is taken, the sensitivity can be written as

$$S = \frac{\Delta V}{\Delta T} \qquad (2\text{-}22)$$

It can be seen that compared with the sensitivity of one channel sensing system, the sensitivity of this two channel sensing system is remarkably enhanced. At the same time, the background was completely eliminated by using the differential detection method.

The sensitivity is related to the pulse width of optical beams, the time delay bias T_0 determined by the length of nonlinear crystal, and ΔV, the difference between OUT1 and OUT2. For ultra-short pulses, the sensitivity of the optical pulse correlation sensing

system is possible to be several femoto-seconds in theory. According to Eq.(2-20), we can conclude that ΔV is a constant if the pulse width of two optical beams are fixed. Therefore, the sensitivity and the corresponding measurement range are determined by the time delay bias T_0. We can realize "zoom out" to satisfy a high resolution measurement with a small T_0 by shortening the crystal length, or "zoom in "to acquire a large range measurement with a large T_0 by using a long crystal.

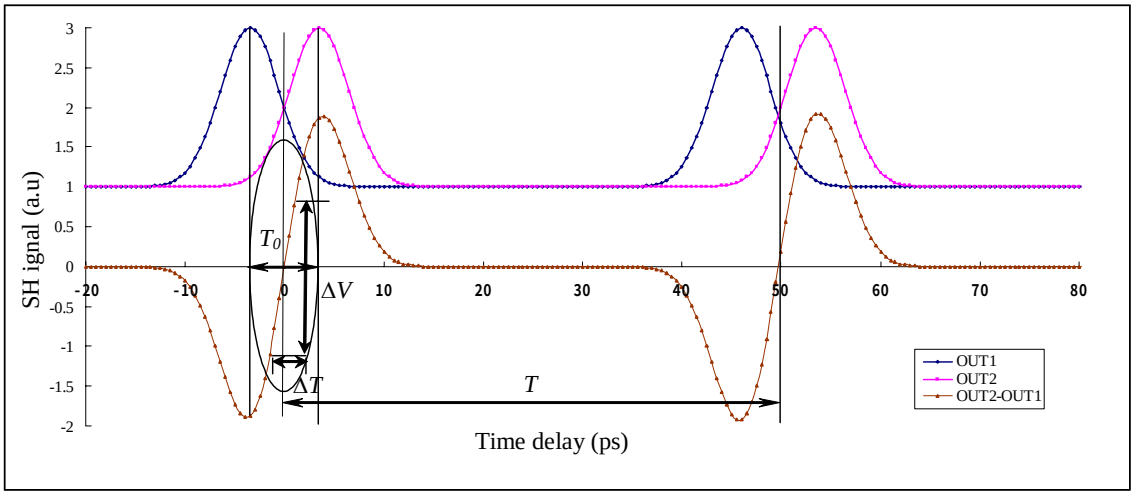

Fig.2.8 SH signal vs. time delay in two channels

2.5 Summary

The concept of an optical pulse correlation sensing was proposed. The available optical pulse correlation measurement methods were discussed and compared. Then the theoretical analysis of optical pulse correlation sensing based on SHG was carried out. The factors related to the sensitivity of the optical pulse correlation sensing system were discussed.

Chapter 3

Optical Pulse Correlation Sensing

3.1 Introduction

The high-sensitivity of the optical pulse correlation sensing system origins from the setting of a time delay bias through a birefringence crystal in the optical signal correlation unit. Just because of the time delay bias, the optical correlation signals in orthogonal directions are generated and measured. Therefore, the high-sensitivity can be obtained by using the difference of two correlation signals. In this chapter, the configuration and principle of the optical correlation sensor will be discussed. The feasibility of the sensor to high-sensitivity measurement will be investigated.

3.2 Configuration of optical pulse correlation sensing system

The configuration of the optical pulse sensing system is shown in Fig.3.1 [39, 53]. The sensing system is composed of three main units, light source unit, sensing unit and optical pulse correlation unit. The optical pulse correlation unit is the crucial part of the sensing system, in which the optical correlation pulse pairs are formed, the correlation signal is generated by using a SHG crystal and the detection is realized. In this section,

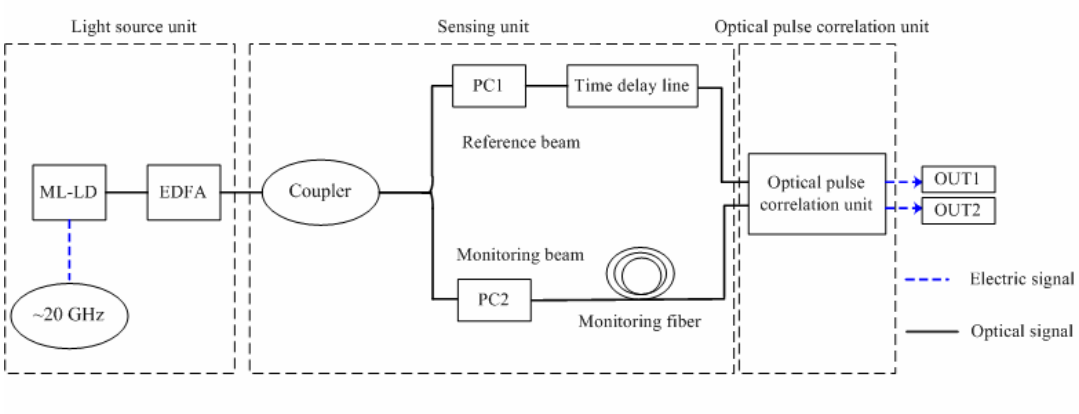

Fig.3. 1 Scheme of optical pulse correlation sensing system

PC1: Polarization controller 1; PC2: Polarization controller 2;

the related components of the correlation sensing system will be introduced to make sure the performance of the whole sensing system.

3.2.1 Light source unit

An active mode-locked laser diode (ML-LD) with electroabsorption (EA) modulation was used as the pulsed light source of the sensing system. The driving circuit diagram, I-P characteristic and stability of the ML-LD are shown in Fig.3.2 (a), (b) and (c). According to Fig.3.2 (b), it can be seen that after warming up several hours, a stable laser output can be obtained. Therefore, it is necessary to warm up the ML-LD for 4-5 hours before the experiment. ML-LD is modulated by a RF signal with a resonant frequency of 19.9 GHz. Therefore, a pulse train with about 50 ps repetition rate is obtained. Then the modulated signal is amplified by an Erbium-doped fiber amplifier (EDFA), the specifications of EDFA are shown in table 3.1.

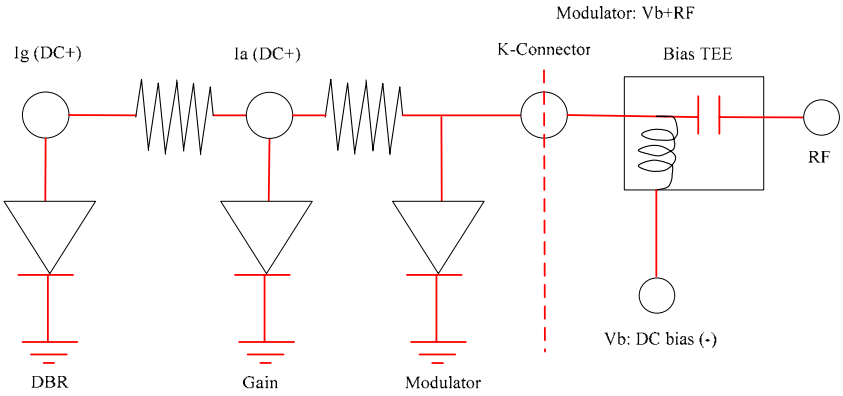

(a)

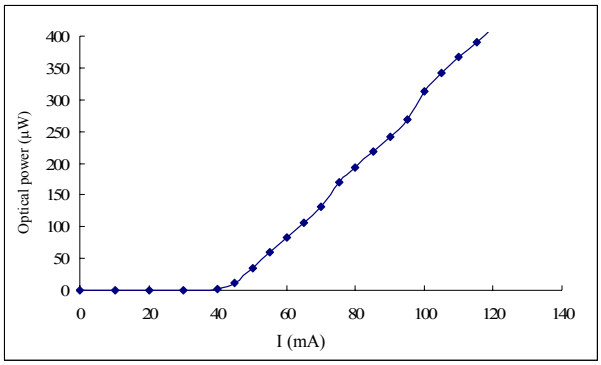

(b)

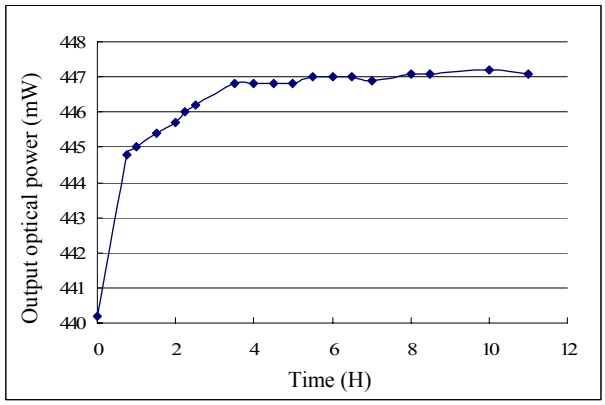

(c)

Fig.3.2 (a) Driving circuit diagram of ML-LD

(b) I-P characteristic of ML-LD

(c) Stability of ML-LD

Table 3.1 Specifications of ErFA1215

Signal wavelength	1530 - 1565 nm
Wavelength of pump laser	1480 nm
Maximum output power	> +15 dBm
Gain	30 dB
Noise figure	≤ 7.5 dB
Polarization dependence of output power	< 0.15 dB
Polarization extinction ratio	> 17 dB

3.2.2 Sensing unit

In the sensing unit, the light beam from ML-LD is split into a reference beam and monitoring beam by using a 3 dB optical coupler. On the reference beam a time delay line is used to initialize the sensing state, which will be discussed in later section. The polarization controllers before the time delay line and monitoring fiber to adjust the polarization state of the reference beam and monitoring beam. The loss characteristic of the time delay line is shown in Fig.3.3. According to the loss characteristic of the time delay line, it can be seen that the loss from 50 ps to 80 ps is a flat loss region. In order to avoid the correlation degradation caused by the signal loss, the flat loss region should be used.

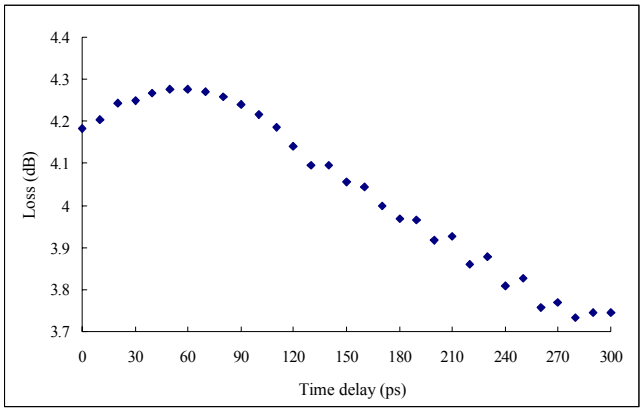

Fig.3.3 Loss characteristic of time delay line

3.2.3 Optical pulse correlation unit

The optical pulse correlation measurement idea was realized by an optical pulse correlation unit, which concludes two sub-units, optical pulse correlation pairs generation unit and optical pulse correlation detection unit as shown in Fig.3.4. The optical pulse correlation pairs generation unit is composed of a birefringent crystal, a half mirror and a polarization beam splitter (PBS). When the reference beam passes through the birefringence crystal, it is split into two beams, Refα and Refβ, which polarize in orthogonal polarization planes *p* and *s*. At the same time, a time interval about 7 ps is produced between Refα and Refβ. This 7 ps time interval is defined as the time delay bias, which is an important fact to determine the sensitivity and dynamic range of the sensing system. Therefore, the time delay bias can be designed according to the requirement of the practical application. The novelty of the optical pulse correlation sensing system lies in the setting of the time delay bias, which makes it possible to realize the optical pulse correlation measurement in two channels and the differential detection is available. By using a polarization controller, the polarization state of the monitoring beam can be adjusted to 45°. Then equal components Sig ξ and Sigζ will be obtained in polarization plane *p* and *s*, respectively. At the half mirror, Refα and Refβ will be combined with Sig ξ and Sigζ in plane *p* and *s*, respectively and form to two optical pulse pairs. After that, the polarization beam splitter will divide the two optical pulse pairs into Ch1 and Ch2. The orthogonal optical pulse pairs generation is realized in a compact component with a size of 5.5 cm×3.0 cm×0.8 cm. The top view of the optical pulse correlation unit and the SHG correlation detection & O/E unit are shown in Fig.3.4 (b).

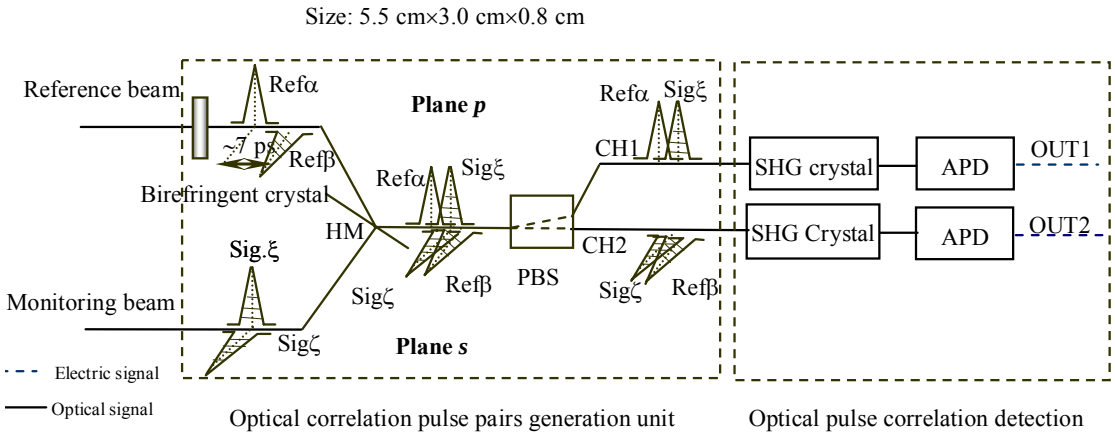

(a)

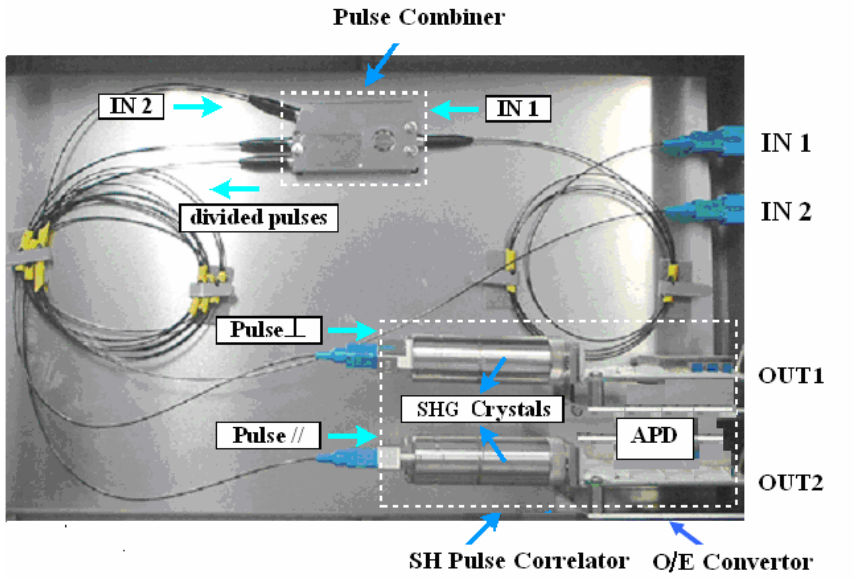

(b)

Fig. 3.4 (a) Diagram of optical pulse correlation unit

HM: Half Mirror; PBS: Polarization beam splitter

(b)Top view of optical pulse correlation unit and SHG correlation detection & O/E unit

The function of optical pulse correlation detection unit composed by SHG & avalanche photon diode (APD) is to generate the correlation signal and convert it to electric output. A KTP crystal is used to generate second harmonic wave. As the signal from SHG

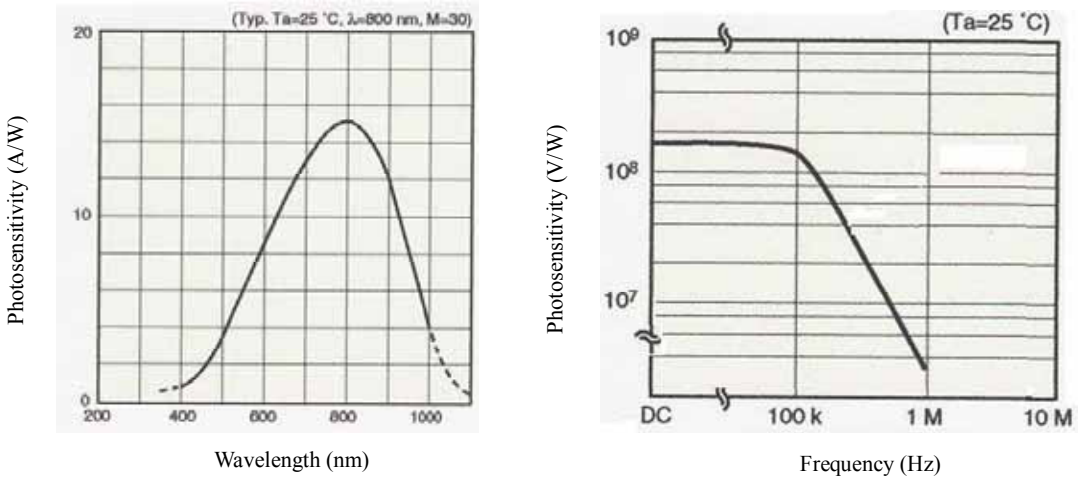

(a) Spectrum response (b) Frequency response

Fig.3.5 Spectrum response and frequency response of APD

Table 3.2 Specifications of APD

		Min.	Typ.	Max	Unit
Cutoff frequency (-3dB)	High	80	100	-	MHz
	Low	-	DC	-	
NEP (800 nm)		-	0.02	0.04	$Pw/Hz^{1/2}$@10MHz
Return resistance		-	10	-	KΩ
Photosensitivity (Including M=30)		-1.4	-1.5	-1.6	10^8 V/W
Maximum incident power		0.05	0.06	-	μW
Minimum detectable power		-	0.0005	0.01	nW

crystal is too weak, an APD with high photo-electronic sensitivity is used to detect the second harmonic signal. The specifications of APD are shown in Fig.3.5 and table 3.2. The relationship between the input power and APD output voltage of SH signal is shown in Fig.3.6.

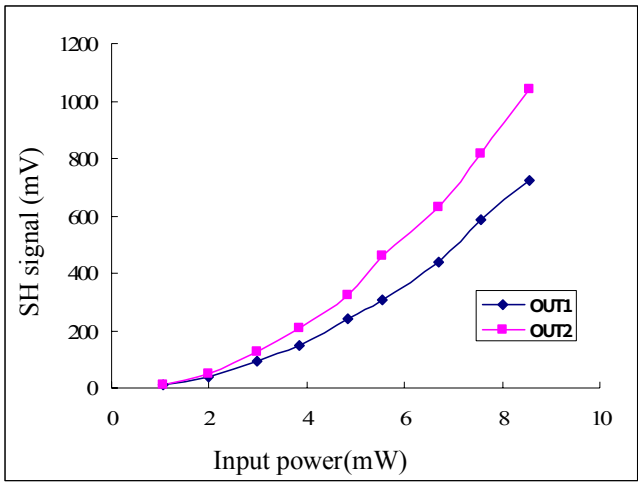

Fig.3.6 Fundamental power vs. SH signal

3.3 Mechanism of optical pulse correlation sensor

A short optical pulse train less than 9 ps from a ML-LD modulated by a RF signal with a frequency of approximately 20 GHz was amplified to 16.5 mw and divided into a reference pulse train and a monitoring pulse train by a 3 dB optical coupler as shown in Fig.3.1. By tuning an optical time delay line, the correlation state of the reference pulse train and the monitoring pulse train was initialized. The pulse splitter in the optical pulse correlation unit separates the reference pulse train into two pulse trains Refα and Refβ, which polarize in orthogonal polarization planes *p* and *s*. At the same time, a stable time delay bias about 7 ps is generated between Refα and Refβ. By tuning the polarization controller before the monitoring fiber, the polarization angle of the monitoring pulse can be adjusted to 45°, and then two equal components Sig ξ and Sigζ will be obtained in polarization plane *p* and *s*, respectively. After passing through the half mirror, the monitoring pulse components will be combined with reference pulse components in orthogonal polarization planes and two optical pulse pairs will be obtained. One is composed of Refα and Sig ξ, the other is composed of Refβ and Sigζ.

PBS will separate these two optical pulse pairs into ch1 and ch2. Then two optical pulse correlation signals will be obtained by using SHG crystal. After the O/E converter, two electric output signals will be obtained.

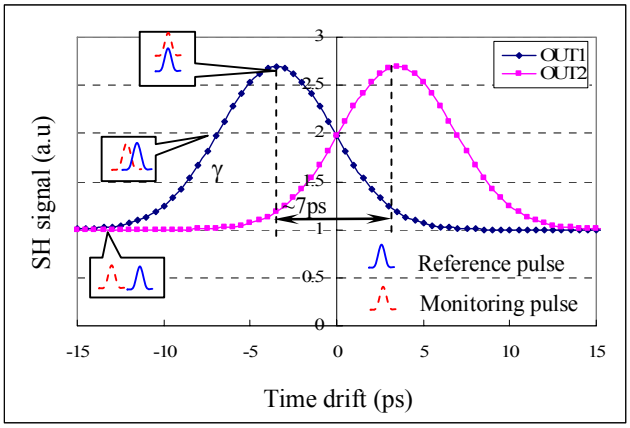

Fig.3.7 SH average versus pulses position in each channel

The relationship between the SH signal, the optical pulse correlation state and time delay between two optical pulses are illustrated in Fig.3.7. It can bee seen that two correlation signals OUT1 and OUT2 have the similar variations with the timing drift. At the beginning, the monitoring pulse locates in the front of the reference pulse component Refα with a large time delay. For the two optical pulse pairs, The output intensity of OUT1 and OUT2 are near to 1, which are correspond to the theoretical value indicated in Eq. (2-20). If the monitoring pulse drifts further, the correlation between Refα and Sig ξ increases gradually. However, there is no obvious change in the correlation signal between Refβ and Sigζ. When the monitoring pulse drifts further, the overlap between Refβ and Sigζ will increased with a speed lower than the correlation between Refα and Sig ξ. When Refα is behind Sig ξ with 3.5 ps, the overlap between Refα and Sig ξ equals to the overlap between Refβ and Sigζ. Thus OUT1 equals OUT2. With the monitoring pulse drift forwardly further, Refα will completely overlap with

Sig ξ, so OUT1 arrives at the peak. In theory, the value of the peak equals to 3, while the peak value in Fig.3.7 is a little less than 3. This is because the conversion efficiency of SHG in practice is less than that in theory. After OUT1 arrives at the peak value, Refα will deviate from Sig ξ and the overlap between Refβ and Sigζ becomes larger and larger. Then OUT1 will decrease gradually, while OUT2 will increase and a peak value can be obtained in OUT2. According to Fig.3.7, it is indicated that the time interval between peaks of OUT1 and OUT2 is about 7ps, which is determined by the time delay bias in the optical pulse correlation unit. For one channel output, a time resolution around 0.1 ps was obtained. In order to improve the resolution of the system; we introduced a differential detection technique. The differential signal between OUT1 and OUT2 was monitored. The resolution of the sensing system with differential detection depended on the balance of OUT1 peak and OUT2 peak, which was determined by the offset polarization angle of monitoring pulse and detector sensitivity. Therefore, an offset polarization angle of the monitoring signal is controlled as 45° to obtain equal components in orthogonal polarization directions. On the other hand, if there is a little difference between sensitivities of two detectors, the offset polarization angle used to eliminate the asymmetry is monitored by the outputs voltages of OUT1 and OUT2 with only the monitoring pulse input. By taking the difference between OUT1 and OUT2, a linear region around 7 ps is obtained as shown in Fig.3.8.

According to Fig.3.8, it can be seen that the time drift direction of the monitoring pulse can be judged through the sign of the difference signal between OUT1 and OUT2. If the monitoring pulse drifts forward, the intensity of OUT1 increases; while that of OUT2 decreases. Then the sign of the differential signal between OUT1 and OUT2 becomes positive. If the monitoring pulse drifts backward, the intensity of OUT1 reduces, while

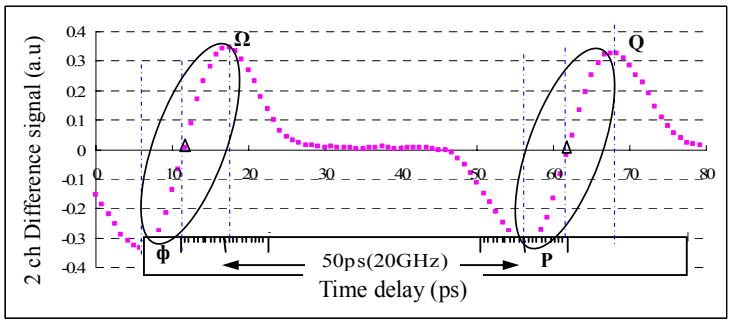

Fig.3.8. Differential signal versus pulse time position (Part II in figure 1)

Φ: Peak of OUT1 Ω: Peak of OUT2 Δ: Decision point

that of OUT2 rises. And the sign of the differential signal becomes negative. The change of the differential signal with pulse time delay is illustrated in Fig.3.8. It indicates that the differential signal varies periodically with pulse time delay. The period is approximately 50 ps due to the repetition rate of optical pulse train from the ML-LD. i.e. when the monitoring pulse N has a small time drift; it overlaps with pulse M in reference pulse train (pulse (N+1) in monitoring pulse train overlaps with pulse (M+1) in reference pulse train). The sensing region is between point ϕ and Ω in Fig.3.8 corresponding to peaks of OUT1 and OUT2, respectively. When time drift of the monitoring pulse is beyond this region, monitor pulse N will overlaps with reference pulse (M+1). Then the region PQ is available. The time resolution of the differential detection system is less than 0.04 ps, which is twice of that of single channel measurement. Therefore, the measure range of the system can be “zoomed in” with rough resolution and “zoomed out” with high resolution. Compared with single channel measurement, the differential signal detection has its unique advantages:

1. It indicates not only the time drift value, but also the drift direction;
2. Its resolution is nearly double that of single channel detection.

3. Background noise was completely eliminated by using the difference of two correlation signals.

In the sensing system, the overlap state of pluses is indicated by the SH signal detected by APD module instead of pulse scanning. SHG signal nearly has no response limit in time. Hence the response time of the sensing system is determined by that of detector module. The response time of the detector module to a stepped pulse is several micro-seconds, which allows the measurement to be immune to fluctuations resulting from external perturbations. Therefore the real-time sensing can be realized with this sensing system. The related performance of the sensor is shown in table 3.3.

Table 3.3 Performance of optical pulse correlation sensor

Specification	Data
Resolution (ps)	0.04
Dynamic range (ps)	7 ps
Nonlinearity	<1%

3.4 Temperature and strain characteristics

3.4.1 Temperature characteristics

According to the relationship between the differential correlation signal and the pulse time position in Fig.3.8, any physical quantity caused to the pulse time drift of the optical signal transmitting in the optical fiber can be monitored. Therefore we can use the system to measure physical quantities such as temperature, strain and pressure around a fiber optic. A typical temperature measurement setup is shown in Fig.3.9.

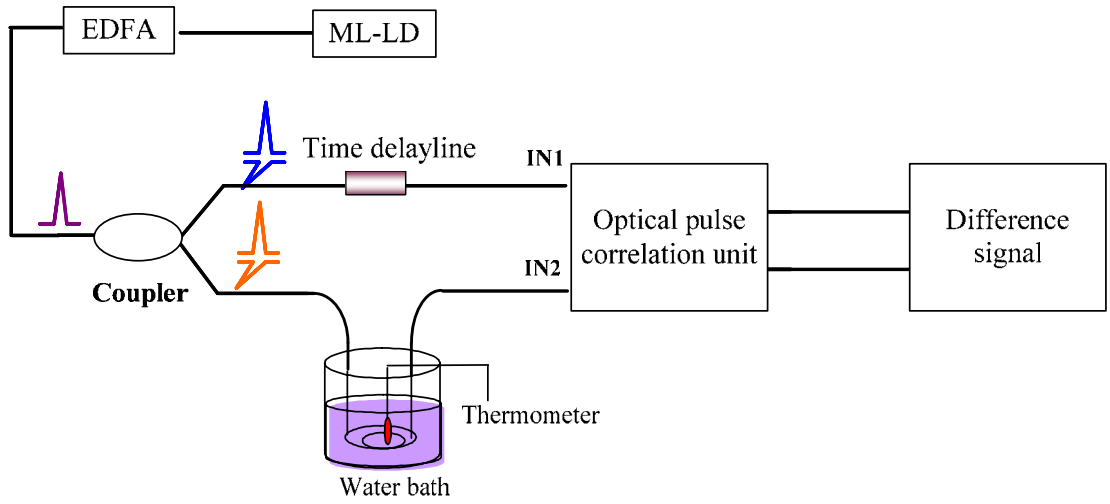

Fig.3.9 Setup of temperature experiment

Before heating the water bath, we located the pulses position around the decision point by tuning the optical time delay line. When the temperature of water was increased, a timing delay was generated in the monitoring pulse train, which caused a change in the differential signal. A single mode fiber of length 1m with Polyamide sleeve was employed. By controlling the temperature of the water bath, the differential pulse correlation signal was monitored by a digital multimeter.

The variation of differential signal with the temperature of water bath was shown in Fig.3.10. A good linearity was observed, when the water bath temperature was increased from 19 °C to 50 °C within several hours. By fitting the experimental data with least square method, a curve correlation coefficient of 99.24% was obtained. A resolution about 0.04 m·°C was obtained, which showed different temperature resolution could be realized with different fiber length to satisfy the corresponding requirements in applications. The temperature sensitivity is in the same order with the high-sensitivity interferometer temperature sensor demonstrated in [54, 55]. As a single-mode fiber with sleeve was used as the monitoring fiber, the sensitivity is related to the sleeve material. Therefore, we can obtain much higher sensitivity by selecting fiber with high thermal

coefficient sleeve.

It should be noted that the correlation signal is not only sensitive to the time delay in the monitoring signal but also sensitive to the polarization change in the monitoring fiber. The polarization state is propone to be affected by the birefringence fluctuation resulted from the uneven thermal effect in the single mode fiber. Therefore, some fluctuations appeared in the correlation signals, when the temperature was enhanced, which is adverse to the application. Thus the birefringence effect should be compensated, which will be introduced in later chapter.

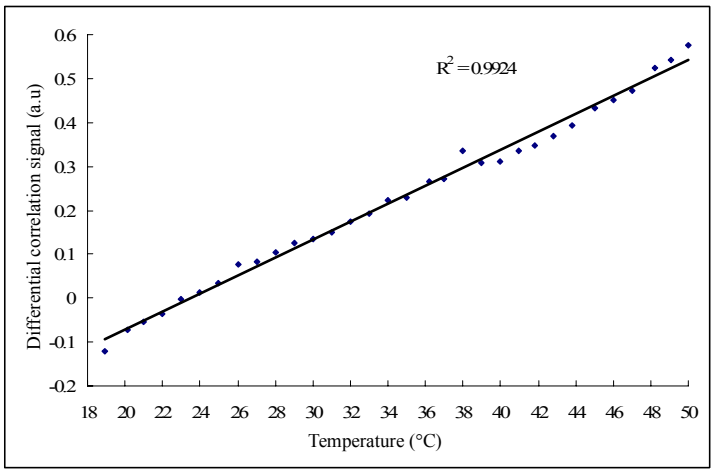

Fig.3.10 Temperature vs. difference of two correlation signals

3.4.2 Strain characteristic

An experiment for strain measurement with a single mode fiber of length 56 cm was carried out by the similar approach as shown in Fig.3.11. Due to the strain, the fiber optic was extended, which yielded a timing delay for the optical pulse through it. The relationship between the differential signal and the manipulator position was shown to be extremely linear with a correlation coefficient rate of 99.78% as indicated in Fig.3.12. According to further experimental study, a resolution of 0.2 με was obtained, which is

comparable with the FBG sensor demonstrated in reference [56, 57].

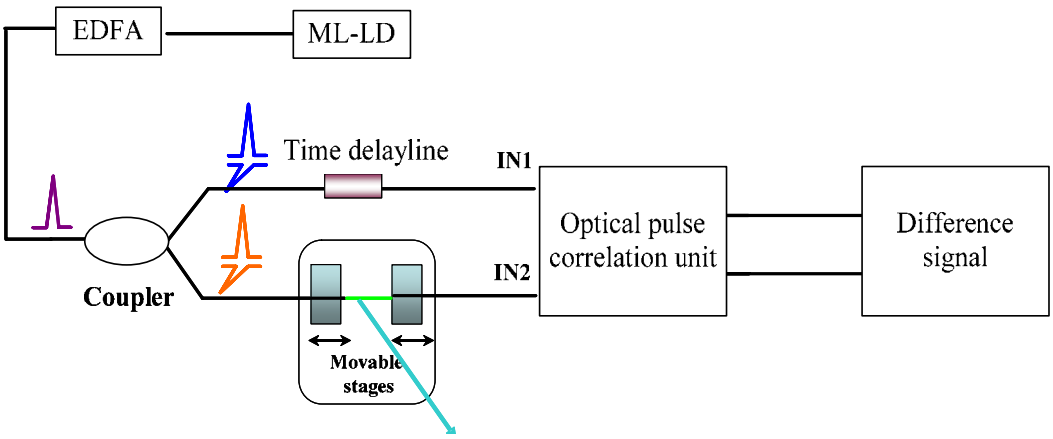

Fig.3.11 Setup of strain experiment

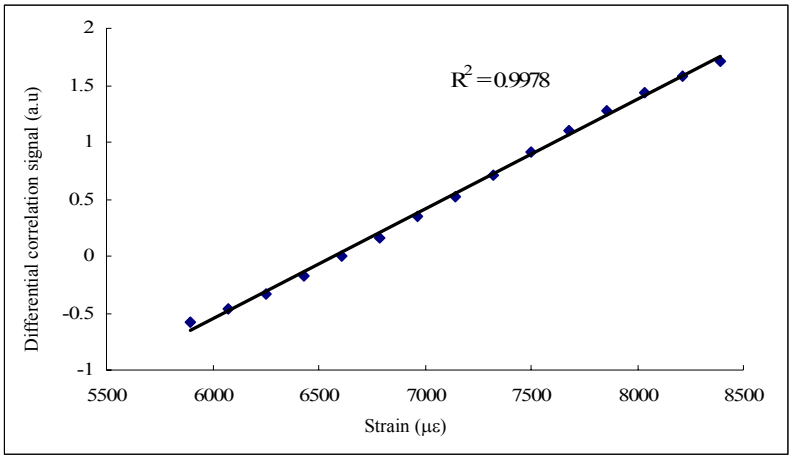

Fig.3.12 Differential signal correlation pulse vs. tensile strain position

According to the temperature and strain experiment, the optical pulse correlation system is feasible to high sensitivity measurement. As the correlation signal is both sensitive to strain and temperature around the monitoring fiber, a discrimination measurement will be discussed in the following section.

3.5 Discussion on discrimination of temperature and strain measurement

The sensing theory of white light optical fiber sensor was discussed in Ref 58. Compared with white light optical fiber interferometer, the sensing parameter of the optical pulse correlation is the time delay instead of the phase in the sensing part, which can be written as

$$t = \frac{n_0 \cdot L}{c} \tag{3-1}$$

Where n_0 is the refractive index of the optical fiber core and L is the length of sensing part in monitoring fiber.

As the optical path S is the function of strain (σ) and temperature (T) exerted on the sensing fiber, therefore the time delay induced in the monitoring signal under he exertion of strain and temperature is

$$t = \frac{S(\sigma,T)}{c} = t(\sigma,T) \tag{3-2}$$

The increment can be expressed as

$$dt = \frac{1}{c}([\frac{\partial t}{\partial \sigma}]_T d\sigma + [\frac{\partial t}{\partial T}]_\sigma)dT \tag{3-3}$$

Where $d\sigma$ and dT are the local change of strain and temperature, respectively. $\partial t/\partial \sigma$ and $\partial t/\partial T$ are the differential of t with respect to σ and T.

Substituting (3-1) to (3-3), we have

$$dt = \frac{1}{c}\{n_0[\frac{\partial L}{\partial \sigma}]_T + L[\frac{\partial n_0}{\partial \sigma}]\}d\sigma + \{n_0[\frac{\partial L}{\partial T}]_\sigma + L[\frac{\partial n_0}{\partial T}]_\sigma\}dT \tag{3-4}$$

The strain ε is defined as

$$\varepsilon = \frac{\Delta L}{L} \tag{3-5}$$

Therefore formula (3-4) can be changed as

$$dt = \frac{1}{c}\{n_0 L[\frac{1}{L}\frac{\partial L}{\partial \sigma}]_T + n_0 L[\frac{1}{n_0}\frac{\partial n_0}{\partial \sigma}]\}d\sigma + \frac{1}{c}\{n_0 L[\frac{1}{L}\frac{\partial L}{\partial T}]_\sigma + n_0 L[\frac{1}{n_0}\frac{\partial n_0}{\partial T}]_\sigma\}dT$$

$$= \frac{n_0 L}{c}\{[\frac{\partial \varepsilon}{\partial \sigma}]_T + \frac{1}{n_0}[\frac{\partial n_0}{\partial \varepsilon}]_T[\frac{\partial \varepsilon}{\partial \sigma}]_T\}d\sigma + \frac{n_0 L}{c}\{[\frac{\partial \varepsilon}{\partial T}]_\sigma + \frac{1}{n_0}[\frac{\partial n_0}{\partial \varepsilon}]_\sigma[\frac{\partial \varepsilon}{\partial \sigma}]_\sigma\}dT\} \quad (3\text{-}6)$$

If the Young's modulus E_f and expansion coefficient α_f are introduced, we can write formula (3-6) as

$$dt = \frac{n_0 L}{c}\{(1 + \frac{1}{n_0}[\frac{\partial n_0}{\partial \varepsilon}]_T)\frac{d\sigma}{E_f} + (\alpha_f + \frac{1}{n_0}[\frac{\partial n_0}{\partial T}]_\sigma)dT\} \quad (3\text{-}7)$$

If $t = \frac{n_0 L}{c}$ and Hawk law $d\varepsilon = d\sigma/E_f$ are considered, formula (3-7) can be simplified as

$$\frac{dt}{t} = (1 + \frac{1}{n_0}[\frac{\partial n_0}{\partial \varepsilon}]_T)\frac{d\sigma}{E_f} + (\alpha_f + \frac{1}{n_0}[\frac{\partial n_0}{\partial T}]_\sigma)dT\} \quad (3\text{-}8)$$

Where C_ε and C_T are defined as

$$C_\varepsilon = \frac{1}{n_0}[\frac{\partial n_0}{\partial \varepsilon}]_T \quad (3\text{-}9)$$

$$C_T = \frac{1}{n_0}[\frac{\partial n_0}{\partial T}]_\sigma \quad (3\text{-}10)$$

3.5.1 Temperature measurement

The time delay caused by the temperature change in the monitoring beam is written as

$$\frac{dt}{dT} = \frac{1}{c}\cdot\frac{\partial}{\partial T}(n_0 \cdot L_0)$$

$$= \frac{1}{c}(\frac{\partial n}{\partial T}\cdot L_0 + n_0 \cdot \frac{\partial L}{\partial T}) \quad (3\text{-}11)$$

Hence $$\Delta t = \frac{1}{c}\cdot(\Delta n_0 \cdot L_0 + n_0 \cdot \Delta L) \quad (3\text{-}12)$$

When the temperature around the optical fiber sensor is changed from T_0 to T, the length change ΔL and refractive index change Δn can be expressed as

$$\Delta L_0 = L_0(T_0)(T - T_0)\alpha \quad (3\text{-}13)$$

$$\Delta n = n_0(\lambda, T_0)(T - T_0)C_T \quad (3\text{-}14)$$

Substitue (3-7) and (3-8) into (3-6), we can obtain

$$\Delta t = \frac{1}{c} \cdot [n_0(\lambda, T_0)(T - T_0)C_T \cdot L_0 + n_0 \cdot L_0(T_0)(T - T_9)\alpha] \tag{3-15}$$

Therefore

$$\Delta T = (T - T_0) = \frac{\Delta t}{\frac{1}{c} \cdot [n_0 C_T \cdot L_0 + n_0 \cdot L_0 \alpha]} \tag{3-16}$$

Formula (3-10) can be expressed as

$$\Delta t = \Delta T \cdot t_T \tag{3-17}$$

Where $t_T = S_T \cdot L_0(T_0)$ is the sensitivity of the optical pulse correlation sensor with a monitoring fiber length of L_0. S_T is the sensitivity coefficient.

3.5.2 Strain measurement

When a strain ε_z is imposed on an optical fiber along the axial direction, the time delay Δt can be expressed as

$$\begin{aligned} \Delta t &= \frac{\Delta n_0 \cdot L_0 + n_0 \cdot \Delta L_0}{c} \\ &= \frac{\Delta n_0 \cdot L_0 + n_0 L_0 \varepsilon_z}{c} \end{aligned} \tag{3-18}$$

The change of the refractive index can be written as [7, 8]

$$\Delta n_0 = -\frac{1}{2} n_0^3 [(1 - v) p_{12} - v p_{11}] \varepsilon_z \tag{3-19}$$

Hence we have

$$\begin{aligned} \Delta t &= \frac{\{n_0 L_0 \varepsilon_z - \frac{1}{2} n_0^3 [(1 - v) p_{12} - v p_{11}] L_0 \varepsilon_z\}}{c} \\ &= \frac{\{n_0 - \frac{1}{2} n_0^3 [(1 - v) p_{12} - v p_{11}]\} L_0 \varepsilon_z}{c} \\ &= \frac{n_{equivalent} L_0 \varepsilon_z}{c} \end{aligned} \tag{3-20}$$

Where, $n_{equivalent} = n_0 - \frac{1}{2} n_0^3 [(1 - v) p_{12} - v p_{11}]$ is the effective refractive index of the

optical fiber.

Therefore the strain of the optical fiber can be obtained as

$$\varepsilon_z = \frac{\Delta t}{n_{equivalent} L_0} \tag{3-21}$$

In the optical pulse correlation sensing system, by using the optical pulse correlation unit with a time delay bias of 7 ps, temperature and strain resolutions around 0.04 m·°C and 0.2 με was obtained within 19°C -50°C and 5800 με -8500 με for single-mode were obtained when the pulse width of the light source less than 9 ps. As the resolution and dynamic range are related to the time delay bias and the fiber length, much more higher resolution or large dynamic range can be obtained by optimizing the time delay bias and fiber length.

3.5.3 Discrimination of temperature and strain measurement

According to the above description, optical fiber is both sensitive to the temperature and strain. Therefore, it is necessary to compensate the cross effect, especially in the strain experiment.

For the temperature change around the optical fiber, due to difference expansion coefficient between the fiber core and the fiber coating, an additional strain will be produced. The strain caused by the thermal effect can be expressed as

$$\Delta\sigma = E_f(\alpha_m - \alpha_f)\Delta T \tag{3-22}$$

Where E_f is Young's module, α_m and α_f are expansion coefficients of fiber core and fiber coating, respectively.

Substitute (3-20) into (3-8), we have the total increment of time delay caused by thermal effect

$$\frac{\Delta t}{t} = (1 + C_\varepsilon)(\alpha_m - \alpha_f)\Delta T + (\alpha_f + C_T)\Delta T$$

$$= (1 + C_\varepsilon)(\alpha_m - \alpha_f)\Delta T + (\alpha_f + C_T)\Delta T$$

$$= [\alpha_m + C_T + (\alpha_m - \alpha_f)C_\varepsilon]\Delta T \qquad (3\text{-}23)$$

Formula (3-21) indicated that the strain caused by the thermal effect can not be neglected in the strain measurement. The temperature effect in the strain measurement is required to be compensated. Therefore, for most strain measurement, the measured strain will be modified by the independent temperature measurement.

Now let us consider the situation in which the optical fiber is simultaneously affected by the temperature and strain, the time delay induce in the monitoring beam can be expressed as

$$\frac{\Delta t}{t} = (1 + C_\varepsilon)\Delta\varepsilon + [\alpha_m + C_T + (\alpha_m - \alpha_f)C_\varepsilon]\Delta T \qquad (3\text{-}24)$$

We can rewrite formula (3-22) as

$$\frac{\Delta t}{t} = A\Delta\varepsilon + B\Delta T \qquad (3\text{-}25)$$

Where

$$\begin{cases} A = (1 + C_\varepsilon) \\ B = [\alpha_m + C_T + (\alpha_m - \alpha_F)C\varepsilon] \end{cases} \qquad (3\text{-}26)$$

If the temperature is measured by a sensor just sensitive to the temperature, the change in (3-24) related to temperature will be known and the strain can be obtained. As far as formula (3-8) is concerned, only the linear item was considered. If Δε and ΔT are too larger, it is necessary to consider the high order item, which is the cross-sensitive item of the temperature and strain. If Cε,T is defined as the cross coefficient of the temperature and strain, we have

$$\frac{\Delta t}{t} = (1 + C_{\varepsilon})\Delta\varepsilon + [\alpha_m + C_T + (\alpha_m - \alpha_f)C_{\varepsilon}]\Delta T + C_{\varepsilon,T}\Delta\varepsilon\Delta T \qquad (3\text{-}27)$$

The cross coefficient is around $C_{\varepsilon,T}$~10^{-8} rad(°C)$^{-1}$(με)$^{-1}$m^{-1} [59]. The above results indicated that, if the strain or temperature is not too large, for the free optical fiber, the cross coefficient can be neglected. However, if the length of the monitoring fiber is too large, the cross coefficient is needed to be considered as the item is proportional to the length of the fiber.

As far as the optical pulse correlation sensor is concerned, in the strain measurement, the strain caused by the thermal effect should be modified.

3.6 Summary

The configuration of the optical pulse correlation sensing system is illustrated. Then fundamental sensing principle and characteristic are explained. According to the relationship between the second harmonic signal intensity and the time delay, a good linearity was obtained. The time resolution was estimated as around 0.04 ps. The temperature and strain characteristic of the optical pulse correlation sensor was investigated. The results indicated that it is feasible to use the optical correlation sensor to measure the temperature and strain around the optical fiber transmission liens with high sensitivity. As the sensor is sensitive to temperature and strain simultaneously, the discrimination measurement of temperature and strain is discussed in theory. During the temperature experiments, the fluctuation caused by the birefringence in the single-mode fiber was observed due to the sensitivity of the correlation signal to the polarization state change of the monitoring signal. Therefore, it is necessary to compensate the birefringence effect.

Chapter 4

Birefringence Fluctuations Compensation in Optical Pulse Correlation Sensing System

4.1 Introduction

As a birefringent medium, a single-mode fiber has the residual birefringence fluctuation, which causes to the polarization state fluctuation of the monitoring signal in the optical pulse correlation sensing system described in chapter 3. Consequently, the components of monitoring signal in orthogonal polarization planes will be changed, which results in the fluctuation of the correlation signal. In order to obtain a reliable optical correlation sensor, the birefringence fluctuation should be compensated. Since the birefringence fluctuations in a single-mode fiber originate from the time dependant difference variation between two orthogonal components of an optical beam, if the orthogonal components experience the same variations at any time along the single-mode fiber, it is available to neutralize the birefringence fluctuations. A FRM enables the polarization state of any optical beam to rotate 90° before being retraced the single-mode fiber, then two orthogonal components will reciprocally change their tracing paths at any point along the fiber. Consequently, the birefringence fluctuations in the single-mode fiber caused by the external perturbations in the forward direction will be completely compensated by the returned beam. This birefringence compensation approach by using

a retracing beam will be introduced into the optical pulse correlation sensor in this chapter. The polarization sensitivity will be investigated and compared with that in the previous sensing system illustrated in chapter 3. After that, an temperature measurement outside of the lab will be carried out.

4.2 Birefringence effect in optical fiber

Birefringence is termed as a phenomenon in which a ray of light is decomposed into two rays, an ordinary ray and an extraordinary ray, when it passed through certain types of materials. This effect will occur if the structure of the material is anisotropic (directionally dependent). The birefringence magnitude is defined as

$$\Delta n = n_o - n_e \tag{4.1}$$

Where n_o and n_e are the refractive indices for polarizations perpendicular (ordinary) and parallel (extraordinary) to the axis of anisotropy, respectively. As the phase of optical signal propagating in a birefringence material is related to the birefringence magnitude and the thickness of the crystal, it is useful for the devise of optical devices such as wave plate, color filter and polarization beam splitter, which are related to the polarization state controlling of optical signals. However, for the optical signal propagating in an optical fiber, birefringence effect is not desirable in some communication and sensing systems.

As far as a single-mode optical fiber is concerned, birefringence effect exits due to the imperfect circular dielectric symmetry of the fiber resulted from the manufacturing process. Although reasonable polarization stability can be obtained for hours in short fiber within the acceptable circular dielectric symmetry [60-62], if some disturbances are exerted by mechanical stress or temperature change, the birefringence will fluctuate randomly in an unpredictable way [63, 64]. The birefringence fluctuation will

change the phase difference between two orthogonal beams, which leads to the random change of state of polarization (SOP) over time. The change of SOP is adverse in the optical fiber interferometers, which is demonstrated by the degradation of the visibility of the coherent fringe [65, 66]. As the correlation signals of the optical pulse correlation sensor are generated in two channels, which have the orthogonal polarization planes, they are not only sensitive to the time drift in the monitoring pulse but also to the change of polarization state of the optical signal. The random fluctuation of the residual birefringence resulted from the uneven thermal effect of optical fiber was observed in the temperature experiment as a form of fluctuations in the correlation signals [53].

4.3 Birefringence fluctuation in optical pulse correlation sensing system

As is shown in Fig.3.1, two optical pulse correlation signals are generated in the orthogonal polarization planes. Therefore, the optical correlation signal is not only sensitive to the time delay between reference pulse and monitoring pulse, but also sensitive to the polarization fluctuation of optical signals. In the optical pulse correlation sensing system, both the reference beam and monitoring beam are required to be stable linear polarization. For the reference beam, the polarization maintaining fiber was used. Therefore it is possible to satisfy the requirement of linear polarization state. But for the monitoring beam, it is impossible to use a high-birefringence fiber especially in the case of long transmission lines. Since the birefringence in a single-mode fiber will fluctuate randomly when some perturbations caused by the uneven thermal effect or external mechanical strain were exerted in the single-mode fiber, the linear polarization state of the monitoring signal is too difficult to maintain. As a result, the fluctuations in the

correlation signal were observed, especially in temperature experiment, which is undesirable for the measurement [65]. Therefore, it is necessary to compensate such birefringence effect in the single-mode fiber.

4.3.1 Birefringence fluctuations compensation approach

As the SOP is an important parameter of an optical signal, birefringence compensation remains one of the open issues to stabilize the SOP in various optical devices. The compensation of stress-induced birefringence is achieved in Nd:YAG laser through two laser rods in tandem and an optical rotator located between the rods that rotates the direction of polarization by ±90° [67]. R.Ulrich realized the stabilization of the SOP at the output end of a long nominally circular single-mode fiber by an active control system, which contains a polarimeter and two electromagnetic fiber squeezers [68]. Using a dual-exposure technique, the birefringence caused by the geometric asymmetry was reduced in side-written photo-induced fiber devices [69]. The birefringence elimination in silica-on-insulate ridge waveguide by using the cladding stress-induced photo elastic effect was proposed [70].

As far as the birefringence compensation to stabilize the SOP in the sensing systems is concerned, a simple and efficient approach is to use a high-birefringence fiber. However, the high cost limits its applications, especially in the case of a long fiber line. Thus, a conventional fiber with some polarization state control technique should be a solution. M. Martinelli developed a universal compensator for polarization changes through a retracing beam [71]. This technique has been widely used to the optical fiber interferometers [72-74]. The application of the birefringence compensation by using the retracing beam to a time delay line was also demonstrated [75].

The birefringence compensation through a retracing beam is realized by a Faraday

rotator mirror (FRM) as shown in Fig.4.1, which consists of a lens, a Faraday rotator and a mirror. When a beam passes through the single-mode fiber in the forward direction, the polarization state will be changed due to the birefringence fluctuation, but when it is returned under the reflection of the mirror and passes through the single-mode fiber again, the birefringent effect in the forward direction will be compensated by the returned one. This process can be clearly described by using a Jones matrix [71, 73].

The net birefringent effect of the single-mode fiber in the forward direction can be denoted in a Jones matrix formalism described by a unitary matrix

$$\vec{R} = \frac{\alpha}{d}\begin{bmatrix} a & -b^* \\ b & a^* \end{bmatrix} \tag{4.2}$$

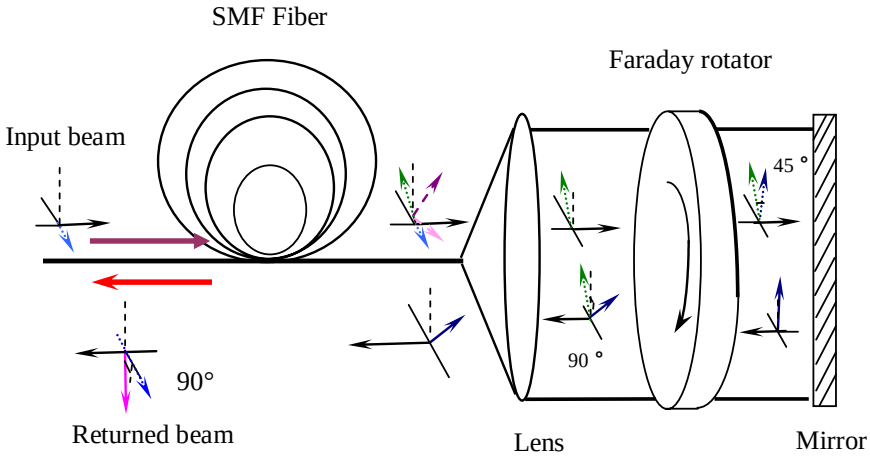

Fig. 4.1. Diagram of FRM

Where $*$ ---the conjugate

α ---the fiber loss

$$d = (a \cdot a^* + b \cdot b^*)$$

a and b depend on the birefringence properties of the fiber

The net effect of the mirror and double pass through the Faraday rotator is described by

$$T = t\begin{bmatrix} 0 & -1 \\ -1 & 0 \end{bmatrix} \tag{4.3}$$

Where t is a coefficient related to the loss and the reflection coefficient of the mirror.

According to formula (4.3), it can be seen that when the beam passes through the Faraday rotator in the forward direction, the polarization state is rotated 45°. With the reflection of the mirror, when the returned beam passes through the Faraday rotator again, it will be rotated another 45° in the same direction. Thus the polarization state of the returned beam is orthogonal to that of the input beam. In the reverse direction through the fiber, the birefringence can be denoted as

$$\overleftarrow{R} = \frac{\alpha}{d}\begin{bmatrix} a & -b \\ b^* & a^* \end{bmatrix} \tag{4.4}$$

Then the transmission of light along a length of fiber through the FRM and back along the fiber path, is thus described by the operation

$$R = \overleftarrow{R}T\overrightarrow{R} = \alpha^2 t\begin{bmatrix} 0 & -1 \\ -1 & 0 \end{bmatrix} \tag{4.5}$$

Formula (4.5) implies that the total effect of the double pass in the fiber is equivalent to the effect of a Faraday rotator mirror, which is independent of the birefringence in the monitoring fiber. Therefore the returned beam always orthogonally polarizes with respect to the incoming one, independent of type, value or direction of the birefringence state occurring in the beam propagation [71]. In theory, the birefringence fluctuation caused by the uneven thermal effect or external stress can be completely compensated by using the retracing beam.

The birefringence compensation of FRM can also be described by the Poincare sphere [71]. The Poincare sphere representation and its equatorial projection about the birefringence compensation process is shown in fig.4.2, which indicates the evolution of the state-of-polarization of the retracing beam. As is shown in fig.4.1, the input beam is

supposed to horizontally polarize (point *H* in Fig.4.2), the retardation produced in formula (4.2), convey point *H* to *R* by means of a rotation around the axis 2θ by an angle of Δ, where θ is the angle the principal axis rotating to a fixed reference direction and Δ is a linear birefringence , which characterizes $\vec{R}$ in (4.2). According to the analysis of Jones matrix, *R* in formula (4.5) is independent of θ and Δ. Half of Faraday rotator effect is produced on the north hemisphere (path *R M*). The presence of the mirror "reflects" the point *M* to *M'* and the Faraday rotator is now acting on the south hemisphere by moving the point *M'* to R'. This point is symmetric to *R* and by means of a further rotation around the axis 2θ, which results to be *V*, i.e. the vertical exit state.

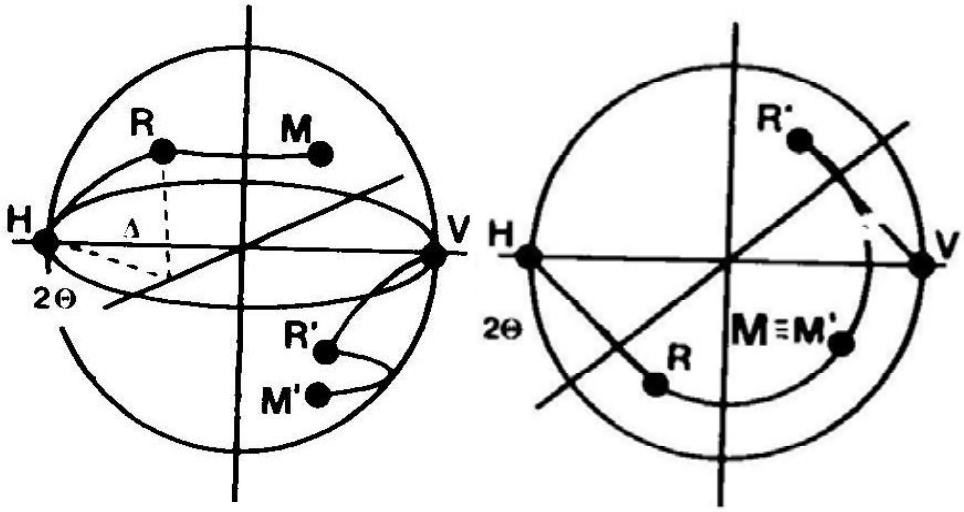

(a) (b)

Fig.4.2 Poincare sphere representation and its equatorial projection [15]

4.3.2 Optical pulse correlation sensor with birefringence compensation

The birefringence compensation approach by using a retracing beam is an effective method to suppress the polarization fluctuation resulted from the birefringence in a single-mode fiber. It provides a passive polarization-insensitive operation of fiber

interferometer based on a reflective configuration [72-74]. To suppress the polarization fluctuation in the optical correlation sensing system, this birefringence compensation method is utilized and a correlation sensing system with birefringence compensation is proposed as shown in Fig.4.3 [76]. In the monitoring arm, a circulator was used to input the optical pulse into the monitoring fiber and FRM, and then the reflected monitoring beam from the FRM can be input into the optical pulse correlation unit. As there are many components in the monitoring arm, the insertion loss will be increased. In order to compensate the unbalanced insertion loss in the reference arm and monitoring arm, an optical coupler with a coupling ratio of 30:70 was used following the EDFA. A remote controllable time delay line was used, which is helpful to realize the automatic data collection and remote monitoring.

The FRM was inserted behind the monitoring fiber. When the signal passes through the monitoring fiber in the forward direction, some birefringence fluctuation will occur in an unpredictable way due to the disturbance from the thermal effect or external stress. After passing through the FRM two times and returned to the monitoring fiber again,

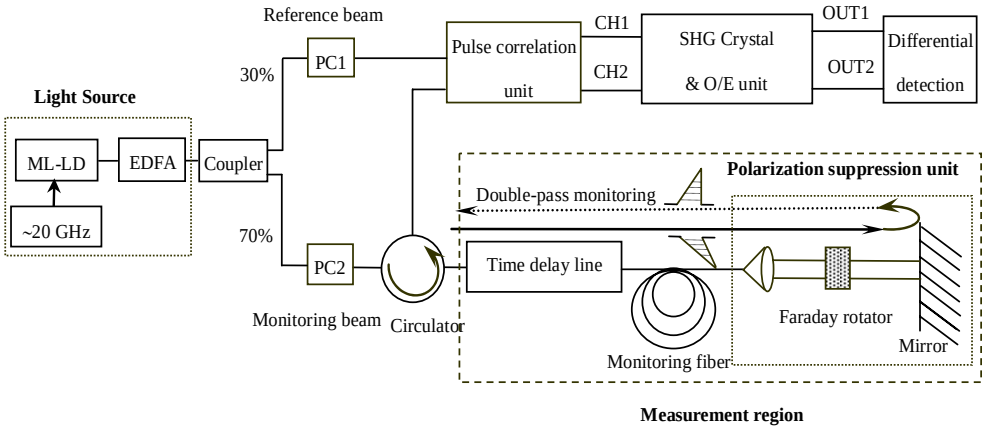

Fig.4.3. Schematic diagram of polarization suppressed fiber optic sensing system

the SOP of the monitoring beam was rotated 90°. Then some birefringence fluctuations

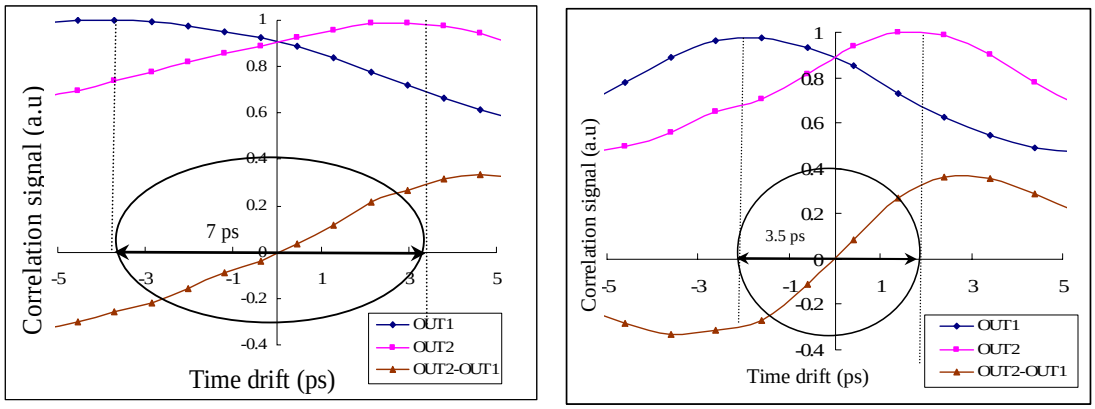

(a)Without FRM (b) With FRM

Fig.4.4. Time drift vs. correlation signals in the optical correlation sensing system

will be exerted on the monitoring beam when it experienced the monitoring fiber again in the backward direction, which will compensate the birefringence fluctuation in the forward direction. The SOP of the returned beam will always orthogonally polarize with respect to the incoming one, independent of type, value or direction of the birefringence state occurring in the beam propagation. Therefore, the birefringence fluctuation in the monitoring fiber caused by the external perturbation was effectively compensated in the optical pulse correlation system. Moreover, with the reflection of the mirror at the end, it makes the optical beam travel in the monitoring beam twice, thus a double-pass monitoring is constructed.

The variation of correlation signals with the time drift in the optical pulse correlation sensing system with birefringence compensation was investigated and compared with that in the previous correlation sensing system without FRM in chapter 3. As shown in Fig.4.4 (a), there is a 7 ps time interval between peaks of the correlation signal OUT1 and OUT2 in the previous correlation sensing system without FRM shown in Fig.3.1. This is because when the reference beam passes through the birefringent crystal, a time delay about 7 ps was generated between two orthogonal components of the reference

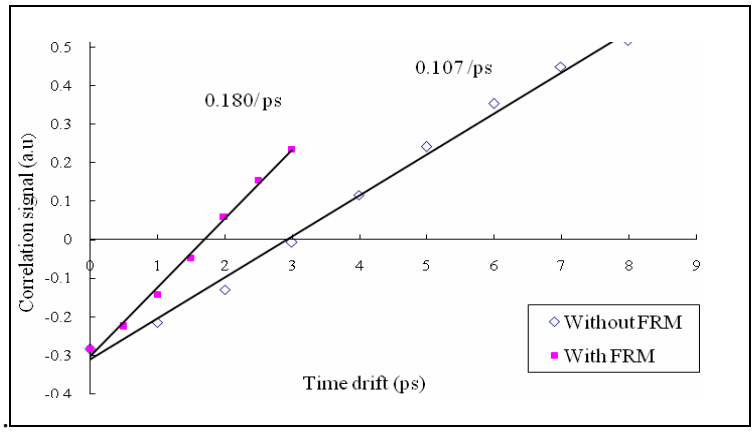

(a)

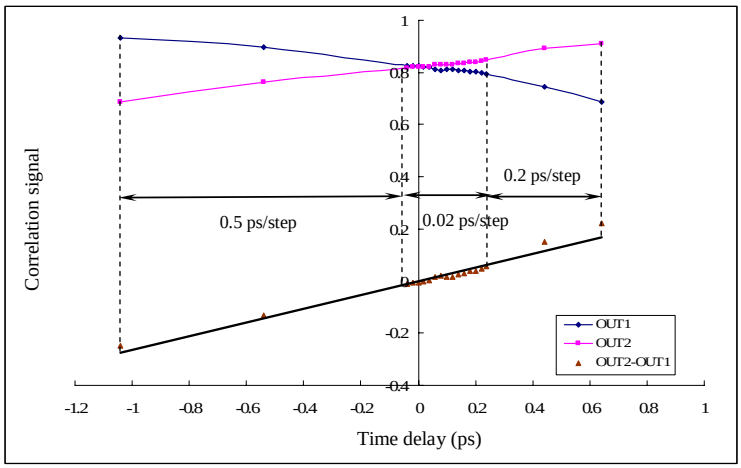

(b)

Fig. 4.5. (a) Sensitivity comparison of correlation sensing system with and without FRM

(b) Time resolution less than 0.02 ps in the correlation sensing system with FRM

beam. In the case of the correlation sensing system with birefringence compensation shown in Fig.4.3, the reflection at the end of FRM makes it possible to establish a double-pass monitoring. Therefore, the time interval between peak OUT2 and peak OUT1 becomes to 3.5 ps in Fig.4.4 (b). The corresponding time sensitivity of the system is doubled as shown in Fig. 4.5 due to the similar levels of the correlation signals in both sensing systems but reduced half time interval. Therefore a time resolution less than 0.02 ps was obtained as shown in the insertion Figure in Fig.4.5.

4.3.3 Investigation of polarization fluctuation in the correlation signal

In order to confirm the performance of the birefringence compensation, the polarization dependency of the correlation signals in the present sensing system was carried out and compared with the previous optical correlation sensing system shown in Fig.3.1. To generate a large polarization perturbation, a fiber polarization controller is inserted in front of the monitoring fiber. Thus the polarization perturbation can be directly imposed on the monitoring signal. The corresponding experimental results were shown in Fig.4.6. When there was no polarization perturbation at the beginning, the correlation signals of OUT1 and OUT2 were stable in both systems. After that, the polarization controller was tuned and polarization perturbation was added to the correlation signals. Compared with the correlation signals of the sensing system without FRM, the polarization dependency of the polarization-suppressed sensing system with FRM was reduced by more than 15 dB. It has to be noticed that after introducing the FRM into the system, there is still some fluctuations, which is caused by the imperfect manufacture of the FRM. In theory, the birefringence fluctuation can be completely compensated. By using a high-quality FRM, the rest fluctuation is expected to be eliminated.

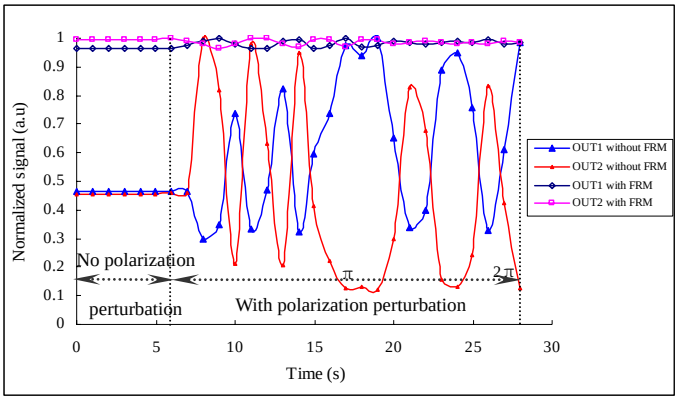

Fig.4.6. Comparison of polarization dependency of the correlation sensing system with and without FRM

4.4 **Temperature and strain characteristics**

For the previous optical correlation sensing system shown in Fig.3.1, during the temperature experiment, the correlation signal was susceptible to the internal and external fluctuations such as the birefringence caused by uneven thermal effect and the wind from the air conditioner. In the correlation sensing system with birefringence compensation, a temperature experiment was also carried out. To avoid any extra strain, a single mode fiber of l m was wound loosely by hand and heated up in a water bath.

According to the experimental results, the degradation of linearity caused by the birefringence of the single-mode fiber in the previous sensing system without birefringence compensation unit was eliminated and the linearity between the temperature and differential signal was obviously improved due to the compensation of birefringence fluctuation. Moreover, the correlation signal fluctuation caused by the external uneven thermal effect was eliminated. In addition as shown in Fig.4.7, the temperature sensitivity was nearly doubled in the optical correlation system with FRM due to the double-pass monitoring.

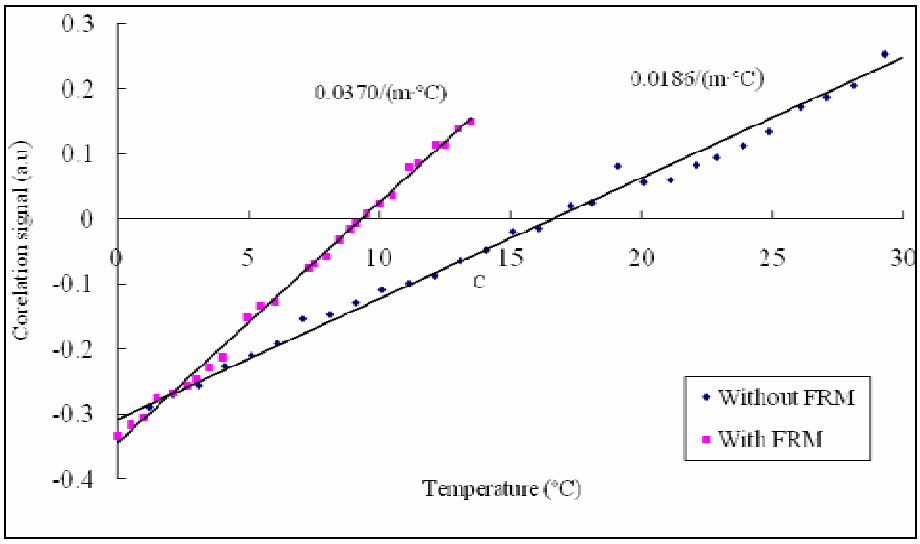

Fig.4.7 Temperature experiment results

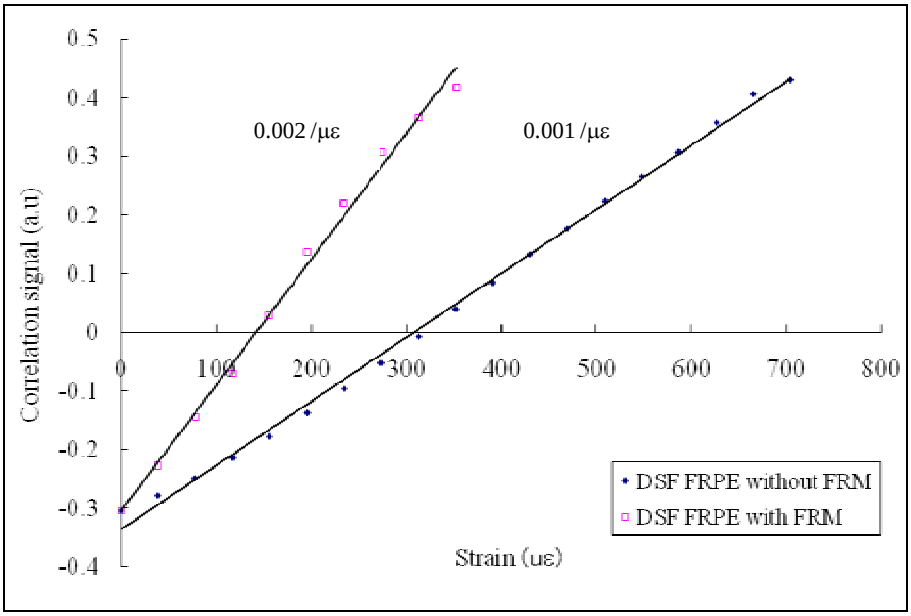

Fig.4.8 Strain experiment result

The strain characteristic of this sensing system was also examined. A dispersion-shifted single mode fiber of length 255.5 cm was used as the monitoring fiber, which was fixed on a stage with a movable section controlled by a micrometer. When the fiber was extended by tuning the micrometer at one end of the stage, time drift was generated, so that the corresponding correlation signal could be obtained. Fig.4.8 revealed the comparison of the strain sensitivities between the sensing system with and without FRM. According to the experimental results, it can be seen that the strain sensitivity in the polarization-suppressed sensing system was also doubled due to the double-pass monitoring.

4.5 Temperature change measurement outside of the lab

In the above section, the fundamental temperature and strain characteristics of the optical pulse correlation sensing system with the compensation of birefringence fluctuation were investigated. In order to make sure the temperature measurement capability in practice, a field temperature experiment is necessary. The temperature

outside of the window of the lab was monitored.

In order to obtain much larger measurement range, an optical pulse correlation unit with 20 ps time delay bias was used. Besides the difference of the time delay bias from the previous correlation unit, two polarizers are added in orthogonal polarization planes, respectively, which is helpful to enhance the stability. The photography of the correlation unit with 20 ps time delay bias. The relationship between the time delay line position and the correlation signal is shown in Fig.4.9. It can be seen that the period of the correlation signal is about 25 ps, while the linear region becomes to 10 ps due to the change of the time delay bias. Therefore, the sensing region of the sensor is enlarged from 3.5 ps to 10 ps, which is useful for large range measurement.

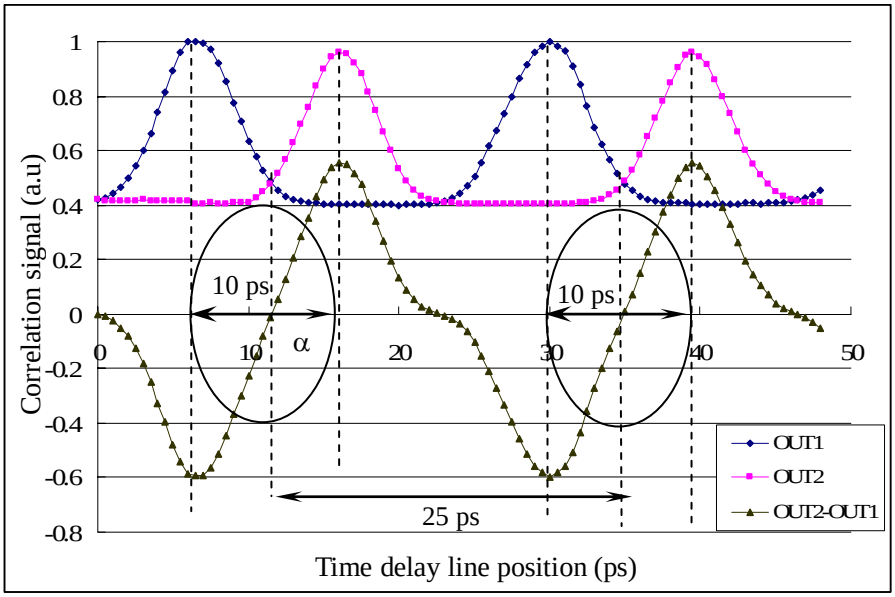

Fig.4.9 correlation signal vs. time delay line position of 20 ps correlation unit

4.5.1 Temperature calibration

Before a sensor is used to the practical measurement, a calibration is required. The schematic diagram of the calibration system is shown in Fig.4.10. It contains three parts, an incubator to control the temperature around monitoring fiber, a commercial available

thermometer (SK-L200 TII) to calibrate the sensor and the optical pulse correlation sensor. The incubator can change the temperature in the range from -15°C to 50°C. Then the temperature around the monitoring fiber can be changed continuously and the time delay of the monitoring pulse will be generated and detected by the correlation signal. By using a commercial available digital thermometer with a USB interface, the temperature change generated by the incubator can be displayed and recorded in a PC. The resolution of the digital thermometer is 0.1 °C and the accuracy is ±0.1°C+1 digit within the measurement range of -9.9 °C~205 °C. The photography of the calibration system is shown in Fig.4.11.

As is shown in Fig.4.9, the linearity is around the decision point α. If the initial position of the time delay line is located at the decision point, not only the change of the temperature can be measured, but also the change direction (increase or decrease) is available, which is determined by the sign of the difference between two correlation signals. This direction identification ability is much important for some physical quantity monitor such as the ocean temperature monitoring.

Before the calibration, in order to reduce the hysteresis of the optical fiber, the natural heat-up and cool-down process was carried out by leaving the monitoring fiber outside of the room for 4 days and nights. Then a single-mode fiber with a length of 3.37 m was calibrated by changing the temperature of the incubator step by step. To make sure the temperature of the fiber core can be accord with the temperature of the incubator, an hour maintaining time was set in each step. The relationships between the correlation signal and temperature of the incubator of two cooling-down and one heat-up process were shown in Fig.4.12. Accuracy around ±0.17 °C was obtained. According to Fig.4.12, all of the data are located in the allowance of the error.

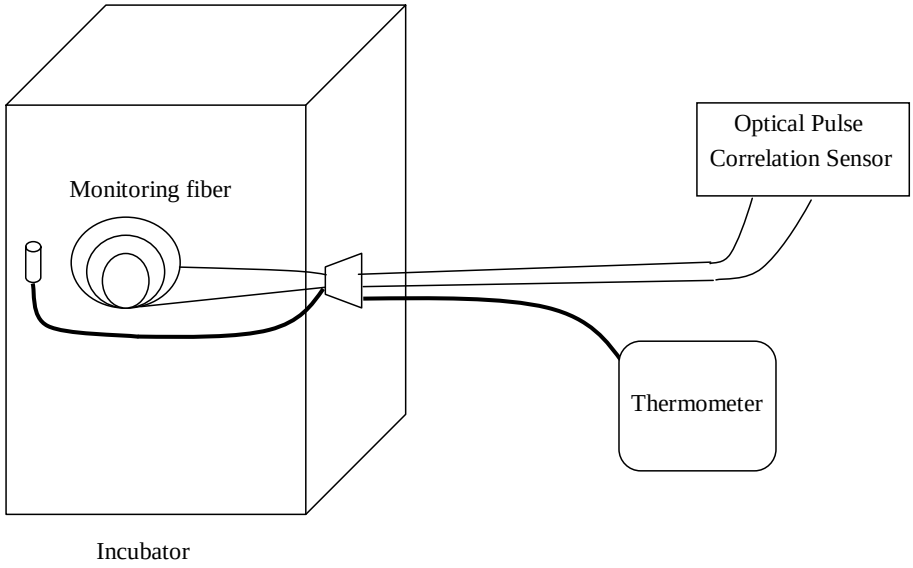

Fig.4.10 Schematic diagram of calibration system

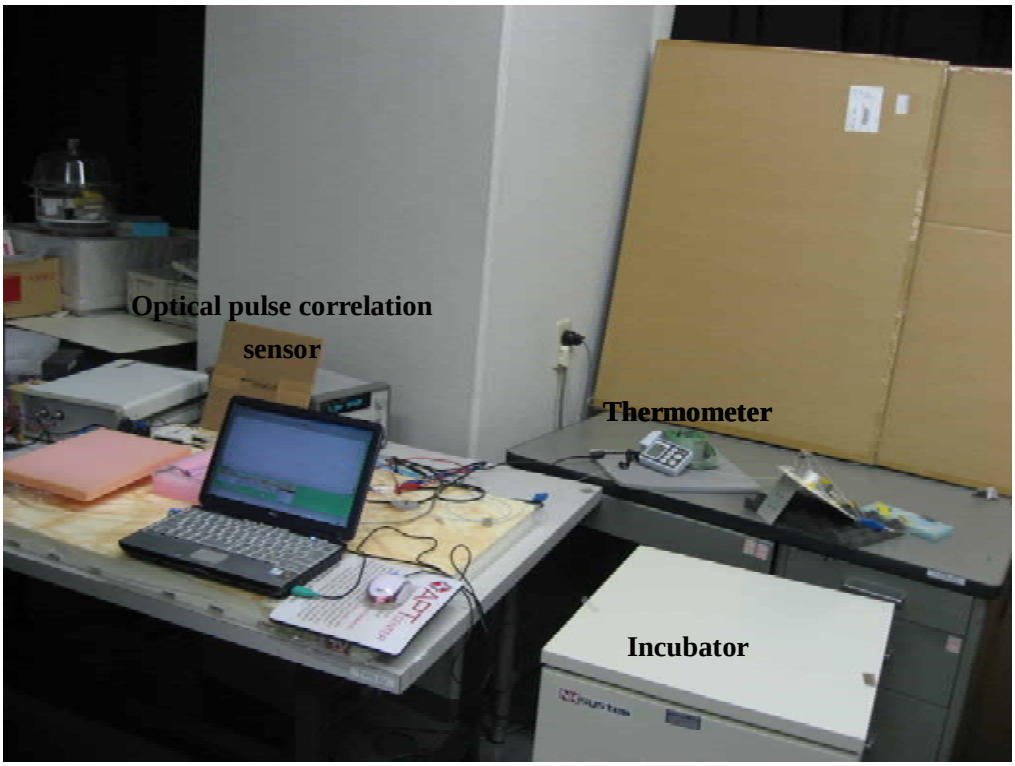

Fig.4.11 Photography of sensor calibration system

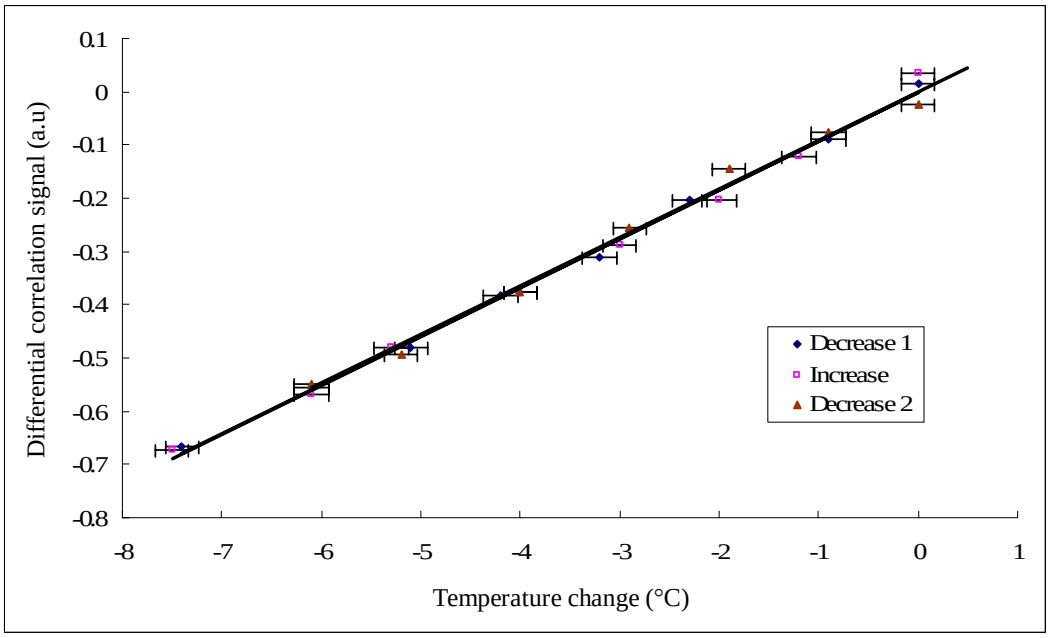

Fig.4.12 Temperature vs. differential correlation signal

4.5.2 Temperature measurement outside of lab

To investigate the performance of the optical pulse correlation sensor in the practical measurement, a field experiment was carried out. The temperature outside of the window of the laboratory was monitored as shown in Fig.4.13. In order to reduce the heat from the concrete due to the absorption, the monitoring fiber was isolated from the concrete of the windowsill as shown in Fig. 4.14.

To confirm the performance of the correlation sensor, a reference digital thermometer (SK-L200) with a resolution of 1 °C was placed near the monitoring fiber as shown in Fig.4.14. The temperature outside of the lab was monitored from 0 o'clock to 8:30 am. During the experiment, besides the real-time data recording from the thermometer and correlation sensor, the temperature change measured by the digital thermometer also was recorded with 20 minutes interval.

Fig.4.13 Test location of temperature measurement

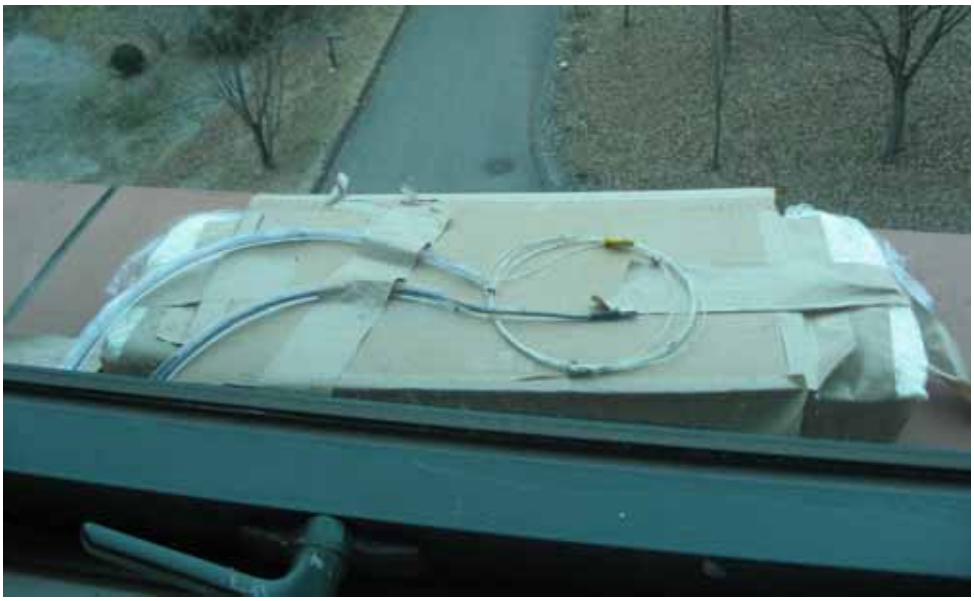

Fig.4.14 Layout of monitoring fiber

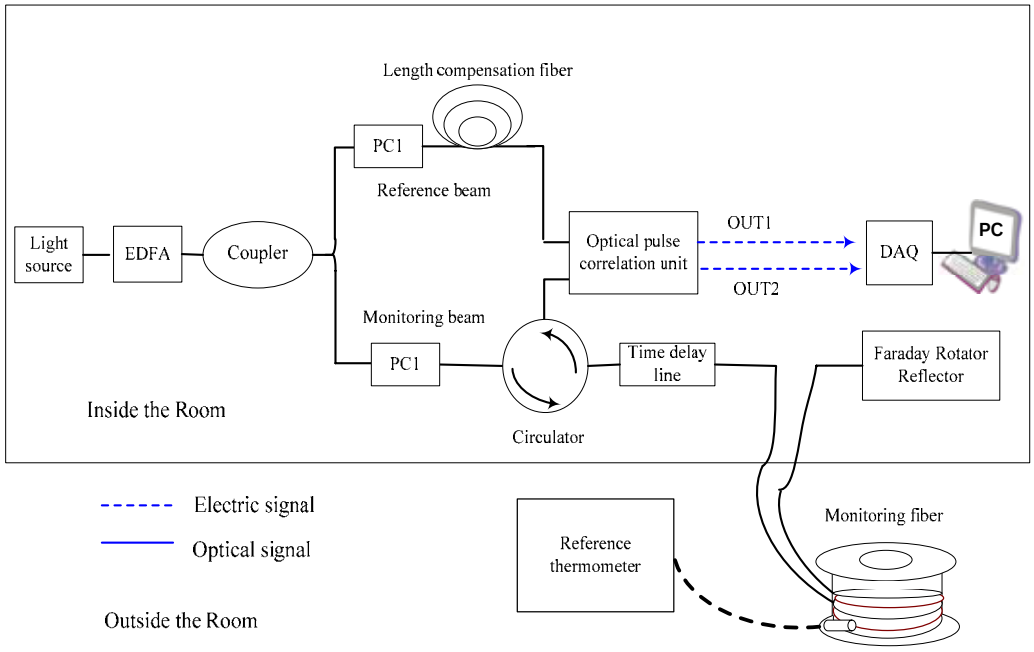

Fig.4.15 Configuration of temperature measurement experiment

The configuration of the experiment is shown in Fig.4.15. To balance the reference arm length and monitoring arm, a length compensation fiber was inserted after PC1. The temperature change measured by the digital thermometer is shown in Fig.4.16 (a), which implies that the air temperature varied slowly but with fluctuation. In the midnight the temperature decreased slowly. At round 3:48 am, there is the lowest temperature. The result from the optical pulse correlation sensor is shown in

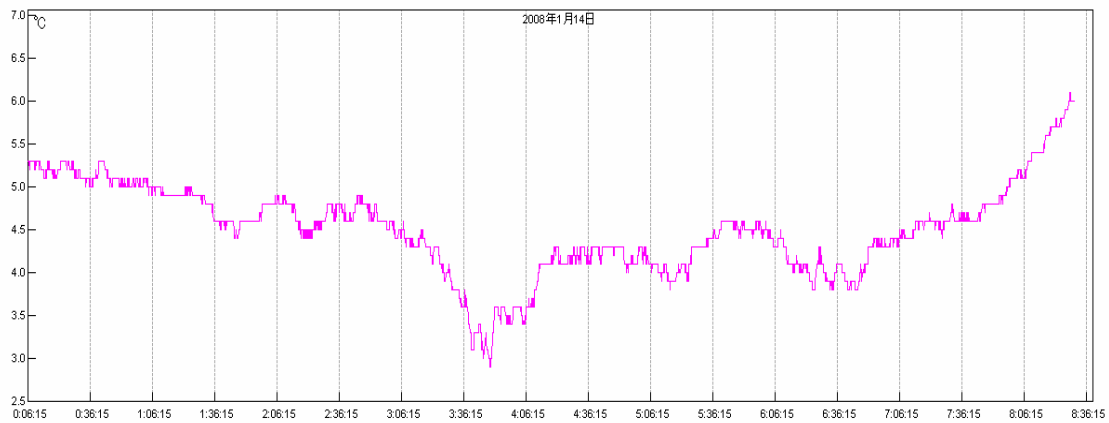

(a)

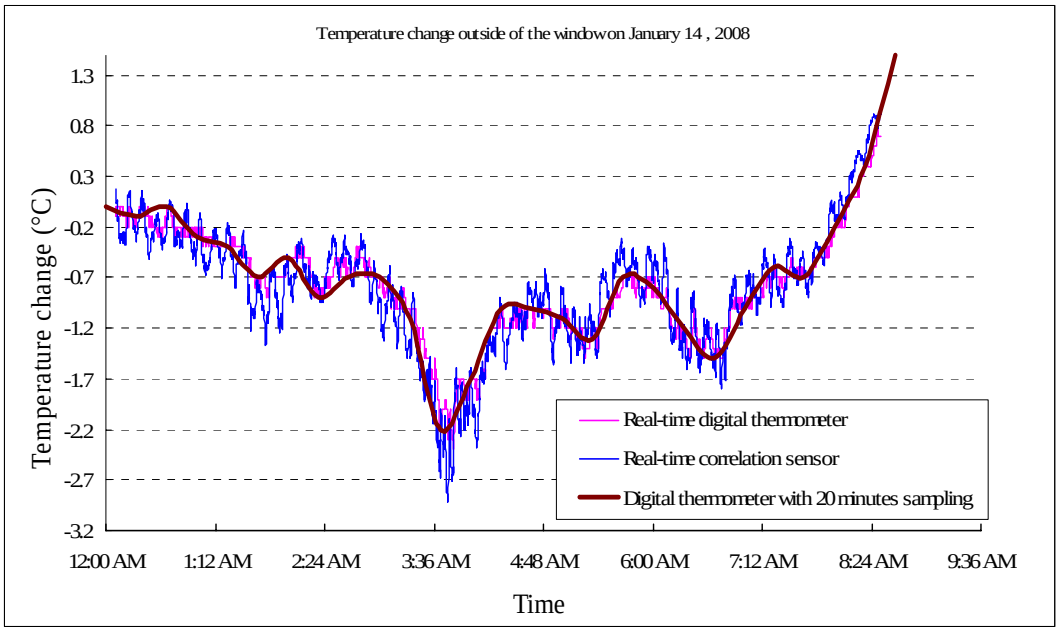

(b)

Fig.4.16 (a) Temperature change from digital thermometer
(b) Comparison of the temperature changes measured from thermometer and correlation sensor

Fig.4.17(b), from which it can be seen that the temperature measured from correlation sensor has the same variation with the thermometer. It is obvious that the result from correlation sensor changes much larger than that of the thermometer, so that some fluctuations were observed. However, these fluctuations are not noise, they reflects the temporary temperature fluctuation around the optical fiber. The larger changes of the temperature from correlation sensing system implied the higher sensitivity than the digital thermometer.

In order to compare with the data from the thermometer, it is necessary to smooth the data from the correlation sensor. A SMA (simple moving average) method was used to SMA is an unweighted mean of the previous *n* data points, which is useful to eliminate the periodical fluctuation in the signal. If the temperature sampled by the digital thermometer or correlation sensor is written as

$$A_N = \{a_1 \quad a_2 \quad a_i \quad \ldots \quad a_n\} \qquad n = 0 \quad 1 \quad 2 \ldots \tag{4.6}$$

After *n*-moving average, the data series will become to

$$S_i = \frac{1}{n}\sum_{j=1}^{i+n-1} a_j \tag{4.7}$$

During the SMA, the average number *n* is taken as 60 corresponding to 10 minutes as the sampling time of the real-time digital thermometer and correlation sensor is 10 s in Fig.4.17. The smoothed signal is shown in Fig.4.18. It can be seen that there is a good accordance between the real-time thermometer and the optical pulse correlation sensor. But we also noticed that the temperature change measured by the optical pulse correlation sensor is larger than that from the real-time digital thermometer at the sharp corner of the curve. The possible reason is the high sensitivity of the optical pulse correlation sensor to the temperature change.

The temperature outside of the lab was successfully monitored by the optical pulse correlation sensor with a high sensitivity, which confirmed the monitor ability of the correlation sensor to the environment around the optical fiber transmission line.

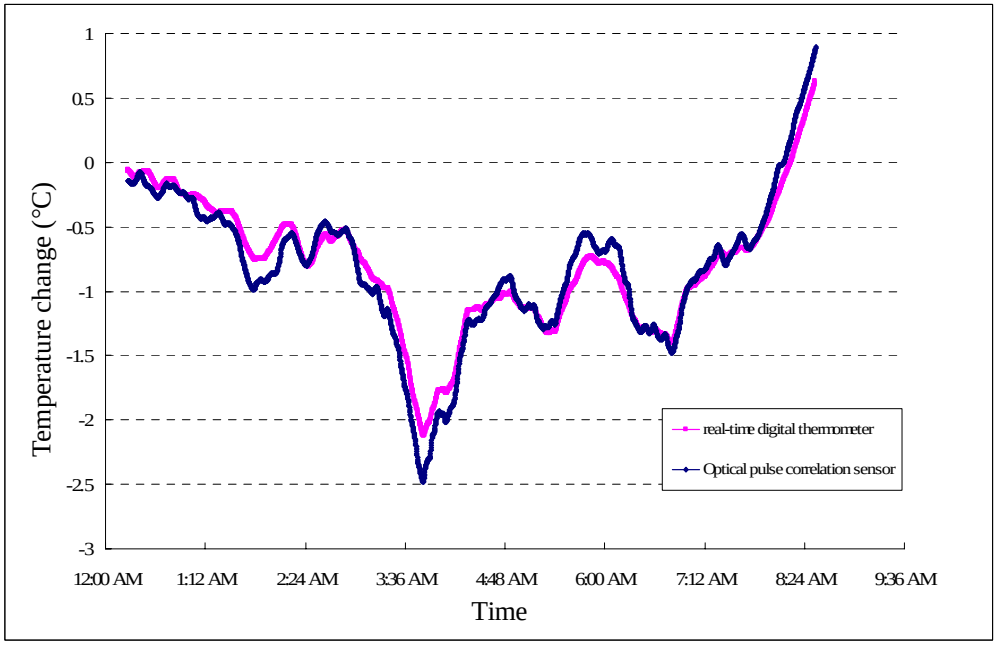

Fig.4.18 Data after SMA

4.6 Summary

In this chapter, The optical pulse correlation sensing system with birefringence compensation was proposed. The birefringence compensation is based on the retracing beam which is realized by a Faraday rotator reflector. The principle of the birefringence compensation was explained in theory by using a Jones matrix. The polarization sensitivity of the sensing system with FRR was investigated and compared with the previous sensing system discussed in chapter 3. The experiment results implied that the fluctuation of the correlation signal caused by the birefringence fluctuation in single-mode fiber was significantly suppressed. Moreover, after introducing the birefringence compensation approach into the optical pulse correlation sensing system, the sensing configuration was changed and a double-pass monitoring was constructed due to the reflection of FRR. Therefore, besides the compensation of birefringence fluctuation in the correlation signal, other performance improvements were also obtained. The sensitivity of the sensing system was nearly doubled due to the establishment of double-pass monitoring. A time resolution as high as 0.02 ps was obtained. At the same time, the linearity between the correlation signals and the time delay was also improved. A temperature measurement experiment outside of the lab was carried out. The experiment result implied that the temperature measured from the correlation sensor accords well with the thermometer, which indicated that the optical pulse correlation sensor can successfully monitor the environment around the optical pulse transmission lines.

Chapter 5

Performance Investigation of Optical Pulse Correlation Sensor in Long-Range Monitoring

5.1 Introduction

An optical pulse correlation sensing system with high time resolution has been developed. Compared with conventional fiber sensors, this correlation sensor is not only able to measure the change of the physical quantities such as temperature, strain or pressure; it can also indicate the change directions of these quantities according to the sign of the differential signal. As the sensing fiber of the optical pulse correlation sensor is not required to be a special fiber as FBGs, the transmission lines for communication purpose is an available medium. Therefore, the environment such as temperature, stress or pressure, around the optical fiber transmission lines can be monitored in long range. Since the monitoring distance will be limited by some factors such as loss, dispersion and nonlinearity, the performance of the optical correlation sensor in long-range monitoring will be discussed in this chapter.

5.2 Long-range monitoring application

The time drift of the optical pulse propagating in the optical fiber resulted from the environmental condition change such as temperature, stress or pressure, is available to be measured by using the optical pulse correlation sensing system. Therefore, the corresponding environment around the optical fiber can be monitored. As the

monitoring fiber is not required to be a special fiber, the optical pulse correlation sensing system is able to monitoring the environment such as temperature, stress or pressure around the optical fiber transmission lines in a long distance.

Recently, the development of the optical fiber sensing system with the long-range monitoring ability such as OTDR, BOTDR, Macro distortion sensor and FBGs, has become a hot topic to predict slope collapse resulted from mud-rock flow, earthquake or flood, due to the potential availability of optical fiber cable for communication purpose [77-79]. By combining the monitoring system with long-range sensing ability and the optical communication network, the alarming signal can be directly sent to user terminal by using the communication transmission line. Some researchers are embarking on the research of monitoring earthquake and tsunami by using the submarine cable [80]. Since the role of the ocean as being critical to understanding the variability of Earth's climate system has been identified by the Intergovernmental Program on Climate Change, the World Climate Research Program CLIVAR, and the U.S. National Research Council [81-83], monitoring of the ocean temperature is significant to study the Earth's climate and to understand the relationship between the ocean climate and the global warming [84]. To realize the ocean temperature monitoring without any adverse effect to the ocean ecosystem, the submarine optical fiber cable for communication purpose is a potential medium.

As far as the optical pulse correlation sensing system is concerned, although the distribution monitoring ability is not realized yet, since it has the long-range monitoring ability, it is also potential to be used to monitor the slope with latent danger. For the ocean temperature monitoring, the average temperature change in a long-range is required instead of the distribution measurement, optical pulse correlation sensor is a

potential solution due to the availability of the optical fiber cable for communication purpose. Since the optical signal will be degraded by some effects such as the loss, dispersion and nonlinearity in a long fiber, it is necessary to investigate the performance of the optical pulse correlation sensing system in the case of long-range monitoring fiber.

5.3 Performance of correlation sensor in long-range monitoring

In order to discuss the performance of optical correlation sensor for long-range monitoring using an optical fiber transmission lines, it is necessary to consider the signal propagation in the optical fiber.

According to the analysis of signal propagation in fibers in Appendix I from Ref 85, we can obtain the basic propagation equation governing pulse evolution inside a single-mode fiber, which is written as

$$\frac{\partial A}{\partial z}+\beta_1\frac{\partial A}{\partial t}+\frac{i\beta_2}{2}\frac{\partial^2 A}{\partial t^2}-\frac{\beta_3}{6}\frac{\partial^3 A}{\partial t^3}=i\beta_{NL}A-\frac{\alpha}{2}A \qquad (5\text{-}1)$$

Where, β_1 is a dispersion parameter, which is inversely related to the group velocity v_g of the pulse as $\beta_1 = 1/v_g$. β_2 and β_3 are known as the second- and third-order dispersion parameters and are responsible for pulse broadening in optical fibers. More specifically, β_2 is related to the dispersion parameter D as

$$D=\frac{d}{d\lambda}\left(\frac{1}{v_g}\right)=-\frac{2\pi c}{\lambda^2}\beta_2 \qquad (5\text{-}2)$$

This parameter is expressed in unit of ps/(km-nm). It varies with wavelength for the fiber and vanishes at a wavelength known as the zero-dispersion wavelength and denoted as λ_{ZD}. The parameter β_3 is related to the dispersion slope S as $S=(2\pi c/\lambda^2)^2\beta_3$. β_{NL} is the nonlinear coefficient, which can be written as

$$\beta_{NL} = \gamma |A|^2, \qquad \gamma = \frac{2\pi n_2}{\lambda_0 A_{eff}} \tag{5-3}$$

the β_1 term simply corresponds to a constant delay experienced by the optical signal as it propagates through the fiber. Since this delay does not affect the signal quality in any way, it is useful to work in a reference frame moving with the signal. This can be accomplished by introducing the new variables *t'* and *z'* as

$$t' = t - \beta_1 z \qquad z' = z \tag{5-4}$$

And rewriting Eq.(5-1) in terms of them as

$$\frac{\partial A}{\partial z'} + \frac{i\beta_2}{2}\frac{\partial^2 A}{\partial t'^2} - \frac{\beta_3}{6}\frac{\partial^3 A}{\partial t'^3} = i\gamma |A|^2 A - \frac{\alpha}{2} A \tag{5-5}$$

Also the third-order dispersive effects are negligible in practice for single-mode fiber as long as β_2 is not too close to zero, or pulses are not short than 5 ps. Setting β_3=0, Eq.(5-5) reduces to

$$\frac{\partial A}{\partial z} + \frac{i\beta_2}{2}\frac{\partial^2 A}{\partial t^2} = i\gamma |A|^2 A - \frac{\alpha}{2} A \tag{5-6}$$

This equation is known as the nonlinear Schrodinger (NLS) equation. The three parameters, α, β_2 and γ, take into account three distinct kinds of degradations that can occur when an optical signal propagates through optical fibers. In the case of long monitoring fiber, the main factors affecting the performance of the optical pulse correlation sensor are loss, nonlinear effect and dispersion.

5.3.1 Loss impact

According to Eq.(5-5), the loss parameter α reduces not only the signal power but it also weakens the strength of nonlinear effect, which can be seen mathematically by introducing [85]

$$A(z,t) = B(z,t)\exp(-\alpha z/2) \tag{5-7}$$

into Eq.(5-5) and writing it in terms of *B(z, t)* as

$$\frac{\partial B}{\partial z} + \frac{i\beta_2}{2}\frac{\partial^2 B}{\partial t^2} = i\gamma e^{-\alpha z}\left|B\right|^2 B \quad . \qquad (5\text{-}8)$$

The above two equations indicate that the power of an optical signal exponentially decreases with a loss coefficient α along the fiber length [85]. The nonlinear effect was also weakened with a coefficient. For the nonlinear effect, we will discuss it in later section.

As far as the power loss is concerned in the optical pulse correlation sensor, the length of the monitoring fiber will be limited due to the conversion efficiency of SHG crystal, i.e. the minimum power of CH1 and CH2 in Fig.5.1. Since the sensitivity and dynamic range of the optical pulse correlation sensing system are related to the time delay bias in the optical pulse correlation unit, we can determine the value of the time delay bias according to the specific requirement in the case of long-range measurement. The insertion losses of related components are shown in table 5.1. The minimum power at point G should be larger than 1 mW, so the length of monitoring fiber will be determined by the inject power to the monitoring fiber at point E and the loss of the transmission line. If the transmission loss of fiber is taken as 0.2 dB/km and the length is *L*, the total loss from point D to point G is

$$L_{Total} = L_{D\to E} + (L_{Delay} + L_{Fiber}) \times 2 + L_{E\to G} + L_{FRM} \qquad (5\text{-}9)$$

Where L_{Fiber}=0.2 × *L* (dB).

Thus the relationship between the injection power and length of monitoring fiber can be written as

$$10\log(\frac{P_{in}}{1}) = L_{D\to E} + (L_{Delay} + L_{Fiber}) \times 2 + L_{E\to G} + L_{FRM} \qquad (5\text{-}10)$$

The numerical simulation in theory is shown in Fig.5.2, if we do not consider the effect of dispersion and nonlinearity in optical fiber.

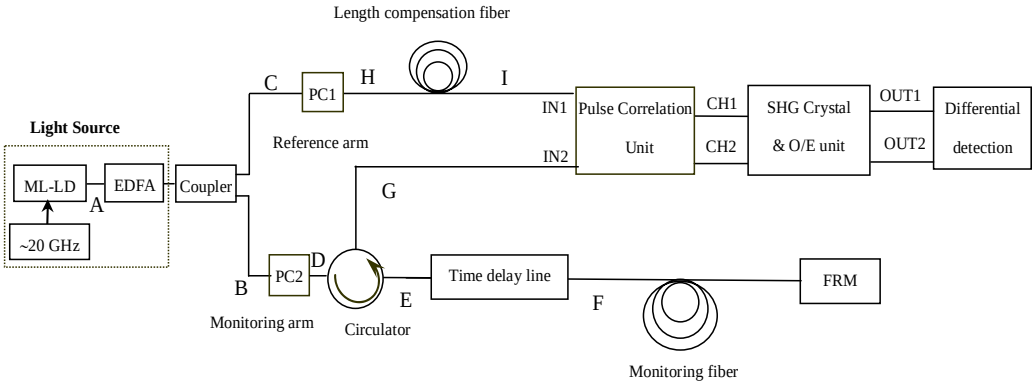

Fig.5.1 Configuration of optical pulse correlation sensing system

Table 5.1 Typical insertion loss of each component

Component		ertion loss (dB)
Coupler	C	1.69
	B	1.9
PC1 (C→H)		1.1
PC2 (B→D)		1.19
Circulator	D→E	0.77
	E→G	0.70
Time delay line (E→F 110 ps- 160 ps)		0.33
FRM		0.56

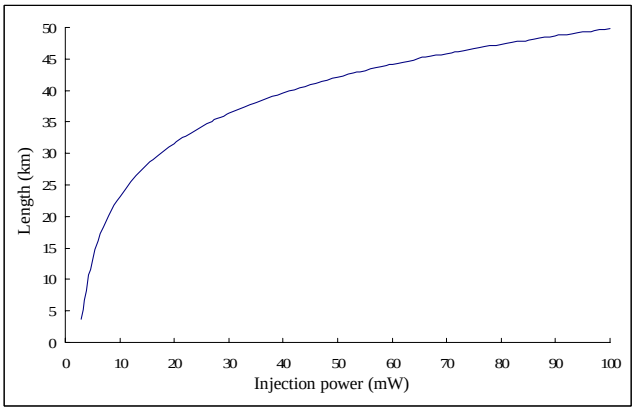

Fig.5.2 Monitoring length limited by injection power

According to Fig.5.2, it can be seen that if only consider the loss impact, when the

average injection power is around 20 mW, the possible length of monitoring fiber is 31.62 km. However, since the existence of dispersion and nonlinear effect in long fibers, the injection power is limited within 10 mW, which will be discussed in later section. So the acceptable length is less than 30 km. It is fortunate that the loss can be compensated by an EDFA; it is possible to obtain much longer sensing length by using an EDFA after point G as shown in Fig.5.3. Therefore, the limitation of SHG threshold is converted to the minimum amplifiable power and the signal to noise ratio of the EDFA. Now the EDFA with minimum input power of 0.01 mW and S/N larger than 20 dB is commercial available such as ErFA 1215 in Furukawa Inc. Therefore, by using an EDFA to compensate the loss, and the maximum injection power of 9 mW is concerned, the maximum monitoring length is

$$l = \frac{10\log(\frac{9}{0.01}) - 0.33\times 2 - 0.56 - 0.7}{2\times 0.2 dB/km} dB = 69.05\, km \qquad (5\text{-}11)$$

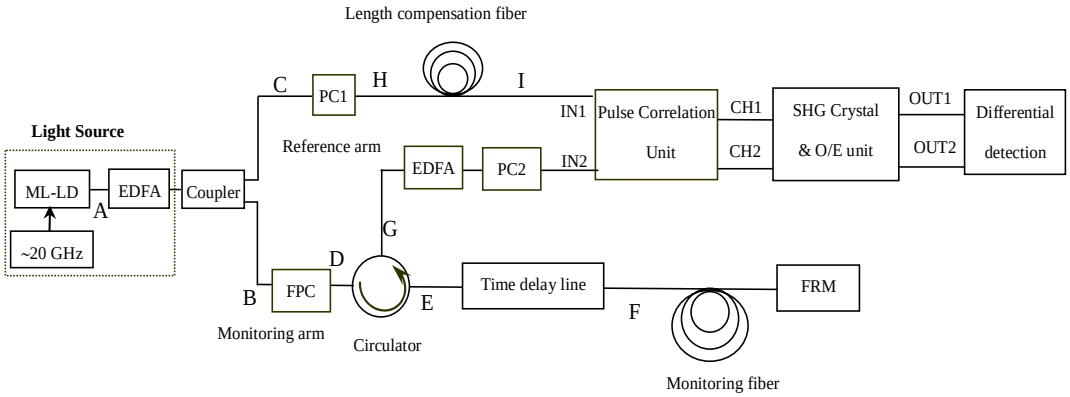

Fig.5.3 Configuration of optical pulse correlation sensing system with loss compensation

5.3.2 Dispersion effect

5.3.2.1 Group-velocity dispersion (GVD)

In the optical pulse correlation sensing system, ML-LD is not the absolute monochromatic light source, which contains several frequency components. Since the

effective refractive index of the fiber mode depends on the frequency of light launched into it. Consequently, there will be a group-velocity dispersion caused by the different group velocity of different spectral components. The GVD is characterized by the parameter β_2 as the effect of β_3 can be neglected [85]. Therefore, β_2 governs the strength of the dispersion of optical signals propagating in the optical fiber. The dispersion parameter β_2 is easy to cause the broadening of the optical pulse. According to the analysis of the dispersion effect on optical pulse with linear chirp in Ref.85, the pulse shape at distance *z* inside the fiber can be written as

$$A(\xi,t)=\frac{A_0}{\sqrt{b_f}}\exp[-\frac{(1+iC_1)t^2}{2T_0^2 b_f^2}+\frac{1}{2}\tan^{-1}(\frac{\xi}{1+C\zeta})] \tag{5-12}$$

Where C is the chirp parameter.T_0 is the half-width of the pulse at *1/e* power point, which is related to the full width at half-maximum (FWHM) of the input pulse by the relation $T_{FWHM}=2(\ln 2)^{1/2}T_0\approx 1.665T_0$. ξ is the normalized distance denoted as $\xi=z/L_D$, in which L_D is defined as the dispersion length by $L_D=T_0^2/|\beta_2|$. The parameters b_f and C_1 vary with ξ as

$$b_f(\xi)=[(1+sC\xi)^2+\xi^2]^{1/2} \qquad C_1(\xi)=C+s(1+C^2)\xi \tag{5-13}$$

Where s=sgn(β_2) takes values +1 or -1, depending on whether the pulse propagates in the normal- or the anomalous-dispersion region of the fiber. The variations of broadening factor and chirp parameter with the relative length are shown in Fig.5.4, in which the anomalous dispersion was considered, i.e. β_2<0.

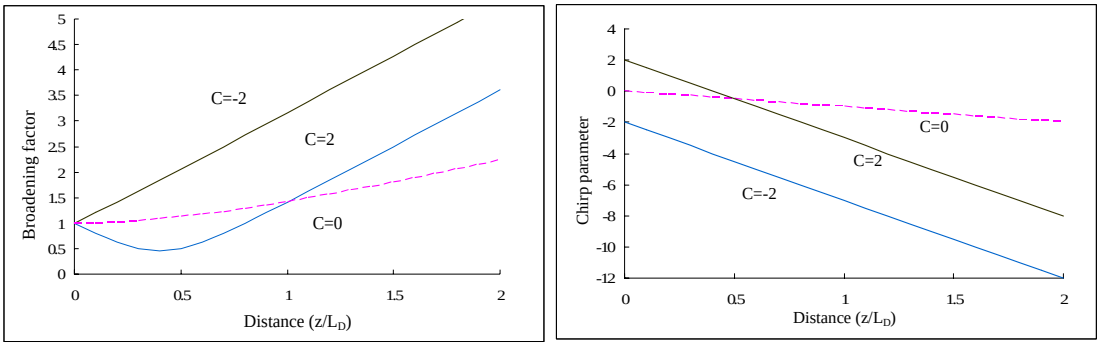

Fig.5.4 Broadening factor and chirp parameter in long fiber

It can be seen that an unchirped pulse (C=0) broadens monotonically by a factor of $(1+\xi^2)^{1/2}$ and develops a positive chirp such that $C_1=\xi$. While the chirped pulse, may broaden or compress depending on whether β_2 and C have the same or opposite signs [86]. When $\beta_2 C>0$, a chirped pulse broadens monotonically at a rate faster than that of the unchirped pulse. The reason is related to the fact that the dispersion-induced chirp adds to the input chirp because the two combinations have the same sign. As far as the chirp parameter is concerned, in the case of $\beta_2 C>0$, the chirp will be monotonically increased or decreased depending on the sign of β_2. As shown in Fig.5.4 (b), when $\beta_2<0$, the chirp parameter C_1 is decreased. On the other hand, if $\beta_2>0$, C_1 will increase. In the case of $\beta_2 C<0$, the chirped pulse will be compressed first and at the length of $\xi = sC/1+sC$, there is the minimum pulse width. Beyond that point, the pulse will be broadened and its width will be larger than the original value. For the chirp parameter C_1, the contribution of the dispersion-induced chirp is opposite to that of the input chirp. The chirped pulse will be unchirped at the distance $\xi = |C|/(1+C^2)$. After that point, the chirp parameter will be increased in the opposite direction to the original chirp.

According to Fig.5.4, it can been that there is a large broadening caused by the

dispersion effect in a single mode fiber when the transmission length is larger than the dispersion length, which will limit the length of monitoring fiber in optical pulse correlation system. As far as the light source of the optical pulse correlation sensing system is concerned, the FWHM of the optical pulse launched into the dispersion-shifted fiber is around 8.965 ps. For a Corning SMF-28, a Non-zero dispersion shifted fiber (NZ-DSF) and a dispersion-shifted fiber (DSF) with the parameters shown in table 5.2, the dispersion length around 1.32 km, 7.53 km, and 103.91 km, respectively. Therefore, the maximum length of a standard single-mode fiber and NZ-DSF and DSF are limited within 0.66 km, 6.3 km and 51.5 km, respectively. It is fortunate that the pulse width broadening is possible to be compensated by using dispersion compensated fiber, which is applied in the submarine transmission lines for communication purpose. In that case, the dispersion effect will be degraded much. The dispersion broadening effect on the optical pulse correlation sensing system will be discussed in the following section.

Table 5.2 Related parameters of SMF and NZ-DSF

Fiber kinds	Single-mode fiber	NZ-DSF	DSF
D (ps/[km-nm])	17	3	0.218
β_2 (ps^2/km)	-21.81	-3.849	-0.279
L_D (km)	1.32	7.53	103.91

For a DSF with the zero-dispersion wavelength near the wavelength of light source, the dispersion effect caused by β_2 can be neglected, since $\beta_2 \approx 0$ near the zero-dispersion wavelength. However, we have to notice the effect of β_3 written as

$$\frac{\sigma_{p}^{2}}{\sigma_{0}^{2}} = 1 + (1 + C^{2} + V_{\omega}^{2})^{2} (\frac{\beta_{3} L}{4\sqrt{2}\sigma_{0}^{3}})^{2} \qquad (5\text{-}14)$$

Where V_{ω} is a parameter related to the RMS pulse width at the end of a fiber of length L, σ_{ω} is the RSM spectrum width and σ_{0} is the RMS spectrum width [85]. For the signal launched into the monitoring fiber have a spectrum width of 0.515 nm and a FWHM of 8.965 ps. Thus we have

$$V_{\omega} = 2\sigma_{\omega}\sigma_{0} = 0.026 << 1 \qquad (5\text{-}15)$$

We can rewrite Eq.(5-13) as

$$\sigma_{p}^{2} = \sigma_{0}^{2} + (1 + C^{2})^{2} (\frac{\beta_{3} L}{4\sigma_{0}^{2}})^{2} / 2 \qquad (5\text{-}16)$$

If we take a typical value $\beta_{3} = 0.1 ps^{3} / km$, the relationship between the pulse width and

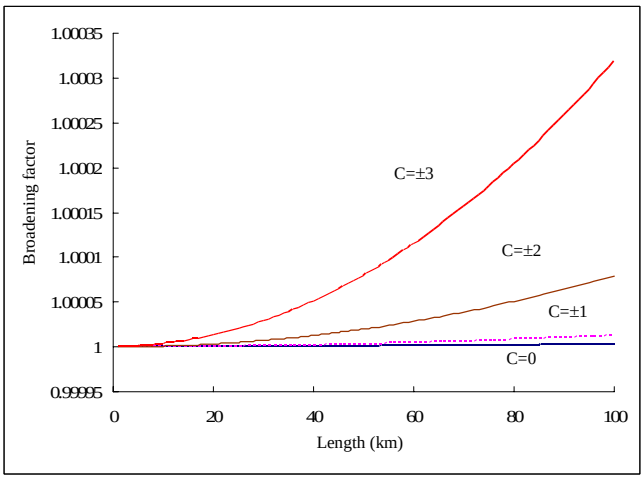

Fig.5.5 Broadening caused by third-order dispersion

the length of monitoring fiber under different chirp parameters can be simulated as shown in Fig.5.5. According to the simulation results indicated that the broadening effect is increased with the increase of chirp parameter *C* and transmission length. For the specific *C*, the broadening factor is increased slowly. Taking an example of C=±3, even the monitoring length is increased to 100 km, the broadening factor is as small as

1.000318. It is obvious that the broadening effect of third-order dispersion in a dispersion-shifted fiber is negligible.

If the bit rate limitation caused by β_3 is considered, we have

$$B(|\beta_3|L)^{1/3} \leq 0.324 \tag{5-17}$$

When B=20 GHz, for dispersion-shifted fiber with β_3~0.1 ps^3/km, L≤21,700 km. Therefore, as long as L≤21,700 km, the effect of β_3 will not be relevant in the optical pulse correlation sensing system since B~20 GHz.

Therefore, if the monitoring fiber is a dispersion-shifted fiber with a zero-dispersion wavelength near 1.5551 μm, the dispersion effect of β_3 is small enough to be neglected.

5.3.2.2 Polarization-mode dispersion (PMD)

The birefringence in the single-mode fiber leads to a dispersion, which is defined as the polarization-mode dispersion. The mechanism of PMD is shown in Fig.5.6, in which differential group delay (DGD) represents the time delay between two polarization modes caused by PMD [85].

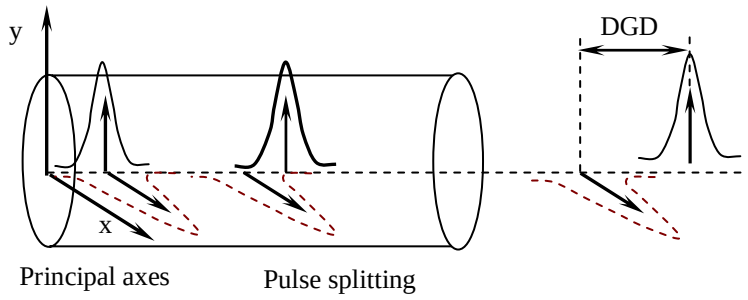

Fig.5.6 Propagation of an optical pulse in a fiber with constant birefringence. Pulse splits into its orthogonal polarized components that separate from each other because of DGD induced by birefringence

Since DGD changes with the transmission lines in a random fashion due to the random fluctuation of the birefringence in a single-mode fiber, the PMD-induced pulse

broadening is characterized by a RMS value of DGD, which can be estimated as the following for the long-range larger than 1 km,

$$\Delta\tau_{RMS} = D_p\sqrt{z} \tag{5-18}$$

Where D_p is known as the PMD parameter, which varies from 0.01 $ps/(km)^{-1/2}$ to 10 $ps/(km)^{-1/2}$ for different fibers. Modern fibers are designed to have low PMD, and typically $D_p < 0.1 \quad ps/(km)^{1/2}$. Therefore, when L=100 km, the PMD-induced broadening is less than 1 ps, which is much small. However, as the birefringence in the single-mode fiber fluctuates randomly with respect to the time, DGD will randomly fluctuate and severely depredates the optical signal.

As far as the optical pulse correlation sensing system is concerned, the birefringence fluctuations have been compensated by balancing the propagation of optical pulse components in orthogonal polarization planes via retracing beam, not only the birefringence fluctuations but also the DGD were compensated. Therefore, PMD will not affect the performance of the correlation sensing system.

5.3.3 Nonlinear impairment

According to nonlinear Schrodinger (NLS) equation shown in Eq.(5-5), γ is an important parameter of degrading the optical signal propagating through optical fiber. For many short-haul communication systems (transmission distance <100 km), the nonlinear effects is small enough to be neglected as the power of the light source is not too high (~1 mW). But for the long-haul system including a chain of cascaded optical amplifiers, nonlinear effect becomes to be essential due to the degradation of signal-to-noise ratio and the accumulation of nonlinear effect from amplifier to amplifier[86-88]. Nonlinear effect in long-haul communication systems includes

self-phase modulation (SPM), cross-phase modulation (XPM), four-wave mixing (FWM), stimulated Raman scattering (SRS) and stimulated Brillouin scattering (SBS).

In the optical correlation sensing system, after being amplified, the average power of the light source is around 16.5 mW, which is potential to stimulate the nonlinear effect in the optical fiber. It is fortunate that such high power only transmit in the length around 3m in an optical coupler. For the launched power of long monitoring fiber, it is around 9 mW, which is a critical value for nonlinear effect in long-range. Therefore, it is necessary to discuss this possibility.

As there is only one signal transmitting in the monitoring fiber, XPM and FWM will not depredate the monitoring signal. As far as SRS is concerned, there will be not much concern in the correlation sensing system as the average optical power of signal launched into the monitoring fiber is around 9 mW corresponding to a peak power of 51.3 mW, which is much less than the threshold power ~450 mW for sing-channel SRS [89]. For the SBS, the threshold for the single-mode fiber is generally around 5 mW, doubled threshold of 10 mW was also observed. However, since the SBS will limit the transmission power of the optical fiber within 3 mW [85], but without interference on the pulse width of the optical signal, it will not give serious impact on the correlation signal as the transmission power is not larger than 3 mW in the usual case. Moreover, it will reduce the SPM effect by limiting the transmission power in the optical fiber. Thus, we just need to consider the effect of SPM.

SPM will affect the pulse width of the optical signal through the frequency chirping due to the nonlinear phase shift ϕ resulted from the large optical power. If neglecting the effect of loss and the dispersion effect, the nonlinear-phase shift can be written as [90]

$$\phi = \gamma P_0 L_{eff} \tag{5-19}$$

Where L_{eff} is the effective length defined as $P_0 L_{eff} = \int_0^L P(z)dz$. P_0 is the peak power of the injection pulse. As discussed in the section of loss effect, the optical power exponentially decreases through the optical fiber, that is

$$P(z) = P_0 \exp(-\alpha z) \tag{5-20}$$

Hence

$$L_{eff} = \frac{\int_0^L P(z)dz}{P_0} = \int_0^L \exp(-\alpha z)dz = \frac{1}{\alpha}[1 - \exp(-\alpha L)] \tag{5-21}$$

The phase shift ϕ varies with time as the optical power changes with time. Thus ϕ is a function of time. Since frequency, by definition, is the derivative of phase shift with respect to time. We have an optical frequency caused by $d\phi/dt \neq 0$. This varying frequency is defined as the chirping. Consequently, pulse broadening due to the frequency chirp will occur. To keep SPM effect to a minimum, it is necessary to keep the nonlinear phase shift small ($\phi << 1$), that is,

$$\phi = \gamma P_0 L_{eff} << 1 \tag{5-22}$$

Therefore,

$$P_0 << \frac{\alpha}{\gamma[1 - \exp(-\alpha L)]} \tag{5-23}$$

Where, γ is the nonlinear parameter, which is written as

$$\gamma = \frac{2\pi n_2}{\lambda_0 A_{eff}} \tag{5-24}$$

n_2 is a constant parameter with a value around 2.6×10^{-20} m^2/W. For a fiber with A_{eff}=50 μm^2. γ is taken as a typical value of 2.1 W^{-1}/km. α is taken as 0.2 dB/km, we can obtain the relationship between the limit of the injection power and the transmission distance as shown in Fig.5.7 (a). It is implied that with the distance increasing, the limit to the injection power is decreased.

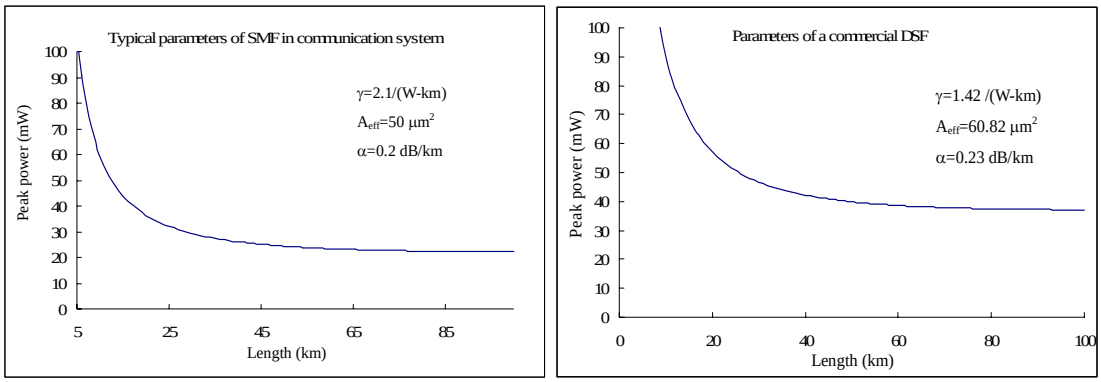

Fig.5.7 Injection power limitation for minimum SPM

As far as the optical correlation sensor is concerned, even the average power of the light source was amplified as large as 16.5 mW corresponding to a peak power around 92 mW, SPM is kept to minimum due to length of the coupler is within 2~3 m. For the monitoring fiber, as the average injection power is around 9 mW corresponding to a peak power around 51.3 mW. According to Fig.5.7 (a), to minimize SPM, the length of the standard single-mode monitoring fiber should be limited within 5.5 km. By considering the limit of less than 0.75 km caused by the dispersion effect, the length is better to limit within 0.75 km, if the loss compensation by using an EDFA and dispersion compensation by using dispersion compensation fiber are not considered. If the loss compensation and dispersion compensation are considered to be used, the length of the monitoring fiber can be extended further.

If the parameters of the commercial DSF of γ=1.42 /(W-km), A_{eff}=60.82 μm^2, and α =0.23 dB/km, are considered, the power limit in different length is shown in Fig.5.7 (b). The length is limited by 24.8 km. However, the frequency chirp caused by the SPM will result in the broadening or compressing determined by the signal of β_2, that is for the normal dispersion β_2>0, SPM causes the broadening and for the anomalous dispersion β_2<0, SPM leads to the pulse compressing. The following analysis proves this conclusion. According to the analysis of the SPM by simultaneously considering

the dispersion effect in Ref 85, the pulse width after transmitting a distance of *z*, can be written as

$$\sigma_p^2(z) = \sigma_L^2(z) + \gamma P_0 f_s \int_0^z \beta_2(z_1)[\int_0^{z_1} p(z_2)dz_2]dz_1 \qquad (5\text{-}25)$$

Where σ_L^2 is the RMS width expected in the linear case (γ=0). The shape of the input pulse enters through the parameter f_s, defined as

$$f_s = \frac{\int_{-\infty}^{\infty} |U(0,t)|^4 dt}{\int_{-\infty}^{\infty} |U(0,t)|^2 dt} \qquad (5\text{-}26)$$

For a Gaussian pulse with $U(0,t) = \exp[-\frac{1}{2}(t/T_0)^2]$, there is $f_s = 1/\sqrt{2} \approx 0.7$.

Eq.(5-21) makes clear the broadening or compressing effect of SPM. The total broadening of a SMF, NZ-DSF, and a DSF under the effect of dispersion and SPM are shown in Fig.5.8. According to the simultaneous consideration of dispersion and SPM, for the standard single-mode fiber and NZ-DSF, the length of monitoring fiber in the optical pulse correlation sensing system should be limited within 1.01 km and 9 km, respectively, to limit the broadening factor with 1.5. While for the DSF, since the dispersion is not so much which can be compensated by the SPM compression, for L=66 km, the broadening is less than 1.5. Therefore, the available length of the monitoring fiber is around 66 km by comprehensively considering the loss, dispersion and SPM.

According to the above analysis, we can conclude that

1. The loss effect limits the length of monitoring fiber within 69.05 km when the average injection power is limited at 9 mW.
2. If there is no any dispersion compensation exerted to reduce the pulse broadening effect and just consider the dispersion effect of β_2 by neglecting the loss and

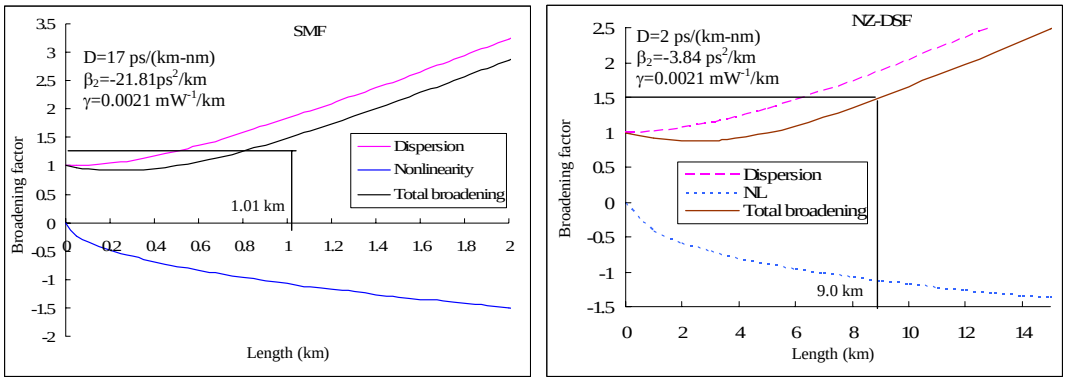

(a) (b)

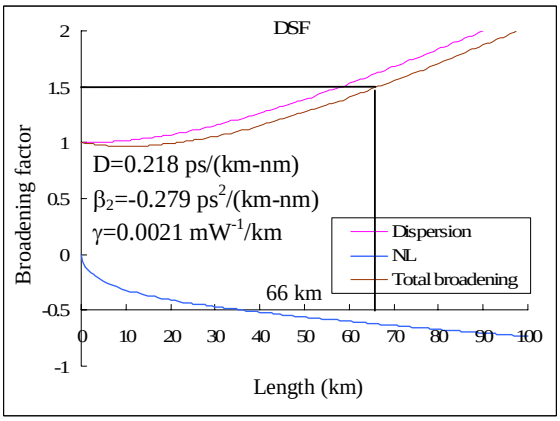

(c)

Fig.5.8 Broadening effect impacted by dispersion and SPM

nonlinearity, for single-mode fiber, NZ-DSF and DSF with some typical parameters, the maximum length of the monitoring fibers are 0.75 km, 6.3 km and 58 km, respectively. For the dispersion-shifted fiber with zero-dispersion wavelength near the wavelength of the light source, the effect of β_2, is very small and the potential dispersion effect from the third-order dispersion parameter β_3 was discussed, the result indicated that the broadening effect from β_3 is small enough to be neglected.

3. For nonlinear effect, by simultaneously considering the dispersion and nonlinear effect, the possible monitoring length for a SMF, a NZ-DSF, and a DSF are 1.01 km, 9 km and 66 km, respectively.

Therefore, the maximum length of monitoring fiber is estimated as long as 66 km in theory.

5.3.4 Relationship between pulse width effect on the sensitivity of optical pulse correlation sensor

According to the above discuss, it can be seen that the loss impact can be compensated by an EDFA and the maximum monitoring length can arrive at 69.05 km. Both the dispersion and nonlinear effect contribute to the pulse broadening, which will affect the sensitivity of the correlation sensing system. Therefore, it is necessary to discuss the broadening effect. As is discussed in chapter 2, the ratio between the peak of the correlation signal and the background should be 3:1 in theory. However, in the practical correlation sensing system, due to the limit of SHG efficiency, the ratio is around 2.7:1. Taking into this effect, the theoretical relationships between the correlation signal and time delay of the correlation unit with 7 ps and 20 ps time delay bias with different pulse width are simulated and shown in Fig.5.9 and Fig.5.10.

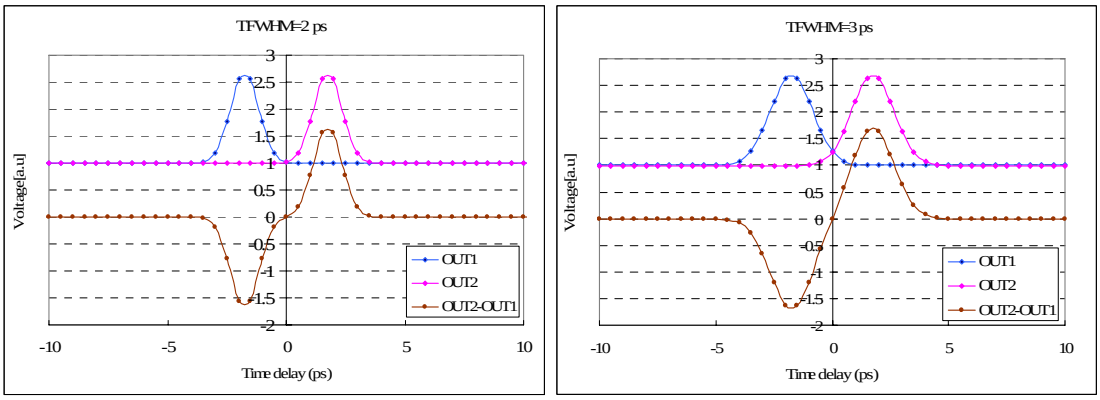

(a) (b)

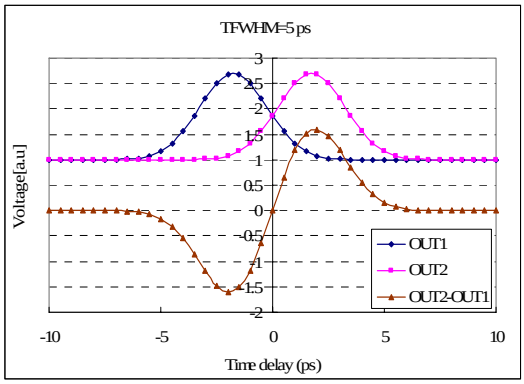

(c)

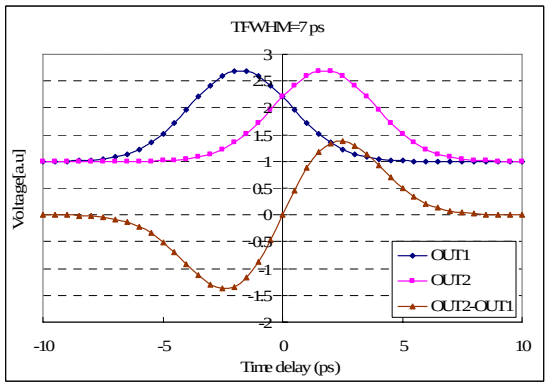

(d)

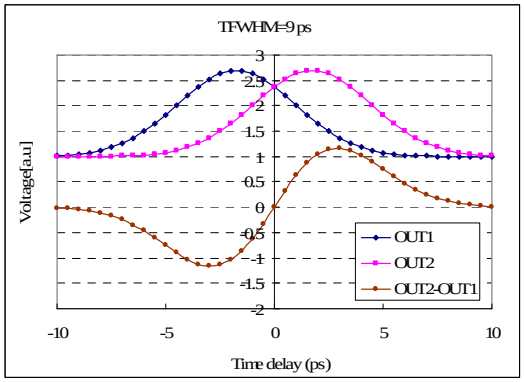

(e)

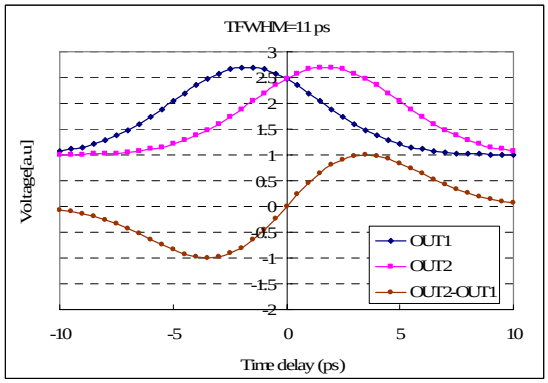

(f)

Fig.5.9 Correlation signal vs. time delay of 7 ps delay bias with different pulse width

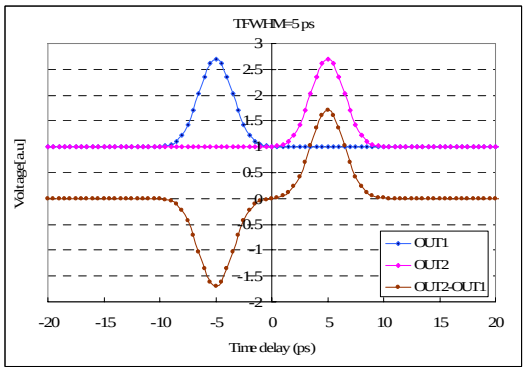

(a)

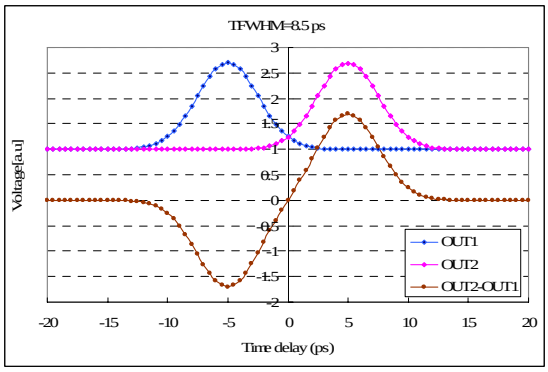

(b)

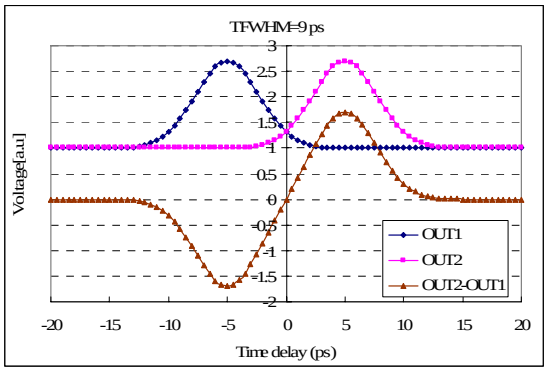

(c)

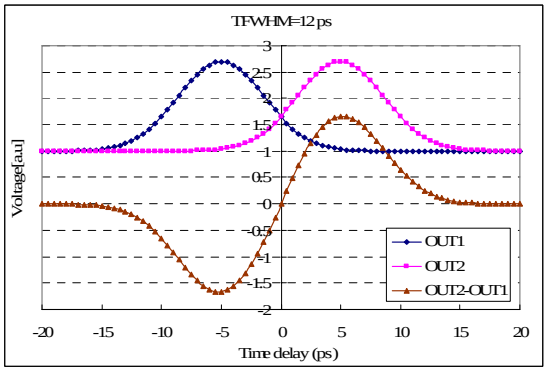

(d)

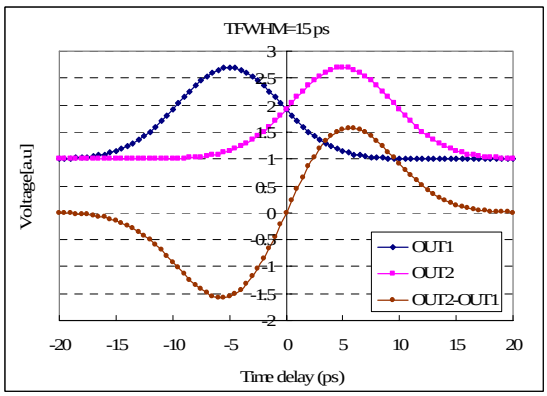

(e)

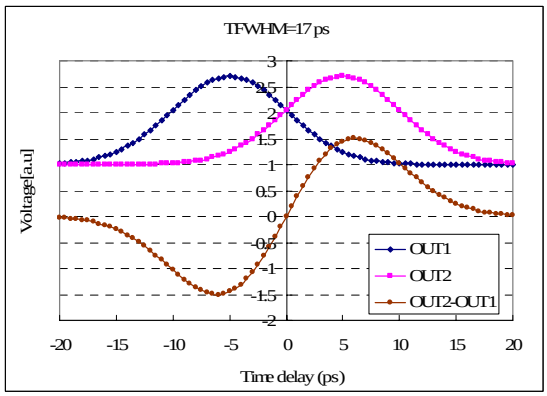

(f)

Fig.5.10 Correlation signal vs. time delay of 20 ps delay bias with different pulse width

According to the simulation result, it can be seen that the sensitivity is closely related to the pulse width of the monitoring beam. As a double-pass is constructed in the optical pulse correlation sensing system with birefringence fluctuation compensation, for the time delay bias of 7 ps and 20 ps, the time interval between the peaks of OUT1 and OUT2 are 3.5 ps and 10 ps, respectively. If the pulse width is too narrow such as T_{FWHM}=2.0 ps in Fig.5.8 (a) and T_{FWHM}=5.0 ps in Fig.5.9 (a), there is nearly no overlap between reference pulse and monitoring pulse. Therefore, it is impossible to realize the differential detection. And the sensitivity is equal to the case of single-channel monitoring. When the pulse width is larger than 3 ps and 8.5 ps as shown in Fig.5.9 (b) and Fig.5.10 (b), there will be overlap between two correlation signals in two channels.

With the pulse width increases, the sensitivity of the correlation sensor will be gradually increased and then decreases as shown in Fig.5.9 (c) (d), (e) and (f) and Fig.5.10(c), (d), (e) and (f) . For the correlation unit with time delay bias of 7 ps, when the pulse width of the monitoring signal is larger than 11 ps, the sensitivity will be decreased dramatically as shown in Fig.5.9 (f). In theory, for the correlation unit with a time delay bias of 20 ps, the signal pulse width as large as 35 ps is acceptable in the correlation sensing if there is no any limit in the repetition rate of the light source. However, in the correlation sensing system, a ML-LD with 20 GHz was used as the light source, which limits the pulse width of the monitoring pulse within 17.5 ps. For long-range measurement, the correlation unit with large time delay bias such as 20 ps should be used to obtain large measurement range. The limit to the pulse width of monitoring beam gives a confinement of the monitoring fiber length due to the dispersion effect. As discussed in the dispersion effect, if just consider the effect of β_2, for standard SMF and he dispersion-shifted fiber, the maximum length of monitoring fiber are 1 km and 69 km respectively. Fig.5.11 indicates the sensitivity changes with the pulse width of monitoring beam for two correlation units with time delay bias of 7 ps and 20 ps. The curves imply that at the beginning, with the increase of the pulse width the sensitivity of the sensing system increased. This is because the sensitivity is determined by the ratio between the difference of two correlation signals and the time interval between the peaks of two correlation signals. In the case of the fixed time delay bias, when the pulse width is very narrow, the decision is located near background. The difference of two correlation signals is mainly up to one channel due to the near static variation of another channel. At that time, the sensitivity is similar to one channel detection and the differential measurement can not take its advantages.

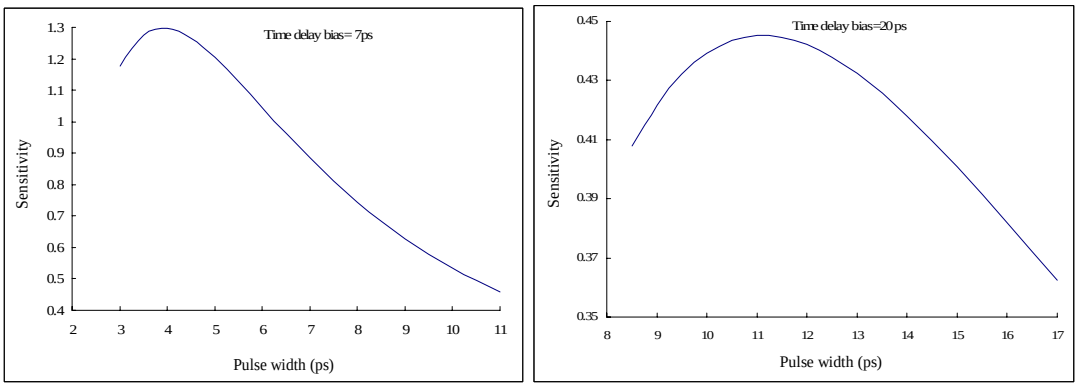

(a) (b)

Fig.5.11 (a) Sensitivity vs. pulse width in correlation unit with 7 ps delay bias

(b) Sensitivity vs. pulse width in correlation unit with 20 ps delay bias

With the increase of the pulse width, the decision point move upside gradually, and the difference between two correlation signals can reflect the variation of two channels and the differential detection begin to work. When the pulse width is 3.9 ps and 11.2 ps in Fig.5.11 (a) and (b), respectively, the sensitivity has the maximum of 1.2988/ ps and 0.5238 /ps, respectively. As indicated in chapter 2, the sensitivity of the correlation sensor is determined by the time delay bias as the correlation signal has the similar levels; the sensitivity of correlation unit with 7 ps delay bias is about three times of that of the correlation unit with 20 ps time delay bias. Therefore, for the measurement requiring high sensitivity, the time delay bias should be designed smaller, while for the measurement in which large measurement range is required, a large time delay bias should be used. If the pulse width is much wider, the decision point will move upside further, and the difference between two channels will decrease due to the similar variation of two correlation signals.

According to the simulation result shown in Fig.5.12, it can be seen that by considering the dispersion broadening and nonlinear effect, when the monitoring fiber length is less than 11 km, the SPM compensated the dispersion broadening in the optical pulse, so the

optical pulse width decreases with the monitoring fiber length increasing. Thus the sensitivity decreases. When the length of monitoring fiber is around 11 km, there is the narrowest pulse width, and the sensitivity has the minimum. When the monitoring fiber length is increased, the dispersion broadening effect is larger than that of the SPM compression. Therefore the pulse width will be increased and the sensitivity will be increased. Until the fiber length is around 49 km, the pulse width is around 11.2 ps, so that the sensitivity has the maximum. After that when the fiber length is increased, the pulse width is much larger so that the decision point will move upside, and the sensitivity will be reduced.

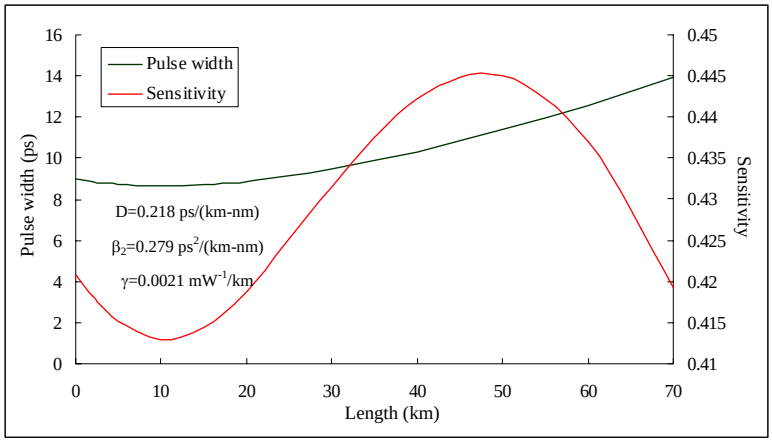

Fig.5.12 Variation of sensitivity with length

5.3.5 Experiment investigation with long monitoring fiber

In this section, the time drift sensitivities of the optical pulse correlation sensing system with monitoring fiber of length 30 km, 50 km and 60 km are investigated in experiment. The experiment configuration is shown in Fig.5.13. The power and pulse width of the optical beam in the case of monitoring fiber with a length of 30 km is shown in table 5.3.

In the experiment investigations, an EDFA with a S/N=20 dB at P_{in}=-20 dBm is used

after the circulator to compensate the loss in the long monitoring fiber. When the optical pulse passes through the 30 km DSF, the pulse width was broadening from 8.965 ps to 10.874 ps, which is slightly deviated from the estimated value in theory, the possible reasons are the GVD resulted from the slight deviation of the light source wavelength

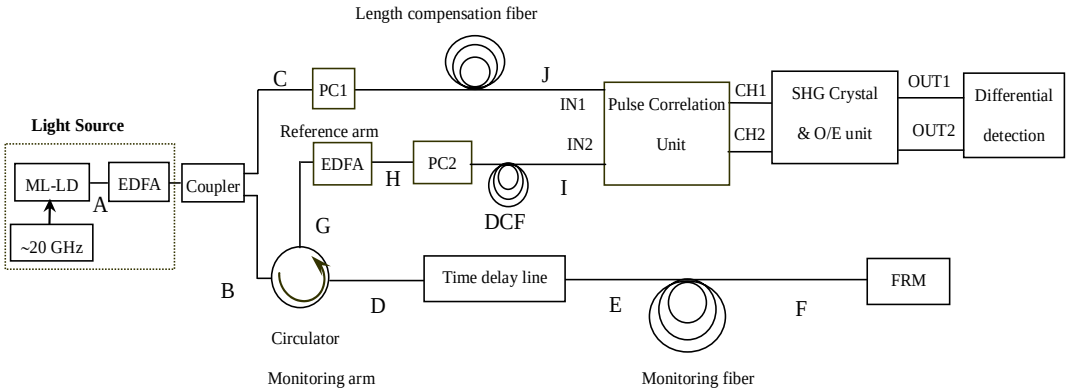

Fig.5.13 Schematic configuration of correlation sensor with long monitoring fiber

Table 5.3 Power and pulse width at each point

Location	Power (mW)	Pulse width (ps)
A	0.4512	8.965
B	10.517	8.965
C	4.989	9.629
D	8.815	8.882
E	8.176	8.965
F	1.665	10.874
G	0.2294	12.532
H	6.436	16.516
I	3.346	10.791
J	3.402	9.38
K	3.402	9.38

from the zero-dispersion wavelength of the DSF and the chirp form the light source. The same situation occurs when the optical signal returned from the FRM to the circulator output port. After passing through an EDFA, the monitoring signal was

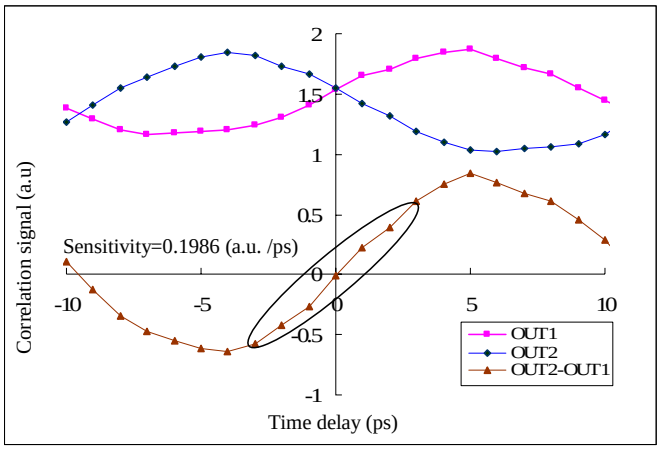

Fig.5.14 Time delay vs. correlation signal for L=30 km without dispersion compensation

broadened again. As the parameters used in Fig.5.12 are the typical value of the DSF instead of the accurate value, the pulse width of correlation signal after 30 km is different from the theoretical estimation.

The sensitivity of the experiment is estimated as 0.1986 a.u./ps as shown in Fig.5.14, which is much less than the theoretical value due to the big difference between the reference pulse width and monitoring pulse width. To balance the pulse widths between reference beam and monitoring beam, dispersion compensated fiber was used. The relationship between the time drift and correlation signal is shown in Fig.5.15, in which sensitivity around 0.427 a.u./ps was obtained, which accords well with the theoretical sensitivity of 0.431 a.u./ps when the pulse width is 10.791 ps.

Fig.5.16 (a) and (b) illustrate the relationship between the time delay and the correlation signal when L=50 km and L=60 km, respectively. It can be seen that when the monitoring fiber is as long as 50 km and 60 km, the ratio between the peak and the background of the correlation signal are much less than 3:1, which causes to the large

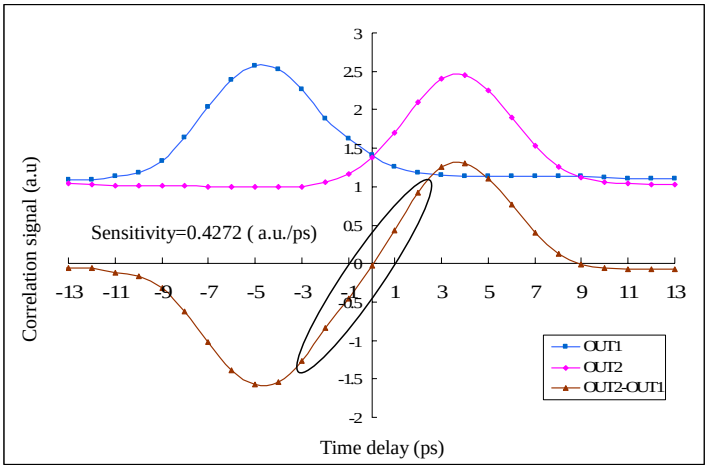

Fig.5.15 Time delay vs. correlation signal for L=30 km with dispersion compensation

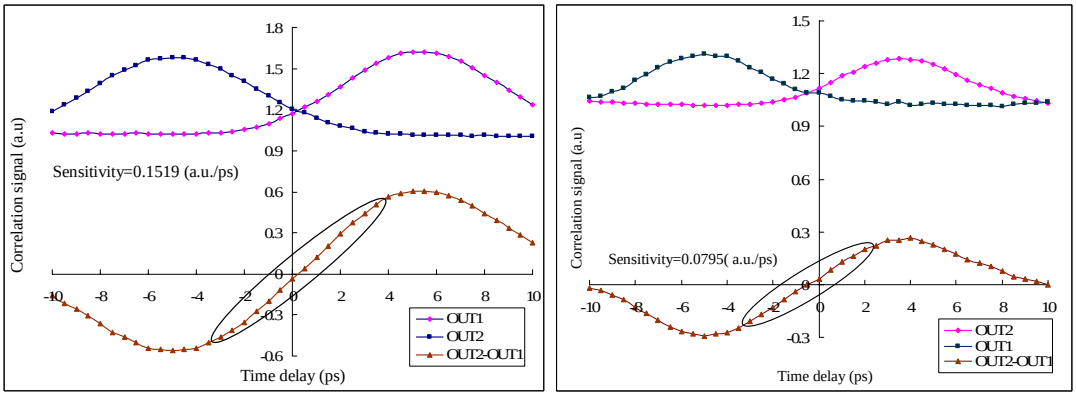

(a) (b)

Fig.5.16 Time delay vs. correlation signal for L=50 km and L=60 km

deviation of the sensitivity in experiment from the theory. The mainly reason is the lager pulse width of the monitoring beam due to the dispersion effect in the DSF and the larger amplification frequency range of the EDFA for loss compensation. If a filter with narrow bandwidth is used after the EDFA, the ratio between the peak and background of the correlation signals and the sensitivity of the optical pulse correlation sensing system are expected to be enhanced.

According to the above experiments, although the sensitivity of the optical pulse correlation sensing system is not large, when L=60 km, the sensing is available. By

inserting a filtering technique, the monitoring fiber length as long as 60 km with higher sensitivity is available to be realized.

5.4 Summary

In this chapter, the performance of the optical pulse correlation sensing system in the long-range measurement was discussed in theory and experiment. According to the theoretical analysis, the possible length of single-mode fiber and NZ-DSF are estimated as long as 1 km and 9 km, respectively. If the loss compensation was considered by using an EDFA with a minimum input power -30 dBm and S/N larger than 20 dB, the possible monitoring length around 66 km was estimated in theory. The time drift sensitivity of the optical pulse correlation sensing system with monitoring fiber lengths of 30 km, 50 km and 60 km were investigated in experiments. The corresponding time drift characteristics were successfully obtained, which indicated that the monitoring fiber length as long as 60 km is available to be realized.

Chapter 6

Conclusions

A optical pulse correlation sensing system based on the time drift monitoring of an optical signal was developed in this work. According to the measured time drift generated in the optical fiber due to the change of environment conditions such as the temperature, strain or pressure around the optical fiber, the corresponding environment conditions monitoring is realized. The optical pulse correlation sensing system is not only able to detect the physical quantities change such as temperature, strain or pressure with high sensitivity, but also it can indicate the change direction of the physical quantities according to the sign of the differential signal between two correlation signals. Moreover, since the optical pulse correlation sensor is not required the special fiber as the monitoring fiber, the optical fiber transmission line is available to be used to long-range monitoring such as slope collapse and ocean temperature measurement with real-time. The development of optical pulse correlation sensor offers a new method for high-sensitive sensing and real-time optical fiber remote sensing.

Chapter 2 proposed the concept of optical pulse correlation sensing based on the optical pulse correlation measurement. The theoretical analysis of the optical pulse correlation sensor was carried out and the related characteristics were discussed. As the sensitivity and dynamic range are determined by the ratio of the correlation signal and the time delay bias, we can obtain a high-sensitive sensor by using a short time delay bias and enlarge the measurement range by making the time delay bias larger. Therefore,

according to the requirement of practical measurement, the high-sensitivity and long-range monitoring can be realized respectively.

The mechanism and the fundamental characteristics of the optical pulse correlation sensor were explained in chapter 3 in detail. By using the differential detection of two correlation signals in orthogonal polarization planes, the background in the SH signal was eliminated and a time resolution as high as 0.04 ps was obtained by using the correlation unit with 7 ps time delay. The temperature and strain characteristic investigation results indicated the high-sensitive sensing ability of the optical correlation sensor to the temperature and strain around the optical fiber transmission lines with high sensitivity. As the sensor is sensitive to temperature and strain simultaneously, the discrimination measurement of temperature and strain is discussed in theory. During the temperature experiments, the fluctuation caused by the birefringence fluctuation in the single-mode fiber was observed due to the sensitivity of the correlation signal to the polarization state change of the monitoring signal. Therefore, it is necessary to compensate the birefringence fluctuation.

By improving the sensing system structure, the optical pulse correlation sensing system with the birefringence fluctuations compensation was proposed in chapter 4. The compensation of birefringence fluctuation method by using a retracing beam was introduced into the optical pulse correlation sensing system and a double-pass monitoring was constructed due to the reflection of FRM. As a result, besides the compensation of correlation signals fluctuation caused by the birefringence fluctuation, the sensitivity of the sensing system was nearly doubled by virtue of the double-pass monitoring. By using an optical pulse correlation unit with 20 ps time delay bias, the temperature change outside of lab was successfully measured.

Chapter 5 theoretically and experimentally investigates the performance of the optical pulse correlation sensing system in long-range measurement. According to the theoretical analysis, the length of monitoring fiber is mainly limited by the loss, dispersion and nonlinear effect. It is fortunate that the dispersion effect can be compensated by using a DSF, the nonlinear effect can be minimized by reducing the injection power into the monitoring fiber, and the corresponding loss compensation by using an EDFA is available. Therefore, a long-range monitoring as long as 66 km is estimated in theory. Since the dispersion can not be completely reduced due to the unavailability of absolute monochromatic light source. Thus the reduced dispersion will give some impact on the performance of the correlation sensor. So the dispersion effect on the sensitivity was investigated by numerical simulation, which indicated that the sensitivity will be degraded if the pulse was broadened much. This result is much helpful for determining the related parameters of the monitoring fiber, especially in the case of single-mode fiber without dispersion shifting. Finally, the time drift sensitivity of the optical pulse correlation sensing system with long monitoring fiber was investigated in theory by using an EDFA with 25 dB gain, 20 dB S/N at input power -20 dBm to compensate the loss impact in a DSF. The result confirms the available monitoring length of the optical pulse correlation sensor is as long as 60 km.

The work in this research successfully developed an optical pulse correlation sensing system based on the optical pulse correlation concept which is completely different from the conventional sensors. The experimental results confirmed the performance of the correlation sensor in the real-time, high-sensitivity measurement with long-range sensing ability.

Acknowledgement

I would like to express my sincere gratitude to my advisor, Professor Koji Nonaka, for his patient guidance and encouragement throughout the research. His technical and editorial advice was essential to the completion of this dissertation. Words are too limited to express my appreciation to Professor Koji Nonaka not only for his guidance in research but also for his help in life.

Especial and sincere thanks is given to my vice advisor, Prof. Iwashita, who gave me much valuable advice and provide me with the convenience of some instruments during this work. I would also like to thank Prof. Hiroshi Kanbe, Prof. Masahiro Kimura, and Associate Hiroshi Furusawa as the members of my committee and for their valuable suggestions. I also specially acknowledged to Prof.Kanbe, who gave me so much help in my experiment by offering some important instuments.

Prof.Takashi Kurokawa, and Dr. Tatsutoshi Shioda in Tokyo University of Agriculture and Technology are sincerely acknowledged for their valuable discussion and advice.

The deep appreciation is also expressed to my advisor of Master degree, Prof.Libo Yuan and senior Dr.Jun Yang for their advice and encouragement. I also sincerely express my sincere thanks to my dear friends Ms. Ai Zhou, Mr. Yinlai Jiang, and Mr. Xueyuan Zhang for their help and encouragement when I was in the difficult time.

I would like to thank all my colleagues and friends at the Nonaka group, especially Mr. Charoen Tangtrongbenchasil, Mr. Hiroshi Mizuno, Mr.Toshinori Suzuki, for their help in the research and life.

I also thank to the support of SSP of KUT and Gakusyu Shoreihi Scholarship.

My sincerely thanks but not the last belong to my dear parents and my younger brother for their love and supports.

References

[1] K. Osaka, T. Kosaka, et.al, “Effects of pressure on measurement of strains in EFPI optical .fiber sensors embedded in FRP laminates”, *Adv .Composite Mater*. **10,** 169–176, 2001

[2] E.A. Zak and N.P. Kravchenko, “Industrial applications of amplitude-type fiber-optic sensors”, *Measurement Techniques*. **34,** 1211-1214, 1991

[3] O.S. Wolfbeis, B. Kovács, K. Goswami, S.M. Klainer, “Fiber–optic fluorescence carbon dioxide sensor for environmental monitoring”, *Microchemica Acta*. **129,** 181-188, 1998

[4] P.V. Preejith, C.S. Lim, A. Kishen, M.S. John, A. Asundi, “Total protein measurement using a fiber optic evanescent wave-based biosensor”, *Biotechnology Letters*. **25,** 105–110,2003

[5]Daniele Inaudi, “Overview of fibre optic sensing to structural health monitoring applications”, *ISISS'2005, International Symposium on Innovation & Sustainability of Structures in Civil Engineering*, Nanjing, China, November 20-22, 2005

[6] Kazuo Hotate, “Fiber-optic gyros”, *Optics & Laser Technology***. 25,** 262, 1993

[7] S.Kato et.al “Investigation on road slop monitoring system by using optical fiber sensing technology”, Japan Road Association Meeting, 2001

[8] R.O.Cook and C.W.Hamm, Fiber optic lever displacement transducer, *Appl. Opt* 18, 3230-3241, 1979

[9] Lagakos, Nicholas; Cole, J. H.; Bucaro, J. A.,” Microbend fiber-optic sensor”, *Appl. Opt*, Vol. **26**, 2171-2180, 1987,

[10] Sung-Hoon Jung, Dong-Ho Lee, Kwang-Hee Kwon, and Jae-Won Song,” Water sensor using macrobending-sensitive fiber for real-time submersion monitoring”, *Opt.Comm*., Vol. **260**, Issue 1, 105-108, 2006

[11] Chuan Li, Yi-mo Zhang, Hui Liu, Sheng Wu and Cai-wen Huang, “Distributed fiber-optic bi-directional strain–displacement sensor modulated by fiber bending loss”, *Sensors and Actuators A: Physical* ., Vol.**111**, Issues 2-3, 236-239, 2004

[12] J.Deng, “development of novel optical fiber interferometric sensors with high sensitivity for acoustic emission detection”, PhD. Thesis. *Virginia Polytechnic Institute and State University*, 2004.

[13] J.D.C.Jones, “Interferometry and polarimetry for optical sensing”, *Handbook of optical fiber sensing technology*, John Wiley & Sons Ltd 228 2002

[14] A. Dandridge and A. D. Kersey, “Overview of mach-Zehnder sensor technology and applications”, *Proceedings of SPIE, Fiber Optic and Laser Sensors VI*, Boston, Sept. 985 1988.

[15] V.Vail,R.W.Shorthill, “Fiber ring interferometer”, *Appl. Opt.* **15** 1099-1100, 1976

[16] T. Li, A. Wang, K. Murphy, and R. Claus, "White-light scanning fiber Michelson interferometer for absolute position-distance measurement," *Opt. Lett.* **20**, 785- (1995)

[17] T. K. Lim, et al., ‘fiber optic acoustic hydrophone with double Mach-Zehnder interferometers for optical path length compensation’, *Optics Communicatons*.. **159**, 301, 1999

[18] Habel W. & Hofmann D, “Determination of Structural Parameters Concerning Load

Capacity Based on Fiber Fabry-Perot-Interferometers", *Proc. SPIE,* Vol. **2361**, pp. 176-179,1994

[19] N. Furstenau et al., 'Extrinsic Fabry-Perot Interferometer Fiber-Optic Microphone', IEEE Trans. Intrum. Measurement, Vol. 47. No. 1 138(1998)

[20] V. Bhatia, K.A. Murphy, R.O. Claus, M.E. Jones, J.L. Grace, T.A. Tran, J.A. Greene, "Optical fibre based absolute extrinsic Fabry-Perot interferometric sensing system", Meas. Sci. Technol. **7**, 58–61, 1996

[21] Markus Schmidt, BerndWerther, and Norbert Fürstenau, "Fiber-Optic Extrinsic Fabry-Perot Interferometer Strain Sensor with < 50 pm displacement resolution using three-wavelength digital phase demodulation", *Optics Express*, Vol. **8**, No. 8, 475-480, 2001

[22] Markus Schmidt, BerndWerther, and Norbert Fürstenau, "Fiber-Optic Extrinsic Fabry-Perot Interferometer Strain Sensor with < 50 pm displacement resolution using three-wavelength digital phase demodulation", *Optics Express*, Vol. **8**, No. 8, 475-480, 2001

[23] Y.J.Rao, J.Jiang, and C.X.Zhou, "Spatial-freuqency-multiplexed fiber-optic Fizeau strain sensor system with optical amplification", *Sens.Actuat.A* 120, 354-359, 2005

[24] D.Donglagic, E.Cibula,"All-fiber high-sensitivity pressure sensor with SiO_2 diaphragm", Opt.Lett. 30, 2071-2073, 2005

[25] G.Meltz, W.W.Morey, W.H.Glenn, "Formtion of Bragg gratings in optical fibers by a transverse holographic method", *Opt. Lett.* 14, 823-825, 1989

[26] Byoungho Lee, Review of the present's status of optical fiber sensors *Optical Fiber Technology* **9**. 57-79, 2003

[27] W.W. Morey, Distributed fiber grating sensors, in: Proceedings of the 7th International Conference on Optical Fibre Sensors, IEEE, Sydney, Australia, 285–288, 1990

[28] Y.J.Rao, "Fiber Bragg grating sensors: principles and applications", in: K.T.V.Grattan, B.T.Meggitt (Eds.),*Optical Fiber Sensor Technology,* Chapman & Hall, London, Vlo.2, 355-389, 1998

[29] W.W. Morey, Distributed fiber grating sensors, in: Proceedings of the 7th International Conference on Optical Fibre Sensors, IEEE, Sydney, Australia, 285–288, 1990

[30] Volanthen, M., Geiger, H., Cole, M. J., Laming, R. I. and Dakin, J. P,"*Low coherence technique to characterise reflectivity and time delay as a function of wavelength within a long fibre grating"* , *Electron. Lett.*, 32 (8). 757-758, 1996

[31] Peng-Chun Peng, Jia-He Lin, Hong-Yih Tseng, and Sien Chi," Intensity and wavelength-division multiplexing FBG sensor system using a tunable multiport fiber ring laser", *IEEEPhotonicsTechnology Letters*, Vol. 16, Issue 1, 230 – 232, 2004

[32] H. Igawa, H. Murayama, T. Kasai, I. Yamaguchi, K. Kageyama, K.Ohta, Measurement of strain distribution with a long gauge FBG sensor using optical frequency domain reflectometry *OFS-17 Conference (Bruges, Belgium).* 547-549, 2005

[33] H. Yokosuka, S. Tanaka, N. Takahashi High-sensitive fiber Bragg grating vibration sensor using

intensity-modulated laser source, *OFS-17 Conference (Bruges, Belgium).* 731-734, 2005

[34] M. Seaver, S.T.Trickey, and J.Nichols, Strain measurements from FBGs embedded in rotating composite propeller blades, *OFS-18 Conference (Cancun, Mexico)*, ThD2, 20066

[35] S. Chung, J. Kim, Bong-Ahn Yu, and Byoungho Lee, A fiber Bragg grating sensor demodulation technique using apolarization maintaining fiber loop mirror, *IEEE Photonics Technology Letters,* 13, 1041-1135**,** 2001

[36]X.Bao, D.J.Webb, and D.A.Jackson, "22-KM distributed temperature sensor using Brillouin gain in an optical fiber", *Opt.Lett.*, Vol.18, No.17, 552-554, 1993

[37] Koyamada, Y.; Sakairi, Y.; Takeuchi, N.; and Adachi, S, "Novel Technique to Improve Spatial Resolution in Brillouin Optical Time-Domain Reflectometry**",** *IEEE Photon.Technol.Lett.* **19** 1910-1912, 2003

[38] K. Uchiyama, K. Nonaka, H. Takara, "Subpicosecond timing control using optical double-pulse correlation measuremen", *IEEE Photon. Technol. Lett.***16**, 626-628, 2004

[39] K. Nonaka, M. Sako, T. Suzuki, "Optical pulse time drift sensing for fiber delay monitoring using pulse correlation and differential detection", *OFS-17 Conference (Bruges, Belgium).* 76-79, 2005

[40] H. B. Song, K. Nonaka, "A novel stable and high-sensitivity fiber strain sensor based on optical pulse correlation measurement", *International Conference on Smart Materials and Nanotechnology in Engineering*, Harbin, China, 2007

[41] E. B. Li , J. Xi and J. F. Chicharo, "Characteristics of a UV beam generated by a frequency doubled Ar-ion laser", *Optics Communications*, 234 329-335,2004

[42] S. A. Mitchell, M. Mehendale, D. M. Villeneuve and R. Boukherroub, "Second harmonic generation spectroscopy of chemically modified Si surfaces". *Surface Science.,* **488,** 367-378, 2001

[43] G. COX, E.Kable, A. Jone, I. Fraser, F. Manconi and M. D. Gorrell, "3-Dimensional imaging of collagen using second harmonic generation", *Journal of Structural Biology*., **141**, 53-62, 2003

[44] N. J. Vasa, Y. Kawata, R. Tanaka and S. Yokoyama, "Development of an electric field sensor based on second harmonic generation with electro-optic material", *Journal of Material Processing Technology*., **185**, 173-177, 2007

[45] S. L. Shapiro, *Ultrashort light pulses : picosecond techniques and applications*, Springer-Verlag, Berlin ; New York , pp 83-93, 1977

[46] W. A. Lopes, M. O. Morales, M. A. Rieffel, J. A. Giacoletti, J. T. Thorpe and L. A. Westling, "Intensity autocorrelation measurements of an AlGaAs diode laser", *Opt.Lett*., **18**, 820-822, 1993

[47] Amnon Yariv, *Optical electronics in modern communication*, Oxford series in electrical and computer engineering, pp 286, 1997

[48] http://www.rp-photonics.com/phase_matching.html

[49] Gopel, J. Hesse, J. N. Zemel, *Sensors: a comprehensive survey*, New York Basel. Cambridge, pp342, 1998

[50] J.A.Giordmaine, P.M.Rentzepis, S.L.Shapiro, and K.W.Wecht, ""Two Photon Excitation of fluorescence by picosecond light pulses", *Appl.Phys. Lett.*, 11, 216, 1967

[51] S. K. Sudheer, S. Vijay Shuklaa, S. M. Oak, R. Arya, and V. P. N. Nampoori, "Characterization of a pulse width tunable picosecond Nd:YAG laser", *Journal of Optoelectronics and Advanced Materials*., Vol. **4**, No. 4, p. 893 – 899,2002

[52] Amnon Yariv, "Optical electronics in modern communications" 5th edition., Maruzen Co., Ltd., 235-239, 2000

[53] H. B. Song, T. Suzuki, M.Sako and K.Nonaka, "High time resolution fiber optic sensing system based on optical pulse correlation and differential technique", *Meas. Sci. Technol.,* **17,** 631-634, 2006

[54] E. De la Rosa, L. A. Zenteno, A. N. Starodumov, and D. Monzon,"All-fiber absolute temperature sensor using an unbalanced high-birefringence Sagnac loop **",** *Opt.Lett.*, Vol.**22**, No.7, 1997

[55] Y. Chen, and H.F.Taylor "Multiplexd fiber Fabry-Perot temperature sensor system", *Opt. Lett.*, Vol.**27**, No.11, 903-905, 2002

[56] Michael L. Dennis et. al, "Grating sensor array demodulation by use of a passively mode-locked fiber laser ", *Opt.Lett.*, Vol.**22**, No.17, 1362-1364, 1997

[57] T.Coroy, and R.M.Measures, "Active wavelength demodulation of a Bragg grating fiber optic strain sensor using a quantum well electroabsorption filtering detector", *Electron.Lett.*, **32**, 1811-1812,1996.

[58] J. Yang,"Research on distributed fiber-optic white light interferometric deformation measuring technique", PhD. Thesis, Harbin Engineering University, 2005

[59] Farahi. F, Webb. D. J, Jones. J. D. C, and Jackson. D. A, "Simultaneous measurement of temperature and strain: cross-sensitivity considerations", *J. Lightwave Tech***.,** **8**, 138-142,1990

[60] S.C.Rashleigh, W.K. Burns, R.P.Moeller, and R.Ulrich, "Polarization holding in birefringence single-mode fibers", Opt.Lett., Vol**.7**, 40-42, 1981

[61] V.Ramaswamy, R.Standley, D.Sze, and W.G.French, "Polarization effects in short length single mode fibers", Bell syst.Tech., J.**57**, 635-651, 1978

[62]Gregory D.VanWiggeren and Rajarshi Roy, "Thansmission of linearly polarized light through a single-mode fiber with random fluctuations of birefringence", Applied Optics., Vol.**38**, No.18, 3888-3892,1999.

[63]E,Giese, K.Schatazel, and E.O.Schulz-Dubois, "single-loop polarization stabilization for single-mode fiber", *Opt.Lett*., Vol**.7**, No.7, 337-338, 1982

[64] R. Ulrich, S. C. Rashleigh,* and W. Eickhoff, **"**Bending-induced birefringence in single-mode fibers", Opt.Lett., Vol.**5**, No.6, 273-275, 1980

[65] D. W. Stowe, D. R. Moore, and R. G. Priest, "Polarization fading in fiber interferometeric sensors", *IEEE J. Quantum Electron*., **QE-18**, 626-665, 1982

[66] A.D.Kersey, M.J.Marrone,"Input-polarization scanning technique for overcoming polarization-

induced signal fading in interferometric sensors", *Elec. Lett.* **24,** 931-933,1988.

[67] W. C. Scott and M. de Wit, "Birefringence compensation and TEM_{00} mode enhancement in a Nd:YAG Laser," *Appl. Phys. Lett.* **18**, 3-4 (1971)

[68] R.Ulrich, "Polarization stabilization on single-mode fiber", Appl.Phys.Lett., Vol.**35**, No.11, 840-842, 1979

[69] Ashish M. Vengsarkar, Qian Zhong, Daryl Inniss, W. A. Reed, Paul J. Lemaire, and S. G. Kosinski, "Birefringence reduction in side-written photoinduced fiber devices by a dual-exposure method", Opt.Lett., Vol.**19**, No.16, 1260-1262, 1994

[70] D.-X. Xu, P. Cheben, D. Dalacu, A. Delâge, S. Janz, B. Lamontagne, M.-J. Picard, and W. N. Ye," Eliminating the birefringence in silicon-on-insulator ridge waveguides by use of cladding stress", Opt.Lett., Vol.**29**, No.20, 2004

[71] M. Martinelli, "A universal compensator for polarization changes induced by nonlinear on a retracing beam", *Opt. Commu.* **72,** 341-346, 1989

[72]A. D. Kersey, M. J. Marron, M. A. Davis, "Polarization-insensitive fiber optic Michelson interferometer," *Electron. Lett.* **27,** 518-520, 1991

[73] L. A. Ferreira, J. L. Santos,F. Farahi, "Polarization insensitive fiber-optic white-light interferometry," *Opt. Commu.*, **114,** 386-392, 1995

[74] D. Moteki,C. Samuel,T. Shioda, Y. Tanaka, T. Kurokawa Polarization-insensitive measurement by fiber optic interferometer with faraday rotator elements." in 11th *Microoptics Conference (MOC`05)*, Tokyo 112-116, 2005

[75] T. Okoshi, Y. H. Cheng, and K. Kikuchi, Electron. Lett. "New polarization-control scheme for optical heterodyne receiver using two Faraday rotators", *Electron. Lett.*, **21**, 787 (1985).

[76] H.B.Song, T. Suzuki, T.Fujimura, K. Nonaka, T.Shioda and T. Kurokawa , "Polarization fluctuation suppression and sensitivity enhancement of an optical correlation sensing system" *Measurement Science and Technology*., **18**, 3230-323, 2007

[77] S.Kato et.al "Investigation on road slop monitoring system by using optical fiber sensing technology", Japan Road Association Meeting, 2001 [In Japanese]

[78] K.Fujihashi et.al. "Prevention of disaster by using optical fiber sensing technology", http://www.ntt.co.jp/journal/0709/files/jn200709052.pdf, 2007 [In Japanese]

[79] S.Miki, "Development of rock bed and slope risk management technology", *Projector report of Civil Engineering*,2002. [In Japanese]

[80] K. Fujihashi, T. Aoki, K. Okutsu, K. Arai, T.Komori, H. Fujita, Y. Kurosawa, Y. Fujinawa, and K. Sasaki:"Development of Seafloor Seismic and Tsunami Observation System", *Underwater Technology and Workshop on Scientific Use of Submarine Cables and Related Technologies*, TB3.2, pp. 349-355, 2007.

[81] Intergovernmental Program on Climate Change, *ClimateChange 1995: The Science of Climate*

Change, the Contribution of Working Group 1 to the Second Assessment Report of the Intergovernmental Panel on Climate Change (Cambridge Univ. Press, Cambridge, UK, 1996

[82] CLIVAR, *CLIVAR Science Plan*, World Climate Research Programme, WCRP-89 (WMO/TD NO. 690), 1995

[83] National Research Council, *Global EnvironmentalChange: Research Pathways for the Next Decade* (National Academy Press, Washington, DC, 1999

[84] N.C.Wells, W.J.Gould, and A.E.S.Kemp, "The role of Ocean circulation in the changing climate", Oceanography edited by C.P.Summaerchayes and S.A.Thorpe, Manson Publishing Ltd, 41-42, 1996

[85] Govind P. Agrawal, "Signal propagation in fibers", *Light wave technology telecommunication systems*, A JOHN WILEY and SONS, Inc., 66-104, 2005

[86] G.P.Agrawal, *Nonlinear Fiber Optics*, 3rd ed., Academic Press, San Diego, CA 2001

[87] G.P.Agrawal, *Applicatins of Nonlinear Fiber Optics*, Academic Press, San Diego, CA 2001

[88] M. Morin, M. Piche and R. Tremblay," Active mode-locking through loss modulation: Chirped pulse solutions", *Optics Communications*, Volume 68, Issue 3, 213-219, 1988

[89] Djafar K. Mynbacy, and Lowell L. Scheiner, "Nonlinear Effects in a Single mode Fiber", *Fibe-Optic Communications Technology*, Pearson Education Inc., 202-204, 2002

[90] G.P.Agrawal, *Fiber-optic Communication Systems*, 3rd ed., Wiley New York, 2002.

Appendix A

Abbreviations and Symbols

OTDR: Optical time domain reflectometer

BOTDR: Brillouin optical time domain reflectometer

MZI: Mach-Zehnder interferometer

FOG: Fiber optic gyroscope

FPI: Fabry-Perot interferometer

WLI: White light interferometer

EFPI: Extrinsic Fabry-Perot interferometer

FBC: Fiber Bragg grating (FBG)

SHG: Second-harmonic generation

TPF: Two-photon fluorescence

CCD: Charge-coupled device

ML-LD: Mode-locked laser diode

EA: Electric absorption

EDFA: Erbium-doped fiber amplifier

RF: Ratio frequency

PBS: Polarization beam splitter

HM: Half mirror

PC: Polarization controller

KTP:Potassium Titany Phosphate

APD: Avalanche photon diode

FRM:Faraday rotator mirror

SOP: State of polarization

SMA:Simple moving average

NLS: Nonlinear Schrodinger

GVD: Group-velocity dispersion

NZ-DSF:Non-zero dispersion-shifted fiber

DSF: Dispersion-shifted fiber

FWHM: Full width at half-maximum

SPM: Self-phase modulation

XPM: Cross-phase modulation

FWM: Four-wave mixing

SRS: Stimulated Raman scattering

SBS: Stimulated Brillouin scattering

Appendix B

Signal propagation in fibers

In chapter 5, we just give the conclusions about the nonlinear Schrodinger (NLS) equation. The derivation in detail shown in the following originates from "*Light wave]technology telecommunication systems*" by Govind P. Agrawal in chapter 3: Signal propagation in fibers, published by A JOHN WILEY and SONS, Inc., 66-104, 2005.

When an optical signal from the transmitter is launched into a single-mode fiber, it excites the fundamental HE_{11} mode of the fiber, and its transverse spatial distribution does not change during propagation. Thus the electric field associated with the optical bit stream can be written as

$$\vec{E}(\vec{r},t) = \mathrm{Re}[\hat{e}F(x,y)A(z,t)\exp(i\beta_0 z - i\omega_0 t)] \qquad (1)$$

Where $\hat{e}$ is the polarization unit vector, *F(x,y)* is the spatial distribution of the fundamental fiber mode, *A(z,t)* is the complex amplitude of the field envelope at a distance *z* inside the fiber, and β_0 is the mode-propagation constant at the carrier frequency ω_0. The polarization unit vector $\hat{e}$ changes in a random fashion along the fiber because of a small but fluctuation birefringence. Here, such birefringence effects will be ignored and treat $\hat{e}$ as a constant. Since *F(x,y)* does not depend on z, the only quantity that changes with propagation in Eq.(1) is the complex amplitude *A(z,t)* associated with the optical signal shown.

As the frequency component of the optical field propagates in a single-mode fiber with a slightly different propagation constant, it is useful to work in the spectral domain. The Fourier transform of *A(z,t)* is

$$A(z,t) = \frac{1}{2\pi}\int_{-\infty}^{\infty} \tilde{A}(z,\omega)\exp(-i\Delta\omega t)d(\Delta\omega) \qquad (2)$$

Consider a specific spectral component $A(\tilde{z},\omega)$. It propagates inside the optical fiber with the propagation constant $\beta_p(\omega)$ that is different from β_0 appearing in Eq.(1). Thus the phase shift can be written as

$$\tilde{A}(z,\omega) = \tilde{A}(0,\omega)\exp[i\beta_p(\omega)z - i\beta_0 z] \qquad (3)$$

Where $\tilde{A}(0,\omega)$ is the Fourier transform of the input signal *A(0,t)* at *z*=0.The propagation constant β_p is, in general, complex and can be written in the form

$$\beta_p(\omega) = [\bar{n}(\omega) + \delta_{nNL}(\omega)](\omega/c) + i\alpha(\omega)/2 \qquad (4)$$

Where $\bar{n}$ is the effective mode index and α is the attenuation constant responsible for fiber losses. The nonlinear effects are included through δn_{NL} that represents a small power-dependent change in the effective mode index.

Pulse broadening results from yes frequency dependence of the mode index $\bar{n}$. Since the exact functional form of this dependence is not known in general, it is useful to write the propagation constant β_p as

$$\beta_p(\omega) = \beta_L(\omega) + \beta_{NL}(\omega) + i\alpha(\omega_0)/2 \qquad (5)$$

Where $\beta_L(\omega) = \bar{n}(\omega)\omega/c$ is its linear part, βNL is the nonlinear part and α is the fiber-loss parameter. Usually α and β_{NL} can be treated as frequency-in dependent over the signal bandwidth and expand $\beta_L(\omega)$ in a Taylor series around ω_0. If we retain terms up to third order, we obtain

$$\beta_L(\omega) \approx \beta_0 + \beta_1(\Delta\omega) + \frac{\beta_2}{2}(\Delta\omega)^2 + \frac{\beta_3}{6}(\Delta\omega)^3 \qquad (6)$$

The three dispersion parameters appearing in this equation are known in practice for any fiber used for signal transmission.

Physically, the parameter β_1 is related inversely to the group velocity v_g of the pulse as $\beta_1 = 1/v_g$. β_2 and β_3 are known as the second- and third-order dispersion parameters and are responsible for pulse broadening in optical fibers. More specifically, β_2 is related to the dispersion parameter D as

$$D = \frac{d}{d\lambda}\left(\frac{1}{v_g}\right) = -\frac{2\pi c}{\lambda^2}\beta_2 \qquad (7)$$

This parameter is expressed in unit of ps/(km-nm). It varies with wavelength for the fiber and vanishes at a wavelength known as the zero-dispersion wavelength and denoted as λ_{ZD}. The parameter β_3 is related to the dispersion slope S as $S = (2\pi c/\lambda^2)^2\beta_3$.

Substitute Eq.(5) and (5.6) in Eq.(3), calculate the derivative $\partial\tilde{A}/\partial z$ and convert the resulting equation into the time domain by replacing $\Delta\omega$ with the differential operator $i(\partial/\partial t)$. The resulting time-domain equation can be written as

$$\frac{\partial A}{\partial z} + \beta_1\frac{\partial A}{\partial t} + \frac{i\beta_2}{2}\frac{\partial^2 A}{\partial t^2} - \frac{\beta_3}{6}\frac{\partial^3 A}{\partial t^3} = i\beta_{NL}A - \frac{\alpha}{2}A \qquad (8)$$

This is the basic propagation equation governing pulse evolution inside a single-mode fiber. Before using it, we need to write the nonlinear term in its explicit form. From Eq. (4), the nonlinear part of the propagation constant is given by $\beta_{NL} = \delta_{nNL}(\omega/c)$. For optical fiber, the nonlinear change in the refractive index has the form $\delta_{nNL} = n_2 I$ (similar to a Kerr medium), where n_2 is a constant parameter with values around 2.6×10-20 m2/W and I represents the optical intensity. The intensity is related to

optical power at any distance z as $I(z,t) = P(z,t) / A_{eff}$, where A_{eff} is the effective core area of the fiber and is generally different than the physical core area because a part of the optical mode propagation outside of the core. It is common to normalize the amplitude A in Eq.(8) such that $|A|^2$ represents optical power. With this identification and using $\omega_0 = 2\pi c / \lambda_0$, where λ0 is the carrier wavelength, we obtain

$$\beta_{NL} = \gamma |A|^2, \qquad \gamma = \frac{2\pi n_2}{\lambda_0 A_{eff}} \tag{9}$$

Where the parameter γ, takes into account various nonlinear effects occurring within the fiber. the values of this parameter can be tailored to some extent by controlling the effective core area of an optical fiber.

We simplify Eq.(8) somewhat by noting that the β_1 term simply corresponds to a constant delay experienced by the optical signal as it propagates through the fiber. Since this delay does not affect the signal quality in any way, it is useful to work in a reference frame moving with the signal. This can be accomplished by introducing the new variables *t'* and *z'* as

$$t' = t - \beta_1 z \qquad z' = z \tag{10}$$

And rewriting Eq.(8) in terms of them as

$$\frac{\partial A}{\partial z'} + \frac{i\beta_2}{2}\frac{\partial^2 A}{\partial t'^2} - \frac{\beta_3}{6}\frac{\partial^3 A}{\partial t'^3} = i\gamma |A|^2 A - \frac{\alpha}{2} A \tag{11}$$

Where we also used Eq.(5-9). For simplicity of notation, we drop the primes over *z'* and *t'* whenever no confusion is likely to arise. Also the third-order dispersive effects are negligible in practice as long as β2 is not too close to zero, or pulses are not short than 5 ps. Setting β_3 =0, Eq.(11) reduces to

$$\frac{\partial A}{\partial z} + \frac{i\beta_2}{2}\frac{\partial^2 A}{\partial t^2} = i\gamma |A|^2 A - \frac{\alpha}{2} A \tag{12}$$

This equation is known as the nonlinear Schrodinger (NLS) equation. The three parameters, α, β_2 and γ, take into account three distinct kinds of degradations that can occur when an optical signal propagate through optical fibers.

Publication list

(A) Journal papers

1.High time resolution fiber optic sensing system based on correlation and differential technique
H.B. Song, T. Suzuki, M. Sako and K. Nonaka
Measurement Science and Technology,17,631-634 (2006).

2.Polarization fluctuation suppression and sensitivity enhancement of an optical correlation sensing system
H.B. Song, T. Suzuki, T. Fujimura, K. Nonaka, T. Shioda and T. Kurokawa
Measurement Science and Technology,18, 3230-3234 (2007)

(B) International conference

1. The 11th Micro optics Conference (MOC'05)
High time resolution fiber-optic sensor based on optical pulse correlation measurement (Poster presentation)
H.B. Song, T. Suzuki, M. Sako and K. Nonaka
Tokyo, Japan, 31/10/2005-2/11/2005

2. The 18th Internatioanl Optical Fiber Sensors (OFS-18)
Polarization stabilized optical fiber sensor with high time resolution based on Optical Pulse Correlation and FRR (Poster presentation)
H.B. Song, T. Suzuki and K. Nonaka, T. Shioda, and T. Kurokawa
Cancun, Mexico, 23/10/2006-27/10/2006

3. The 12th Micro optics Conference (MOC'06)

Direct fiber dispersion measurement using low time jitter multiwavelength pulsed LD array (Oral presentation)

K. Nonaka, H. Mizuno, Y. Mimoto, and **H.B. Song**

Seoul, Korea 10/9/2006-14/9/2006

4.International Conference on Smart Materials and Nanotechnology in Engineering

A novel stable and high-sensitivity fiber strain sensor based on optical pulse correlation measurement (Oral presentation)

H.B. Song, K. Nonaka

Harbin, China, 1/7/2007-4/7/2007

5.The 13th Micro optics Conference (MOC'07)

Low time jitter optical pulse generator with frequency tenability (Poster presentation)

H.B. Song, N. Kitaoka, K. Nonaka

Takamatsu, Japan, 28/10/2007-31/10/2007

(C) Domestic conferences

1. Proceedings of the 2007 IEICE General Conference

Suppression of polarization fluctuations in high resolution optical fiber sensor based on optical pulse correlation sensor

T. Suzuki, **H.B. Song**, T.Fujimura, and K. Nonaka

Nagoya, Japan, 20/3/2007—23/3/2007

2. Symposium of Optical Application, Vision and Measurement

Optical fiber sensing based on optical pulse correlation

K. Nonaka, **H.B. Song**, and N. Kitaoka

Kochi, Japan, 18/1/2008